17698

NATIONAL LIBRARY
OTTAWA

CANADA

BIBLIOTHÈQUE NATIONALE
OTTAWA

NAME OF AUTHOR.....GORDON.....STEAD.....

TITLE OF THESIS.....A.....FINITE.....ELEMENT.....
.....APPROACH.....TO.....SOUND.....
.....TRANSMISSION.....BETWEEN.....ROOMS

UNIVERSITY..OF..ALBERTA.....

DEGREE FOR WHICH THESIS WAS PRESENTED.....M..Sc.....

YEAR THIS DEGREE GRANTED.....1973.....

Permission is hereby granted to THE NATIONAL LIBRARY OF CANADA to microfilm this thesis and to lend or sell copies of the film.

The author reserves other publication rights, and neither the thesis nor extensive extracts from it may be printed or otherwise reproduced without the author's written permission.

(Signed)..Gordon Stead

PERMANENT ADDRESS:

....#102 - 10549...80 AVE
.....EDMONTON, ALTA
.....

DATED..Oct...1.....,....19 73

NL-91 (10-68)

THE UNIVERSITY OF ALBERTA

A FINITE ELEMENT APPROACH TO SOUND TRANSMISSION BETWEEN ROOMS

BY

© GORDON STEAD

A THESIS

SUBMITTED TO THE FACULTY OF GRADUATE STUDIES AND RESEARCH

IN PARTIAL FULFILMENT OF THE REQUIREMENTS FOR THE DEGREE

OF MASTER OF SCIENCE

DEPARTMENT OF MECHANICAL ENGINEERING

EDMONTON, ALBERTA

FALL, 1973

THE UNIVERSITY OF ALBERTA

FACULTY OF GRADUATE STUDIES AND RESEARCH

The undersigned certify that they have read, and recommend to the Faculty of Graduate Studies and Research, for acceptance, a thesis entitled "A FINITE ELEMENT APPROACH TO SOUND TRANSMISSION BETWEEN ROOMS" submitted by GORDON STEAD in partial fulfilment of the requirements for the degree of Master of Science.

A. Craggs

Supervisor

Gary Faulkner

D. W. Murray

Date . Sept. 6. / . 73.

ABSTRACT

A set of two dimensional finite elements were developed to approximate three dimensional coupled plate-acoustic systems. Though quite generally applicable, these elements were restricted to problems in small enclosure acoustics and sound transmission between rooms.

An experimental apparatus was constructed to substantiate the theoretical results. Agreement was found to be good in all except the most adverse cases.

ACKNOWLEDGMENTS

The author wishes to thank

- Dr. A. Craggs for his guidance and supervision of this thesis
- Dr. J. S. Kennedy, Dr. G. Faulkner and Dr. R. Tait for their helpful suggestions
- The members of the Mechanical Engineering Technical Staff for their assistance in construction and instrumentation of the experimental equipment
- My wife for her patience in typing
- The National Research Council of Canada (Scholarship) and The University of Alberta for their financial support and the National Research Council Research Fund No. A 7431 for computing funds

TABLE OF CONTENTS

		Page
CHAPTER I	INTRODUCTION	1
	1.1 Review of Related Work	2
	1.2 Aim of Thesis	4
CHAPTER II	UNCOUPLED ELEMENTS	6
	2.1 Element Formulation	7
	2.2 Rectangular Acoustic Element	10
	2.3 Triangular Acoustic Element	14
	2.4 Beam Plate Element	20
	2.5 Application of Acoustic Elements	30
	2.5.1 Odd Shaped Room	30
CHAPTER III	COUPLED ELEMENTS	40
	3.1 The Coupling Matrix	40
	3.2 Sound Transmission Between Panel Coupled Rooms	50
	3.2.1 Theoretical Considerations	54
	3.3 Sound Transmission Between Orifice Coupled Rooms	76
CHAPTER IV	DISCUSSION AND RESULTS	78
	4.1 Discussion	78
	4.2 Future Research	79
	4.3 Results	80

Page

BIBLIOGRAPHY 81

APPENDIX A 86

APPENDIX B 97

APPENDIX C 107

LIST OF TABLES

Table		Page
2.1	Convergence of Four Lowest Eigenvalues for Sloped Ceiling Reverberation Chamber	33
3.1	Results of Test Model	49

LIST OF FIGURES

Figure		Page
2.1	Element Shapes and Notation	9
2.2	Convergence of Rectangular Acoustic Element	13
2.3	Convergence of Triangular Acoustic Element	19
2.4	Convergence of Line Plate Element (n=0)	28
2.5	Convergence of Line Plate Element (n=1)	29
2.6	Sloped Ceiling Reverberation Chamber	32
2.7	First Mode - Rooms With Sloped Ceiling	37
2.8	Second Mode - Rooms With Sloped Ceiling	38
2.9	Third Mode - Rooms With Sloped Ceiling	39
3.1	Test Acoustic Model	49
3.2	Experimental Apparatus	51
3.3	Pictorial Layout of Components	52
3.4	First Mode - Sound Transmission Between Symmetric Rooms	56
3.5	Second Mode - Sound Transmission Between Symmetric Rooms	57
3.6	Third Mode - Sound Transmission Between Symmetric Rooms	58
3.7	Fourth Mode - Sound Transmission Between Symmetric Rooms	59
3.8	Fifth Mode - Sound Transmission Between Symmetric Rooms	60
3.9	First Mode - Normalized Longitudinal Pressure Variation and Plate Displacement	61

Figure		Page
3.10	Second Mode - Normalized Longitudinal Pressure Variation and Plate Displacement	62
3.11	Third Mode - Normalized Longitudinal Pressure Variation and Plate Displacement	63
3.12	Fourth Mode - Normalized Longitudinal Pressure Variation and Plate Displacement	64
3.13	Full Coupling Panel - Resonant Frequencies for Sound Transmission	65
3.14	73.7 Per Cent Coupling Panel - Resonant Frequencies for Sound Transmission	66
3.15	42.5 Per Cent Coupling Panel - Resonant Frequencies for Sound Transmission	67
3.16	42.5 Per Cent Orifice Coupling - Resonant Frequencies for Sound Transmission	73
3.17	4.2 Per Cent Orifice Coupling - Resonant Frequencies for Sound Transmission	74
3.18	Example of Orifice Coupling Mode Shapes	75
A1	Infinitesimal Acoustic Element	85
A2	P-V Curve	90
B1	Element Shape for Triangular Integral	100

NOTATION

$[A],[A]^{-1}$	matrices relating the arbitrary constants and the nodal pressure coordinates for a triangular acoustic finite element
$a_{\ell m}$	member of the arbitrary constants for a triangular acoustic finite element
B_a	pressure displacement work at a panel-acoustic interface
c	velocity of sound
D	the plate modulus = $Eh_p^3/12\ (1-\nu^2)$
E	Young's modulus
$f_i(x^*)$	the ith Hermitian Interpolation Polynomial of a variable x^*, $0 < x^* < 1$
$g(x,y)$	vector containing the ten variable elements of a cubic polynomial
h_p	thickness of plate element
$J,\delta J$	Hamiltonian or action integral and its first variation
[K]	stiffness matrix for plate finite element
ℓ,m,n	number of acoustical half-cosine waves between the boundaries in a rectangular room
[M]	mass matrix for plate finite element
M_{xx},M_{yy}	bending moments about the x and y axis, respectively

M_{xy}	twisting moment
n_e	number of elements used in convergence test
$\vec{n}$	unit normal vector to a surface
$[P],[P_e]$	overall and elemental acoustic pressure matrices
$\{p_n\},\{p_n\}_e$	overall and elemental pressure co-ordinates
p_e	elemental pressure
$p,\delta p$	pressure and its first variation
p,p_0	initial and final pressure
p_1	excess acoustic pressure = $p-p_0$
$p_i,\frac{\delta p}{\delta x}_i,\frac{\delta p}{\delta y}_i$	nodal pressure and its directional derivatives at the ith node
Q	plate shear
$[S],[S_e]$	overall and elemental acoustic stiffness
s	condensation
$T,\delta T$	kinetic energy and its first variation
t_1,t_2	end values of a time interval
$\underline{u}$	displacement within the acoustic fluid
$U,\delta U$	potential energy and its first variation
v_0,v	initial and final specific volumes
$\{w_n\}$	plate transverse deflection co-ordinates
w,w_p	transverse deflection of plate
$w_{p,x},w_{p,z}$	slope of the plate in the x and z directions, respectively
$w_{p,xx},w_{p,zz}$	plate curvature about the x and z axis, respectively

$w_{p,xz}$	plate twist
x,y,z	co-ordinate directions
γ	ratio of the specific heats of a gas
Δ	dilatation
Θ	acoustic panel coupling matrix
$[\theta]_a, [\theta]_p$	acoustic and plate rotational matrices
λ	eigenvalue of the eigenvalue problem
ν	Poisson's ratio
ρ, ρ_0	initial and final acoustic densities
ρ, ρ_a	acoustic density
ρ_p	plate density
$\{\phi_n\}, \{\phi_n\}_e$	overall and elemental velocity potential co-ordinates
$\{\eta\}_i, \{\Psi\}$	normalized eigenvectors or principal mode shapes

CHAPTER I

INTRODUCTION

The study of sound, similar to most other forms of science, found its origin in a practical "trial and error" sense long before the mathematical theories were developed. Experimentation on motion by Galileo Galilei [1]* and extensive research on musical instruments and listening rooms by Mersenne [2] were grouped under the field of "new sciences" until the name acoustics was introduced by Sauveur [3]. These early treastises, although mostly non-mathematical, defined the field and even made an approach at dividing it into sub-fields - geometrical, statistical and wave acoustics.

Geometrical and statistical are more generally grouped under architectural acoustics as they were the first techniques to find engineering application. The former allows the sound waves only to have ray characteristics thereby allowing the path of the sound to be traced much as a light ray with its intensity diminishing with distance and reflection. Statistical acoustics derives its name from the requirement of a "statistically diffuse sound field." Diffuse in the sense that the pressure level within the volume can be considered uniform. This can usually be approximated in very large enclosures, i.e. auditoriums, large halls, etc. where the longest sound wavelength present is less than one-tenth the minimum dimension and the multiplicity of sound frequencies is sufficient to eliminate pressure nodes and appreciable pressure maxima. This also allows the wave characteristics of sound

---

*Entries in [ ] square brackets refer to the bibliography.

to be totally neglected. Instead, sound radiation becomes independent of spatial location and the time dependency of a sound is only a function of the statistical average of damping surfaces within the enclosure. Much of the early work done in architectural acoustics [4, 5, 6] took this form of analysis.

Wave acoustics does not neglect the obtrusive wave characteristics of sound, increasing many-fold the difficulty of mathematical calculations. It is necessary to include reflection, absorption, diffraction and phase shift at every incidence of the sound waves with a boundary, not to mention cancellation and reinforcement of sound waves coincident within the enclosure. This approach can be used for any size of enclosure but is usually limited to smaller volumes, i.e. small rooms, ducting, etc. where the sound wavelengths present are of the same order as the enclosure's dimensions. The shear futility of analyzing a geometrically complicated structure can be appreciated. Major early theoretical contributions in wave acoustics were made by Rayleigh [7] and Lamb [8]. Their contributions by no means embody the entire field of acoustics, but it has been said, ". . . it behooves all of us. . . to read Rayleigh's Science of Sound regularly." [9]

It might be well mentioned here that between these two approaches to acoustics lies a zone that must be approached with an extensive "salting" of experience.

1.1 Review of Related Work

In 1944, Morse and Bolt published a "state-of-the-art" article [10] on room acoustics. A discussion of geometric and wave

acoustics was given with special reference to different types of absorbing wall materials. These panels were characterized by an acoustic impedence which was the complex ratio of the acoustic pressure and the air velocity just outside the surface. The real part of this ratio is the dissipative term whereas the imaginary part is the reactive term. The exact analysis of a regular acoustically hard rectangular room with one rigid but absorbing wall was presented but the intricacies in the calculations caused the authors to go to more approximate solutions for general application. The introduction of more rigid, absorbing walls only complicated the analysis. A simplified model that could handle different geometries and absorption at the walls would be desirable.

Principal mode analysis supplies an effective method of studying mechanical vibration. The inclusion of damping (hysteretic and viscous) cause problems but these are not insurmountable. Bishop and Gladwell [11] discuss this method quite fully concluding that ". . . when damping of the most general type is present, the system can vibrate in a principal mode at a natural frequency without there being any phase difference between the displacement at various points." This would tend to indicate that a study of undamped systems would supply an insight into lightly damped systems. The orthogonality of the principal mode allows the deformed shape of the structure to be represented by a linear combination of the principal mode shapes. Though principal mode analysis was discussed in terms of structural systems, it could be applied equally as well to acoustics with the corresponding "stiffness" and "mass" effects (more correctly kinetic and potential effects, respectively).

Later, authors became more interested in cases where the flexural natural frequencies of the panel were in the same range as the acoustical natural frequencies. The previous model of a complex acoustic impedance for an absorbing panel was no longer sufficient. Sound transmission between rooms [12] and noise effects on flexible structural enclosures [13, 14, 15, 16, 17, 18] can only be handled by a coupled plate-acoustic system. The idea of such a coupled system, with slight alteration, is also used in the study of liquid sloshing in containers [19].

1.2 Aim of Thesis

Previous finite element work by Craggs [15, 16] produced large three dimensional acoustic and plate elements. They were used to study transient responses of a plate-acoustic system. Each element required relatively large computer core area, therefore even small problems required a long execution time which is approximately proportional to the square of the storage space required. By assuming two of the boundaries to be parallel and hard, the exact solution can be used for the direction perpendicular to these boundaries, i.e. the z-direction. A similar approach (sometimes credited to Kantorovich) was used by Cheung and Zienkiewicz [20] in the study of plates and shafts. A reduction of element storage area by a factor of 3.0 and a consequent reduction in computation time by 7.0 is realized using this assumption. Though the elements are now effectively two dimensional, total freedom is retained in the remaining coordinate directions as to method of solution. It was proposed to develop second order plate and acoustic elements, i.e. approximating displacements and pressures and their first derivatives.

Also, instead of a transient study of a coupled plate-acoustic system, a principal mode analysis was undertaken. The natural frequencies and principal mode shapes of a system can be obtained by studying the free vibration problem. This entails assuming that all time dependent variables obey the same harmonic function, thus removing the time dependency of the system. The problem then reduces to the solution of an eigenvalue problem.

$$\{[A] - \lambda[B]\}\{x\} = 0$$

The numerical results presented are the natural frequencies and principal mode shapes for:

i) a rigid room with a sloping wall

ii) two rigid rooms coupled by a flexible panel of various widths

iii) two rigid rooms coupled by an air slit of various widths

CHAPTER II

UNCOUPLED ELEMENTS

The finite element method is basically the approximation of the desired solution over a well defined geometric space, i.e. cuboid, tetrahedron, etc. Interpolation functions modified by arbitrary parameters make up the general form of the solution. This general form is then forced to satisfy the equations throughout the well defined geometric space (from now on called an element). Though it is not necessary, the interpolation functions are usually picked in such a way that the arbitrary parameters take on physical significance at certain points in the element (called nodes). What remains is to join several elements into a desired configuration that has some degree of continuity between elements and to satisfy the natural boundary conditions.

Convergence (and rate of convergence) to the correct solution is of interest. It is extremely difficult, if not impossible, to prove convergence to the correct solution for all configurations which can be produced by finite elements. The generally accepted approach [19, 20] is to obtain an approximate solution to a problem that is mathematically solvable. Successively finer "grids" of elements are used to better approximate this solution. Percentage error (between the exact and approximate solution) is plotted against the number of elements on logarithmic graph paper. The slope of the resulting curve is an indication of the rate of convergence. Beyond this, "the proof is in the tasting". Results for other desired geometric configurations obtained from this method must be accepted (with due caution,

of course) and if possible checked out by experimentation.

2.1 Element Formulation

It has been found more convenient to work with functionals than with the actual equations of motion and the boundary conditions because certain symmetries arise in the functionals that can be taken advantage of. If a functional can be found whose stationary condition satisfies the equation of motion and the natural boundary conditions, then the functional can be used just as effectively in the solution of the problem [21]. In fact, the functionals required for the uncoupled panel and acoustic subsystems are the Hamiltonians or action integrals J of the subsystems

$$J = \int_{t_1}^{t_2} [T-U]\, dt$$

where T is the kinetic energy and U is the potential energy. The governing equation and boundary conditions are obtained by setting the first variation to zero

$$\delta J = 0$$

The first variation is obtained by replacing the required parameters by themselves plus a small arbitrary increment (i.e. p is replaced by $p + \delta p$) then the resulting equation $J + \delta J$ and the original equation J are subtracted to give the first variation.

Appendix A offers a relatively detailed formulation of the acoustic finite element. From the basic acoustic and energy equations (Appendices A1 and A2, respectively) through to the finite element or matrix formulation of the acoustic functional (Appendix A4), there was no assumption made as to the form of time dependency. This would

allow the study of transient acoustic systems; however, since the steady-state response of an undamped system is desired, the time function was written as

$$\sin (\omega t + \theta)$$

where ω is the cyclic frequency and θ is a phase angle defined by initial conditions. Since all variables in the system obey this time function (A16)* of Appendix A4 can be written

$$\{[S_e] - \omega_e^2[P_e]\} \{p_n\}_e = 0$$

which is a standard form of the eigenvalue problem with $\{p_n\}_e$ corresponding to the elemental nodal pressure coordinates. For a system composed of several elements, the 'e' subscript can be dropped.

The overall [S] matrix can be derived by noting that the energy of the total system is a linear summation of its component energies [8, 22]

$$T = \Sigma T_e = \frac{1}{2} \{p_n\}^T [S] \{p_n\}$$

$$= \frac{1}{2} \Sigma \{p_n\}_e^T [S_e] \{p_n\}_e$$

with a similar formula for [P]. Leading to

$$\{[S] - \omega^2[P]\} \{p_n\} = 0 \qquad (2.1)$$

where $\{p_n\}$ is the overall pressure coordinate.

---

*Entries in ( ) refer to equations.

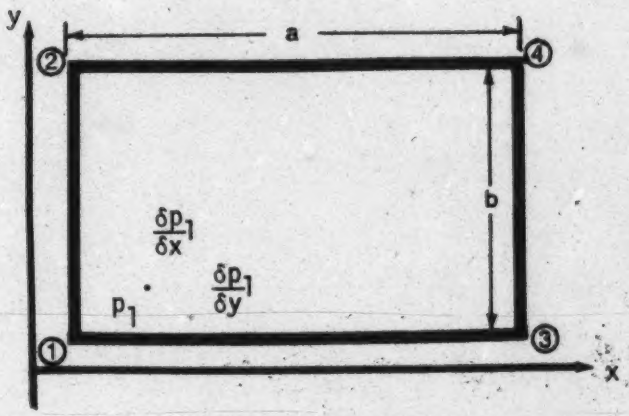

Figure 2.1 (a) RECTANGULAR ACOUSTIC ELEMENT

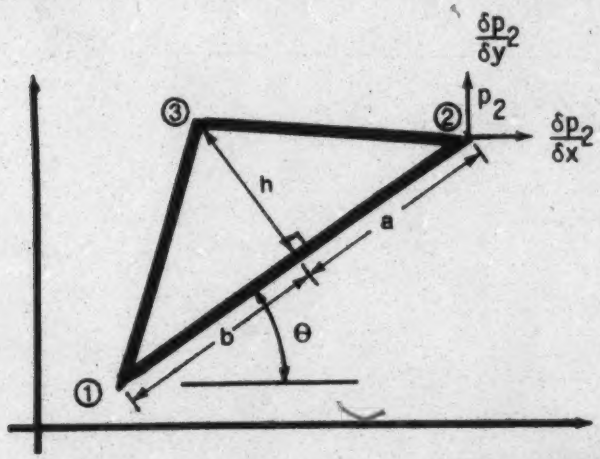

Figure 2.1 (b) TRIANGULAR ACOUSTIC ELEMENT

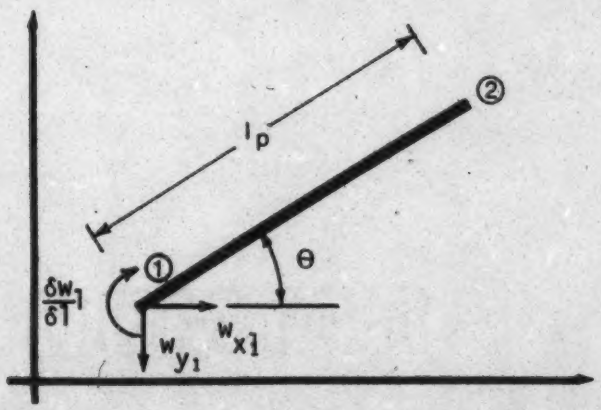

Figure 2.1 (c) LINE PLATE ELEMENT

Figure 2.1 ELEMENT SHAPES AND NOTATION

2.2. Rectangular Acoustic Element

Figure 2.1(a) gives the element shape and dimension in the x-y plane. The encircled numbers are the nodal numbers and the nodal values of p, $\frac{\delta p}{\delta x}$, $\frac{\delta p}{\delta y}$ are p_i, $\frac{\delta p_i}{\delta x}$, $\frac{\delta p_i}{\delta y}$, i = 1, 2, 3, 4 which are functions of time. Since this is a "pseudo" three dimensional approach, there should be an identical x-y plane at a distance d behind the plane shown. These planes were previously defined as rigid and parallel, allowing the exact solution for the z-direction to be found. This solution, a single Fourier cosine series, can easily be used to approximate many mode shapes in the z-direction (as is shown in Appendix B1), although only the nth term of the series will be used in the following calculations to simplify the notation. In the x-y plane, pressure and pressure variation can be approximated by the product of two sets of Hermitian interpolation polynomials f(x*), f(y*), where x* = x/a and y* = y/b. These polynomials, their characteristics and their integrals are given in Appendix B2. The desirable characteristics of these interpolation polynomials allow p_e, the pressure distribution throughout the element for the nth node in the z-direction, to be expressed as

$$\begin{aligned} p_e = \{ & p_1 f_1(x^*) f_1(y^*) + \frac{\delta p_1}{\delta x} a f_2(x^*) f_1(y^*) + \frac{\delta p_1}{\delta y} b f_1(x^*) f_2(y^*) \\ & + p_2 f_1(x^*) f_3(y^*) + \frac{\delta p_2}{\delta x} a f_2(x^*) f_3(y^*) + \frac{\delta p_2}{\delta y} b f_1(x^*) f_4(y^*) \\ & + p_3 f_3(x^*) f_1(y^*) + \frac{\delta p_3}{\delta x} a f_4(x^*) f_1(y^*) + \frac{\delta p_3}{\delta y} b f_3(x^*) f_2(y^*) \\ & + p_4 f_3(x^*) f_3(y^*) + \frac{\delta p_4}{\delta x} a f_4(x^*) f_3(y^*) + \frac{\delta p_4}{\delta y} b f_3(x^*) \cdot \\ & f_4(y^*)\} \cos \frac{n\pi z}{d} \end{aligned} \tag{2.2}$$

where the dimensions a, b are a result of the chain-rule, i.e. $\frac{\delta p}{\delta x} = \frac{\delta p}{\delta x^*} \frac{\delta x^*}{\delta x}$ or $\frac{\delta p}{\delta x^*} = a \frac{\delta p}{\delta x}$. A simpler short-hand notation will be introduced here

$$p_e = \{f(x^*)\ f(y^*)\}^T \{p_n\}_e \cos \frac{n\pi z}{d}$$

where the superscript "T" indicates the transpose of the vector and

$$\{f(x^*)\ f(y^*)\} = \begin{bmatrix} f_1(x^*)\ f_1(y^*) \\ af_3(x^*)\ f_1(y^*) \\ \cdot \\ \cdot \\ \cdot \\ bf_3(x^*)\ f_4(y^*) \end{bmatrix} \quad \text{and} \quad \{p_n\}_e = \begin{bmatrix} p_1 \\ \frac{\delta p_1}{\delta x} \\ \cdot \\ \cdot \\ \cdot \\ \frac{\delta p_4}{\delta y} \end{bmatrix}$$

It would be best to note here that

$$\frac{\delta p}{\delta x}_e = \frac{1}{a} \{f'(x^*)\ f(y^*)\}^T \{p_n\}_e \cos \frac{n\pi z}{d}$$

$$\frac{\delta p}{\delta y}_e = \frac{1}{b} \{f(x^*)\ f'(y^*)\}^T \{p_n\}_e \cos \frac{n\pi z}{d}$$

$$\frac{\delta p}{\delta z}_e = \frac{-n\pi}{d} \{f(x^*)\ f(y^*)\}^T \{p_n\}_e \sin \frac{n\pi z}{d}$$

The prime "'" denotes differentiation with respect to the variables in round brackets.

Substituting these formulas in the energy equation as done in Appendix A4, the acoustic stiffness $[S_e]_R$ and pressure $[P_e]_R$ matrices can be written

$$[S_e]_R = \frac{ab}{\rho} \int_a^1 \int_o^1 \left[\frac{1}{a^2} \{f'(x^*)\ f(y^*)\} \{f'(x^*)\ f(y^*)\}^T \right.$$

$$\left. + \frac{1}{b^2} \{f(x^*)\ f'(y^*)\} \{f(x^*)\ f'(y^*)\}^T \right] dx^* dy^* \cdot \int_o^d \cos^2 \frac{n\pi z}{d}\ dz$$

$$+ \frac{ab}{\rho} \left(\frac{m\pi}{d}\right)^2 \int_o^1 \int_o^1 \{f(x^*)\ f(y^*)\} \{f(x^*)\ f(y^*)\}^T dx^* dy^* \cdot \int_o^d \sin^2 \frac{n\pi z}{d}\ dz \tag{2.3}$$

$$[P_e]_R = \frac{ab}{\rho c^2} \int_o^1 \int_o^1 \{f(x^*)\ f(y^*)\} \{f(x^*)\ f(y^*)\}^T dx^* dy^* \int_o^d \cos^2 \frac{n\pi z}{d}\ dz \tag{2.4}$$

The integrals with respect to z are defined in Appendix B1, and the integrals with respect to x* and y* are defined in Appendix B2.

The rectangular acoustic element was programmed for the IBM 360/67 computer and with the aid of the IBM Scientific Subroutine Package, the eigenvalue problem, as shown by (2.1) was performed. A cubical room of unit side and rigid boundaries was approximated as a check for convergence. This system has an exact set of principal mode solutions

$$p = p^* \cos \ell\pi x \cdot \cos m\pi y \cdot \cos n\pi z$$

$$\omega^2 = c^2 (\ell^2 + m^2 + n^2)$$

where the pressure p* is a periodic function of time and ℓ, m, n are the number of half-cosine waves between the boundaries in the x, y, z directions, respectively. Grid refinement was done only in the x-direction. Percentage error in the eigenvalue (the square of the natural frequency) versus the number of elements is plotted for various (ℓ, m, 0) mode shapes in Fig. 2.2.

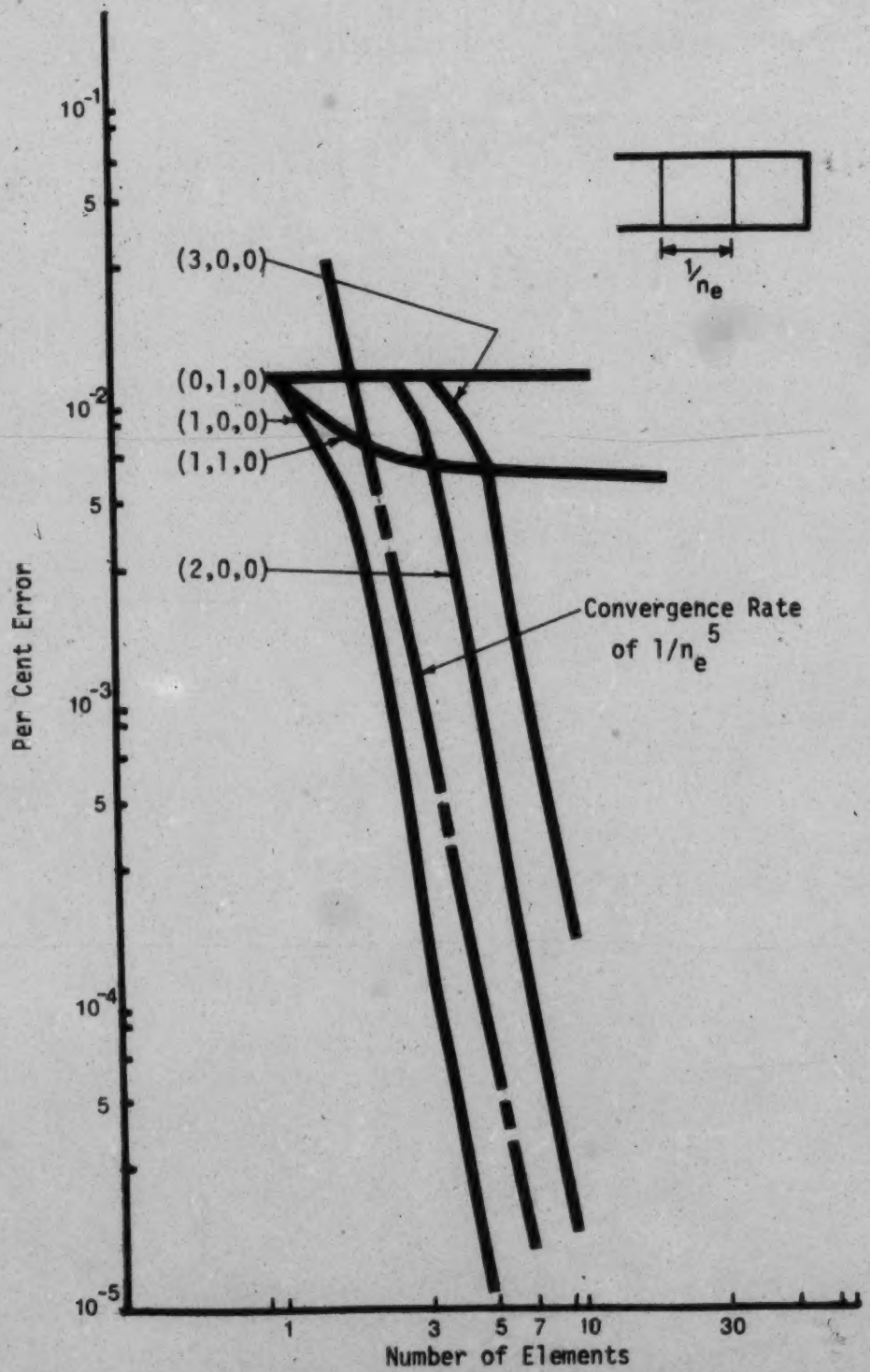

Figure 2.2 CONVERGENCE OF RECTANGULAR ACOUSTIC ELEMENT

The convergence of the results is at the rate of $1/n_e^5$, (n_e being the number of elements) for (ℓ, 0, 0) modes because of the x-direction grid refinement. The two (ℓ, 1, 0) modes plotted, which had no y-direction grid refinement, show no improvement with increase in element number. Note that even one element made a good initial approximation. Although not plotted, (ℓ, m, n) modes would give exactly the same type of curves as (ℓ, m, 0) curves because the exact solution between rigid boundaries is used in the formulation of the elements for the z-direction.

2.3 Triangular Acoustic Element

Because of the change in geometry, the method of approximating the pressure p_e within the element was done by a cubic polynomial in x and y, and the exact solution in the z-direction.

$$p_e = \left(\sum_{m=0}^{3} \sum_{\ell=0}^{3-m} a_{\ell m} x^{\ell} y^{m}\right) \cos \frac{n\pi z}{d}$$

where the $a_{\ell m}$ were a set of arbitrary constants.

A complete cubic polynomial has ten arbitrary parameters, but to approximate the pressure and the pressure variation in x and y-directions for three nodes required only nine parameters. There are several methods to remove the extra parameter; two were tried but the one presented in Appendix C1 was rejected, in this case because the added computational time required did not improve (and in some cases worsened) the element's accuracy. The method chosen was to simply equate the a_{21} and a_{12} coefficients, so the elemental pressure p_e was written as

$$p_e = \{a_{00} + a_{10}x + a_{01}y + a_{11}xy$$

$$a_{20}x^2 + a_{02}y^2 + a_{12}(x^2y + xy^2)$$

$$+ a_{30}x^3 + a_{03}y^3\}\cos\frac{n\pi z}{d} \qquad (2.5)$$

The problems with this formulation will be discussed later. A third possibility would have been to define an internal node where pressure was the only parameter, but this would cause problems with the storage and manipulation of the resulting matrices.

Using a notation similar to Section 2.1,

$$p_e = \{g(x,y^*)\}^T \{\underline{a}\}\cos\frac{n\pi z}{d}$$

where

$$\{g(x,y)\} = \begin{bmatrix} 1 \\ x \\ y \\ \vdots \\ y^3 \end{bmatrix} \text{ and } \{\underline{a}\} = \begin{bmatrix} a_{00} \\ a_{10} \\ a_{01} \\ \vdots \\ a_{03} \end{bmatrix}$$

Considering the element and notation of Fig. 2.1(b), it is now necessary to relate the arbitrary constant $\{\underline{a}\}$ to the nodal characteristics p_i, $\frac{\delta p_i}{\delta x}$, $\frac{\delta p_i}{\delta y}$, $i = 1, 2, 3$. This is simply done by writing down the nine simultaneous equations for $z = 0$

$$\{p_n\}_e = [A]\{\underline{a}\}$$

where

$$\{p_n\}_e = \begin{bmatrix} p_1 \\ \frac{\delta p_1}{\delta x} \\ \cdot \\ \cdot \\ \frac{\delta p_3}{\delta y} \end{bmatrix}$$

and [A] is a matrix of the nodal values of $\{g(x,y)\}$ and its directional derivatives $\left\{\frac{\delta g}{\delta x}\right\}$ and $\left\{\frac{\delta g}{\delta y}\right\}$, respectively. Then it can be written

$$\{\underline{a}\} = [A]^{-1} \{p_n\}$$

If the formulation was carried to completion from this point, the resulting integrals over the triangle would be arduous and could only be handled numerically. It is more convenient to set up a localized x' - y' coordinate system, for the triangle, where $x' = \frac{\varepsilon + b}{a + b}$ and $y' = \eta/h$ perform the required integration (shown in Appendix B3) then "rotate" the results into the x-y coordinate system (shown in Appendix B4). The formulation for the x' - y' coordinate system is identical to what has been presented for the x - y coordinate system, but gives some simplifications in [A] and $[A]^{-1}$, as shown in Appendix B5. The formulation can be carried on in terms of x' and y'.

The elemental pressure can be written as

$$p_e = \{g(x',y')\}^T [A]^{-1} \{p_n\}_e$$

Note that the variables in round brackets are omitted in future to simplify the formulation. The acoustical stiffness $[S_e']_T$ and pressure $[P_e']_T$ matrices are derived by substituting into the energy equations (A14).

$$[S_e'] = \frac{1}{\rho} \cdot [A^T]^{-1} \int_{x'} \int_{y'} \left\{ \left\{\frac{\delta g}{\delta x'}\right\} \left\{\frac{\delta g}{\delta x'}\right\}^T + \left\{\frac{\delta g}{\delta y'}\right\} \left\{\frac{\delta g}{\delta y'}\right\}^T \right\} dx'dy' \cdot \int_0^d \cos^2 \frac{n\pi z}{d} dz \cdot [A]^{-1}$$

$$+ \frac{1}{\rho} \cdot [A^T]^{-1} \int_{x'} \int_{y'} \{g\} \{g\}^T dx'dy' \cdot \int_0^d \sin^2 \frac{n\pi z}{d} dz$$

$$\cdot [A]^{-1} \left(\frac{n\pi}{d}\right)^2 \qquad (2.6)$$

where $[A^T]^{-1}$ is the transpose of $[A]^{-1}$

$$[P_e]' = \frac{1}{\rho c^2} \cdot [A^T]^{-1} \int_{x'} \int_{y'} \{g\} \{g\}^T dx'dy' \cdot \int_0^d \cos^2 \frac{n\pi z}{d} dz \cdot [A]^{-1} \qquad (2.7)$$

The integrals with respect to x' and y' are given in Appendix B3. The integrals with respect to z are given in Appendix B1. The rotation of the nodal velocity potential $\{\phi_n'\}_e$ from the x' - y' coordinate system, is shown in Appendix B4. Since energy is independent of coordinate transformation, it can be written

$$T_e = \frac{1}{2} \{\phi_n'\}_e^T [S_e'] \{\phi_n'\}_e \quad \text{in } x' - y' \text{ system}$$

$$= \frac{1}{2} \{\phi_n\}_e^T [\theta]_a^T [S_e'] [\theta]_a \{\phi_n\}_e$$

$$= \frac{1}{2} \{\phi_n\}_e [S_e] \{\phi_n\} \quad \text{in } x - y \text{ system}$$

or

$$[S_e] = [\theta]_a^T [S_e'] [\theta]_a$$

where $[\theta]_a$ is the acoustic rotational matrix defined in Appendix B4.

The triangular element acoustic stiffness and pressure matrices derived above were programmed and the convergence tests were run on the cubical room used in Section 2.2. The orientation of the elements and the percentage error versus number of elements plot, are shown in Fig. 2. 3. The rate of convergence was slightly less than $1/n_e^5$ in the direction of grid refinement with a poorer initial approximation than the rectangular elements, but overall still gave good results. It was interesting to note that by changing the pattern of subdividing the cuboid, even for a one-directional grid refinement, the results (and the resulting percentage errors) were changed, but this could be a study in itself, so will not be gone into here.

By studying the formulation of the exact solution and by comparing the finite element equations (2.3) and (2.5) it is possible to arrive at a natural frequency equation for the (m, n, q) mode in

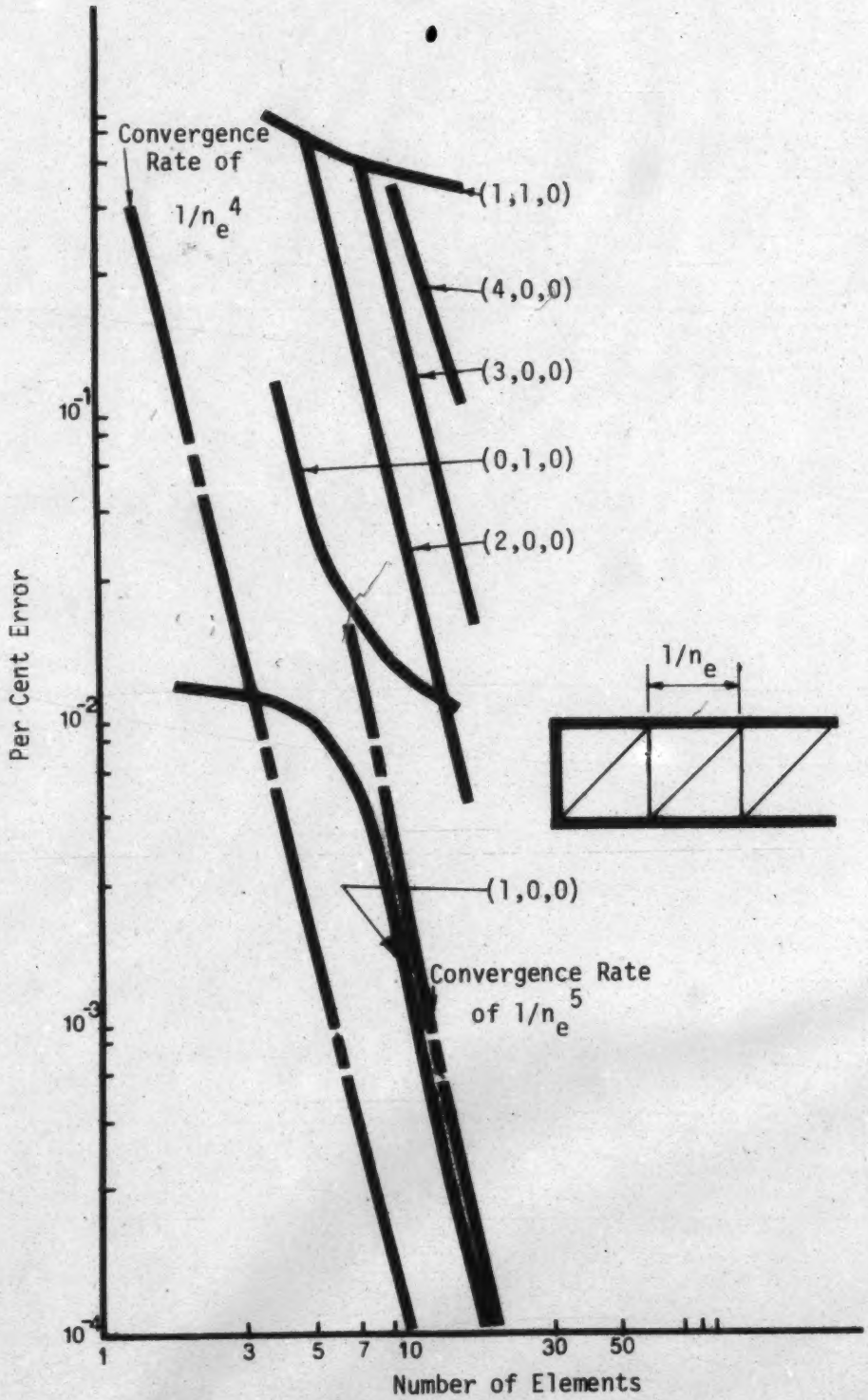

Figure 2.3 CONVERGENCE OF TRIANGULAR ACOUSTIC ELEMENT

terms of the (m, n, 0) mode.

$$\omega_{mnq}^2 = \omega_{mn0}^2 + \left\{\frac{q\pi c}{d}\right\}^2 \tag{2.8}$$

where ω_{mnq} is the natural frequency for the (m, n, q) mode.

c is the velocity of sound

d is the depth of the room

2.4 Beam Plate Element

A similar detailed formulation to the one given in Appendix A could be undertaken for flat plates, but would serve no useful purpose, so will be forgone in favour of writing only the energy equations according to S. Timoshenko [23] for cartesian coordinates. It is, however, initially necessary to discuss the orientation of the plate. To use Kantorovich's approach the plate must be placed between the two rigid planes perpendicular to the z-direction, but the other direction must be general. It will be seen that the same rotational concept used in the triangular acoustic element can be used here. Therefore, the plate will initially take an x-z plane orientation for the formulation and later be rotated to the x' - z'plane by a rotational matrix $[\theta]_p$.

$$T = \frac{1}{2}\rho_p h_p \iint_A \dot{w}_p^2 \, dxdz \tag{2.9}$$

where $\dot{w}_p$ is the time derivative of the transverse deflection of the plate and dxdz is an infinitesimal surface area on the plate in the x-z plane.

It is also convenient to introduce the differentiation convention $w_{,x} = \frac{\delta w}{\delta x}$, $w_{,xx} = \frac{\delta^2 w}{\delta x^2}$ etc. So,

$$U = \frac{D}{2} \iint_A \{w_{p,xx}^2 + w_{p,zz}^2 + 2\nu\, w_{p,xx}\, w_{p,zz} + 2(1-\nu)\,(w_{p,xz}^2)\}\, dxdz \qquad (2.10)$$

where

$D = Eh_p^3 / 12\,(1-\nu^2)$ is the Plate Modulus

E is Young's Modulus

ν is Poisson's Ratio

Again, it is necessary to show that the equation of motion and the natural boundary conditions can be derived from the action integral by variational calculus.

The first variation is

$$\delta J = \int_{t_1}^{t_2} (\delta T - \delta U)\, dt = 0$$

$$\delta J = \int_{t_1}^{t_2} [\rho_p h_p \int_z \int_x \dot{w}_p \, \delta\dot{w}_p \, dxdz - D \int_z \int_x \{w_{p,xx} \, \delta w_{p,xx}$$

$$+ w_{p,zz} \, \delta w_{p,zz} + \nu(w_{p,xx} \, \delta w_{p,zz} + w_{p,zz} \, \delta w_{p,xx})$$

$$+ 2(1 - \nu) \, w_{p,xz} \, \delta w_{p,xz}\} \, dxdz] \, dt = 0 \qquad (2.11)$$

The first term can be integrated by parts with respect to time to give

$$\rho_p h_p \iint_A [\dot{w}_p \, \delta w_p \Big|_{t_1}^{t_2} - \int_{t_1}^{t_2} \ddot{w}_p \, \delta w_p dt] \, dxdz$$

The rest of the terms in (2.11) can be integrated by parts twice, with due care in the evaluation of the integral. The third term in (2.11) can be written as

$$-D \int_{t_1}^{t_2} [\int_x w_{p,zz} \, \delta w_{p,z} \Big|_0^d dx - \int_x w_{p,zzz} \, \delta w_p \Big|_0^d dx$$

$$+ \iint_A w_{p,zzzz} \, \delta w_p \, dxdz] \, dt$$

where the first and second terms are evaluated at the front and rear boundary (z=0 and z=d, respectively) before they are integrated with respect to x. The last term in (2.11) is divided into two halfs and integrated twice by parts; one half is integrated first with respect to x, then with respect to z; the other half is integrated in the

reverse order. Noting again that δw_p and $\delta w_{p,x}$ are arbitrary and small and $\delta w_p = 0$ at t_1 and t_2, the following equations result.

For $x = 0$ or l_p

$$\frac{\delta}{\delta x}\left[\delta w_p \left(w_{p,xx} + \nu w_{p,zz} + (1 - \nu) w_{p,xz}\right)\right] = 0$$

$$\delta w_p\left[w_{p,xxx} + w_{p,xzz} - \frac{\delta}{\delta x}\left(w_{p,xx} + \nu w_{p,zz} + (1 - \nu) w_{p,xz}\right)\right] = 0$$

(2.12)

where l_p is the length of the plate in the x-direction.

For $z = 0$ or d

$$\frac{\delta}{\delta z}\left[\delta w_p \left(w_{p,zz} + \nu w_{p,xx} + (1 - \nu) w_{p,zx}\right)\right] = 0$$

$$\delta w_p \left[w_{p,zzz} + w_{p,zxx} - \frac{\delta}{\delta y}\left(w_{p,zz} + \nu w_{p,xx} + (1 - \nu) w_{p,zx}\right)\right] = 0$$

(2.13)

and within the plate boundaries

$$D(w_{p,xxxx} + w_{p,zzzz} + 2w_{p,xxzz}) + \rho_p h_p \ddot{w}_p = 0 \qquad (2.14)$$

These sets of equations show the power of the functional approach. Besides (2.14) being the equation of motion for a free vibrating plate, (2.12) and (2.13) embody all the natural boundary

conditions on a rectangular plate. According to Timoshenko [24]

$$M_{xx} = - D (w_{p,xx} + \nu w_{p,zz})$$

$$M_{zx} = - D (1 - \nu) w_{p,xz}$$

$$Q_x = - D (w_{p,xxx} + w_{p,xzz})$$

where M_{xx} is the bending moment (in the x-direction on the plate edge perpendicular to the x-direction), M_{zx} is the twisting moment and Q_x is the shear on edges perpendicular to the x-direction.

Using these relations in (2.12)

$$\frac{\delta}{\delta x} [\delta w_p (M_{xx} + M_{zx})] = 0$$

$$\delta w_p [Q_x - \frac{\delta}{\delta x} (M_{xx} + M_{zx})] = 0 \qquad (2.15)$$

$$\text{for } x = 0, l_p$$

For example, a pinned edge on $x = 0$ is defined by $\delta w_p = 0$ and $M_{xx} = 0$. This allows for non-zero Q_x and M_{zx}. All other boundary conditions [24] can be derived from these equations.

Although (2.14) has no assumption as to the time function, it will be considered as harmonic (the time function) and real, i.e. $\sin (\omega t + \theta)$.

For simplicity the exact solution in the z-direction will be taken as a single Fourier sine series, i.e. pinned boundary conditions at z = 0 and z = d. Only one term (the kth) of the exact solution is to be used to simplify notation, although again a multi-term approximation of a mode shape could be handled.

If the notation used in Fig. 2.1 (c) is adopted (noting that $\theta = 0$ for initial consideration), we can write the deflection of plate w_p, in terms of a product of a set of Hermitian interpolation polynomials $\{f(x^*)\}$ and the exact solution where $x^* = \varepsilon/\ell_p$ and $0 \leq \varepsilon \leq \ell_p$.

$$w_p = \{w_1 f_1(x^*) + \ell_p \frac{\delta w_1}{\delta x} f_2(x^*) + w_2 f_3(x^*) + \ell_p \frac{\delta w_2}{\delta x} f_4(x^*)\} \sin \frac{k\pi z}{d} \qquad (2.16)$$

where w_i, $\frac{\delta w_i}{\delta x}$, $i = 1, 2$ - are the nodal characteristics which may vary with time

$f_i(x^*)$, $i = 1, 4$ - are the Hermitian polynomials definition Appendix B2.

This can be written in short hand notation as in Sec. 2.2

$$w_p = \{f(x^*)\}^T \{w_n\} \sin \frac{k\pi z}{d}$$

where

$$\{f(x^*)\} = \begin{bmatrix} f_1(x^*) \\ \cdot \\ \cdot \\ \ell_p f_4(x^*) \end{bmatrix} \quad \text{and} \quad \{w_n\} = \begin{bmatrix} w_1 \\ \cdot \\ \cdot \\ \frac{\delta w_2}{\delta x} \end{bmatrix}$$

The elemental mass $[M_e]$ and stiffness $[K_e]$ can be defined by the equations

$$T_e = \frac{1}{2} \{\dot{w}_n\}^T [M_e] \{\dot{w}_n\}$$

$$U_e = \frac{1}{2} \{w_n\}^T [K_e] \{w_n\}$$

By substituting into the respective energy equations (2.9) and (2.10),

$$[K_e] = D\ell_p \int_0^1 [\{f''(x^*)\} \{f''(x^*)\}^T / \ell_p^4 + \{f(x^*)\} \{f(x^*)\}^T \left\{\frac{k\pi}{d}\right\}^4$$

$$-\frac{\nu}{\ell_p^2} \left\{\frac{k\pi}{d}\right\}^2 (\{f''(x^*)\} \{f(x^*)\}^T + \{f(x^*)\} \{f''(x^*)\}^T)] \, dx^*$$

$$\cdot \int_0^d \sin^2 \frac{k\pi z}{d} \, dz$$

$$+ 2(1-\nu) \frac{D}{\ell_p} \int_0^1 \{f'(x^*)\} \{f'(x^*)\}^T \, dx^* \int_0^d \cos^2 \frac{k\pi z}{d} \, dz \left\{\frac{k\pi}{d}\right\}^2 \quad (2.17)$$

where the third term has been arranged to retain the symmetry of the stiffness matrix.

$$[M_e] = \rho_p h_p \ell_p \int_0^1 \{f(x^*)\} \{f(x^*)\}^T \, dx^* \cdot \int_0^d \sin^2 \frac{k\pi z}{d} \, dz \quad (2.18)$$

The integrals with respect to x* can be found in Appendix B2. The integrals with respect to z can be found in Appendix B1.

This element can now be rotated to any position, letting 1* denote the dimension along the sloped plate as shown in Fig. 2.1(c).

By direct comparison with Appendix B4,

$$\begin{bmatrix} w_i \\ \\ \frac{\delta w_i}{\delta x^*} \end{bmatrix} = \begin{bmatrix} \sin\theta & \cos\theta & 0 \\ \\ 0 & 0 & 1 \end{bmatrix} \begin{bmatrix} w_{xi} \\ w_{yi} \\ \frac{\delta w_i}{\delta l^*} \end{bmatrix}$$

The plate rotational matrix $[\theta]$ can be written

$$[\theta]_p = \begin{bmatrix} \sin\theta & \cos\theta & 0 & & O & \\ 0 & 0 & 1 & & & \\ & & & \sin\theta & \cos\theta & 0 \\ & O & & 0 & 0 & 1 \end{bmatrix}$$

These plate element stiffness and mass matrices were programmed for the IBM 360/67 and convergence tests run on harmonically vibrating plates of unit side with pinned boundary conditions on all edges. This plate has an exact principal mode solution

$$w_p = w_p^* \sin r\pi x \sin k\pi z$$

$$\omega^2 = \frac{\pi^4 D}{\rho_p h_p} (r^2 + k^2)^2$$

where r and k are the number of half-sine waves in the x and z-direction, respectively.

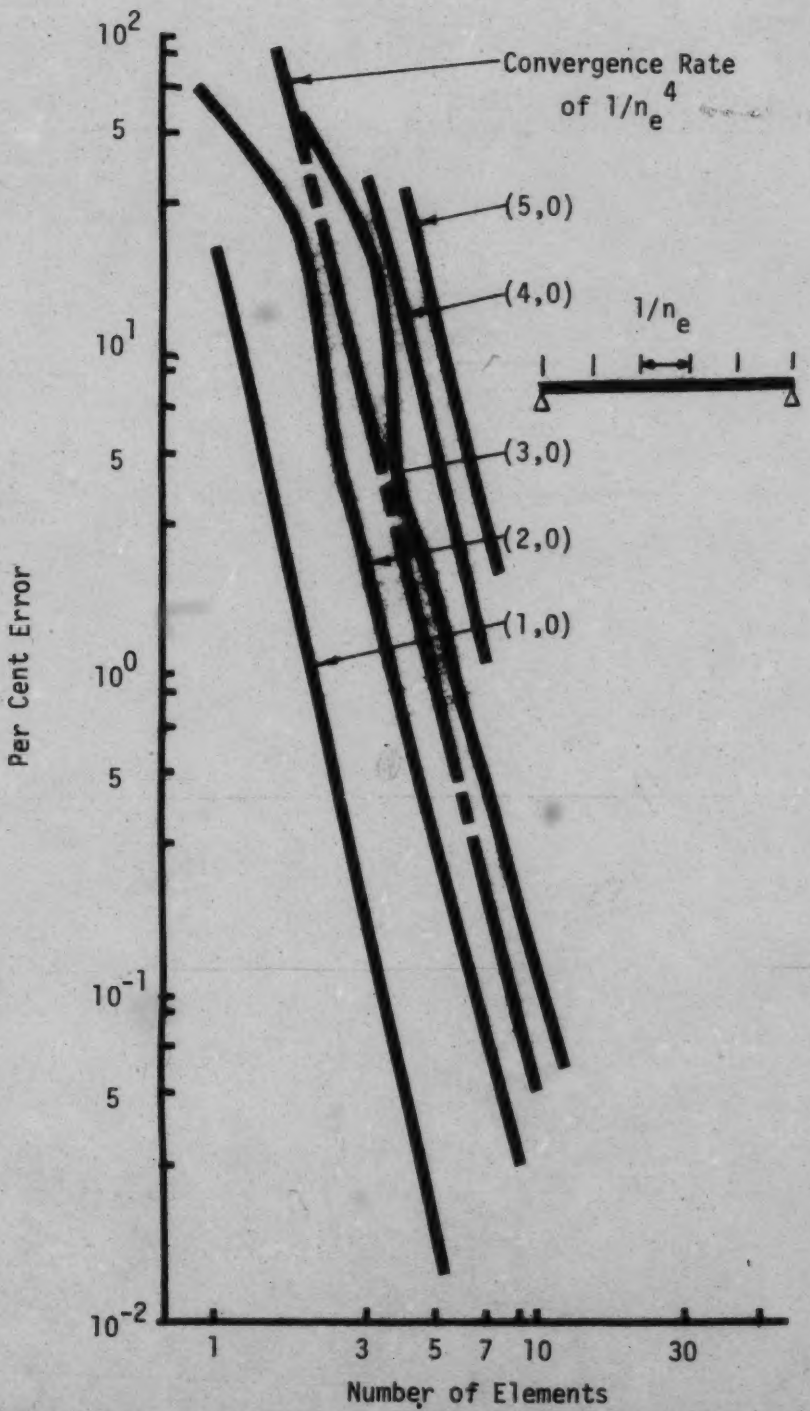

Figure 2.4 CONVERGENCE OF LINE PLATE ELEMENT (n=0)

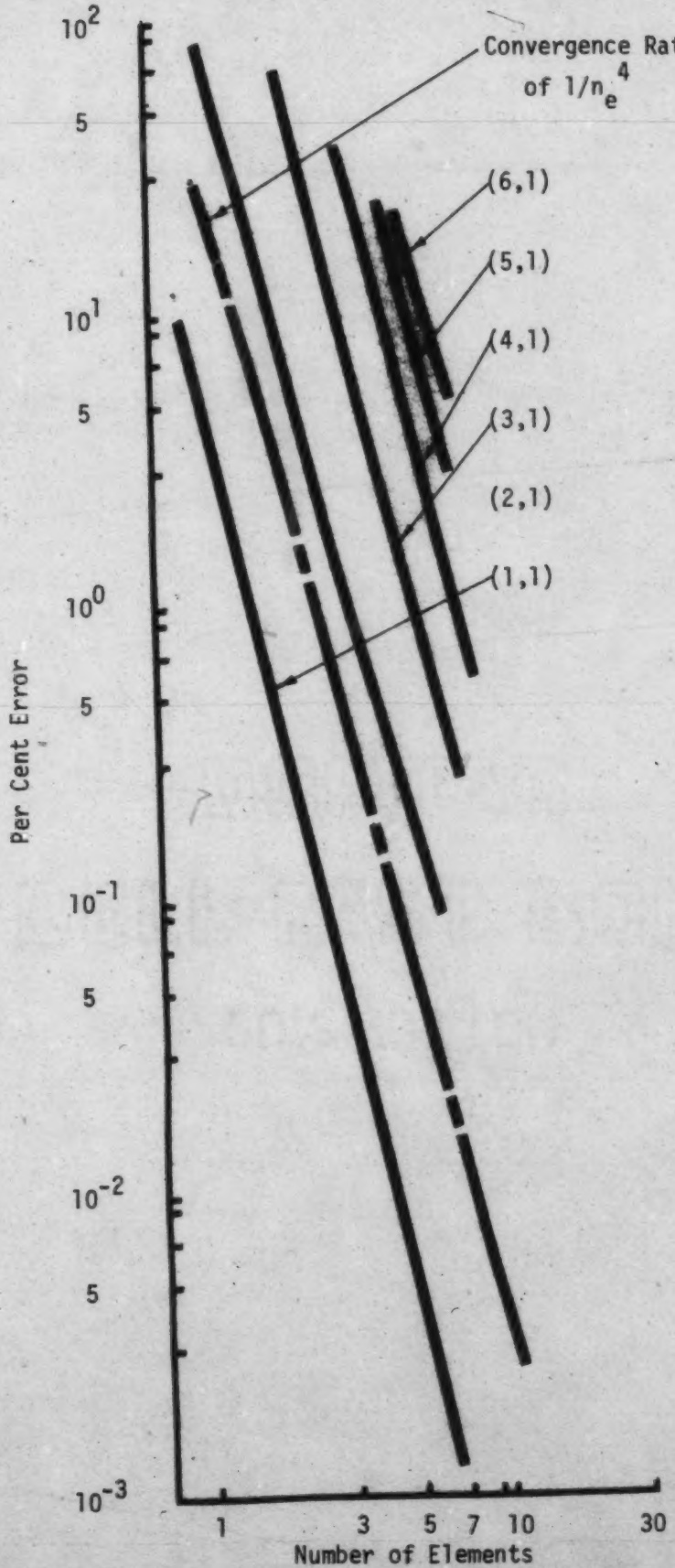

Figure 2.5 CONVERGENCE OF LINE/PLATE ELEMENT (n=1)

ρ_p, h_p and D were picked so the coefficient in front of the natural frequency equation was unity, i.e. $\omega^2 = (r^2 + k^2)^2$.

There is no similar formula to (2.8) that can be easily derived for a plate system so the plots of percentage error versus number of elements are given for both k = 0 and k = 1 (Fig. 2.4 and Fig. 2.5, respectively). The initial approximation in some modes are about 60 per cent in error in the square of natural frequency (8 per cent in the natural frequency). This is not good, but fortunately a slightly higher number of elements gives accuracy of 2 per cent in the lower natural modes. These lower modes will be used in the study of sound transmission. It may also be noted that the results of the theory are integers close to unity for which the error associated with truncation could be significant. Later results tend to bear this up.

The plate element, as developed, was effectively a beam. Independently they can be used to study the vibration of rectangular plates with two parallel pinned boundaries while the other two boundaries can have any combination of free, fixed or pinned boundary conditions. Warburton [25] has produced a very comprehensive analytic paper on such plates. Melosh, Papenfuss, Clough, Adini and Tocher have produced [21] similar plate elements of more general application so the use of the plate elements will be left for the coupled system.

2.5 Application of Acoustic Elements

2.5.1 Odd Shaped Room

A problem was required to test a combination of triangular

and rectangular acoustic elements. The Mechanical Engineering Building on the University of Alberta campus, which was under construction at the time, had a reverberation room which offered an excellent model. Being placed directly under a sloped roof section, required that one half of the room have a sloped ceiling. The exact profile of the room is shown in Fig. 2.6 (c), its depth being 22.0 ft.

One problem, exemplified by this room, is what boundary conditions exist at a corner such as shown in Fig. 2.6 (a). Any node along the sloped edge has the boundary condition

$$\frac{\delta p}{\delta x} = - \text{ctn } \eta \frac{\delta p}{\delta y} \quad \text{or} \quad \frac{\delta p}{\delta y} = - \tan \eta \frac{\delta p}{\delta x}$$

while along an upright edge

$$\frac{\delta p}{\delta x} = 0$$

Right at the corner node, there is a discontinuity, as there would be in a mathematical analysis (unless certain transforms were undergone). Using finite element methods there are three logical possible choices of how to approximate this boundary condition as shown in Fig. 2.6 (b). The first two are not correct, but on element refinement they will converge to nearly the correct result. This occurs by virtue of the fact that as the elements get smaller the effect of the elements containing the incorrect nodal value diminishes

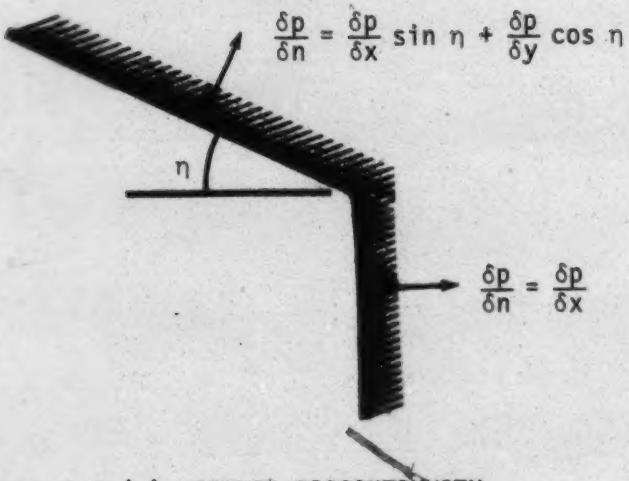

Figure 2.6 (a) CORNER DISCONTINUITY

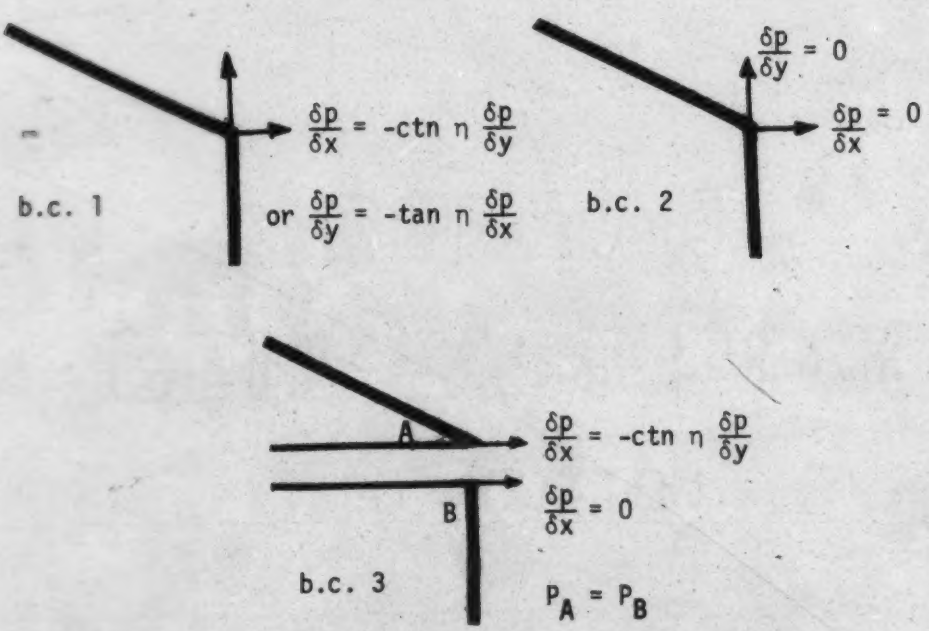
$\frac{\delta p}{\delta x} = -\text{ctn } \eta \frac{\delta p}{\delta y}$
or $\frac{\delta p}{\delta y} = -\tan \eta \frac{\delta p}{\delta x}$
b.c. 1
$\frac{\delta p}{\delta y} = 0$
$\frac{\delta p}{\delta x} = 0$
b.c. 2
A
B
$\frac{\delta p}{\delta x} = -\text{ctn } \eta \frac{\delta p}{\delta y}$
$\frac{\delta p}{\delta x} = 0$
b.c. 3
$P_A = P_B$

Figure 2.6 (b) APPROXIMATING BOUNDARY CONDITIONS

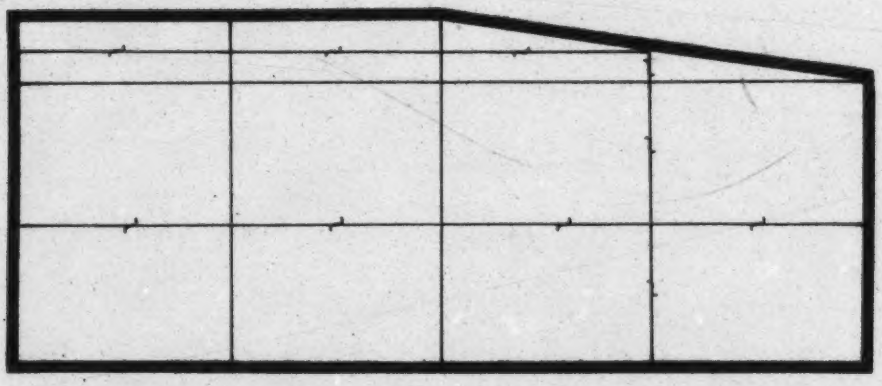

Figure 2.6 (c) FINITE ELEMENT GRIDS

Figure 2.6 SLOPED CEILING REVERBERATION CHAMBER

Table 2.1 CONVERGENCE OF FOUR LOWEST EIGENVALUES FOR SLOPED CEILING REVERBERATION CHAMBER

Segmentation of Sloped Edge (No. of Parts)	Corresponding (x,y,z) Mode Shape to That for a Rectangular Room			
	(0,0,1)	(1,0,1)	(2,0,1)	(0,1,1)
1	.02039	.03274	.06710	.08987
2	.01976	.03215	.06766	.09128
3	.01992	.03202	.06724	.09027
Exact Results for 22 x 29 x 12 Rect. Room	.02040	.03212	.06730	.08895

in terms of the overall acoustical kinetic and strain matrices. Method 3 could converge to the exact result, but it entails larger partitioning operations on the overall matrices (described in Appendix C2) and is therefore more prone to numerical divergence. If looked at from a potential energy viewpoint, 1 and 2 are respectively slightly weaker and slightly stronger than the correct boundary condition 3 giving respectively lower and higher eigenvalues than 3 for any particular grid configuration. Since the approximate solution converges on the exact solution from above, it was deemed interesting to see the effect on convergence of using boundary condition 1. Because of its "relaxing" effect on the overall energy matrices, it is reasonable to assume that for a relatively coarse grid pattern, boundary condition 1 will give eigenvalues closer to the exact solution than a finer grid using the other boundary conditions. The concept of "flexibility" of a system is quite often used to describe deviation from classical results. A more flexible system has less ability to store strain energy and thereby results in a lower natural frequency.

Grid patterns for the coarse grid and refined grid are shown superimposed on one another in Fig. 2.6 (c). There were other grids used including a finer one that divided the sloped surface into three equal sections, but these would only complicate the figure given. The effect of boundary condition 1 is most exemplified for the coarse grid where the entire slope edge has the "relaxed" boundary condition. For computational convenience c, the velocity of sound, was taken as unity.

By close examination of each column of Table 2.1 it is easily

seen that the results for the slope ceiling room are very close to the exact solution for a hard rectangular room that would bound the reverberation room. This is logical since the reverberation room does not deviate much from the classical rectangular form. Column one shows the (0, 0, 1) mode, which is independent of the actual profile of the room, and should therefore converge exactly to the classical result. In accordance with the energy approximation method, the results actually start higher than the correct value, drop below, then start upwards again. This can be explained by the "flexibility" of the structure; the more "flexible" the structure, the lower the eigenvalues. Initially the grid was not flexible enough to approximate the mode shape, but after the first refinement the structure became overly flexible because of b.c. 1. Ensuing refinement would lead to closer convergence because the system has sufficient flexibility to closely approximate the mode shape, while each further subdivision of the sloped ceiling lessens the effect of b.c. 1 (until one enters the region where numerical errors become significant). Similar analysis can be done on the remaining three columns, noting that the sloped roof has almost no effect on the (x, 0, 1) modes but is quite important in the (0, y, 1) modes.

Figures 2.7 through 2.9 show the principal mode shapes of three rooms of different dimension but with the same basic shape. The (a) figures are the actual profiles for the reverberation chamber, whereas the (b) and (c) figures show the changes due to substantially increasing the effect of the sloped wall on the x-direction and x-y directions, respectively. The points of no pressure variation

within the room are of importance when making sound measurements. For a hard rectangular room the zero-pressure nodal line occurs at positions that are simple fractions of the overall dimension, i.e. 1/2, 1/3, etc. Figure 2.7 shows how the zero-pressure node line deviates from the classical position for a rectangular room. The narrowing of the enclosure at one end changes the volume distribution as well as causing localized compression and rarefaction of the sound wave near the roof. A wave travelling in the x-direction, is given an unbalanced y-component of force, tending to bend it into a path where uniform compression (or rarefaction) occurs on both ceiling and floor. In Fig. 2.7 the reflection off the narrow end wall, floor and ceiling, at non-zero angles of incidence, causes "focusing" of the pressure waves in the lower right-hand corner of the room, giving maxima in pressure levels in this region.

Figure 2.8 is actually very similar to Fig. 2.7 except there are now two node lines, i.e. two maxima and a minima, that are substantially affected by the sloped roof. It is interesting that the maxima along the full height wall in Fig. 2.8 moves from the lower left to upper left corner as the slope angle of the roof, η, becomes more than 45°. Figure 2.8 (c) has a higher eigenvalue than Fig. 2.9 (c) so it could be said that the diagram ordering is incorrect, but it is of greater interest to show the development of a mode shape.

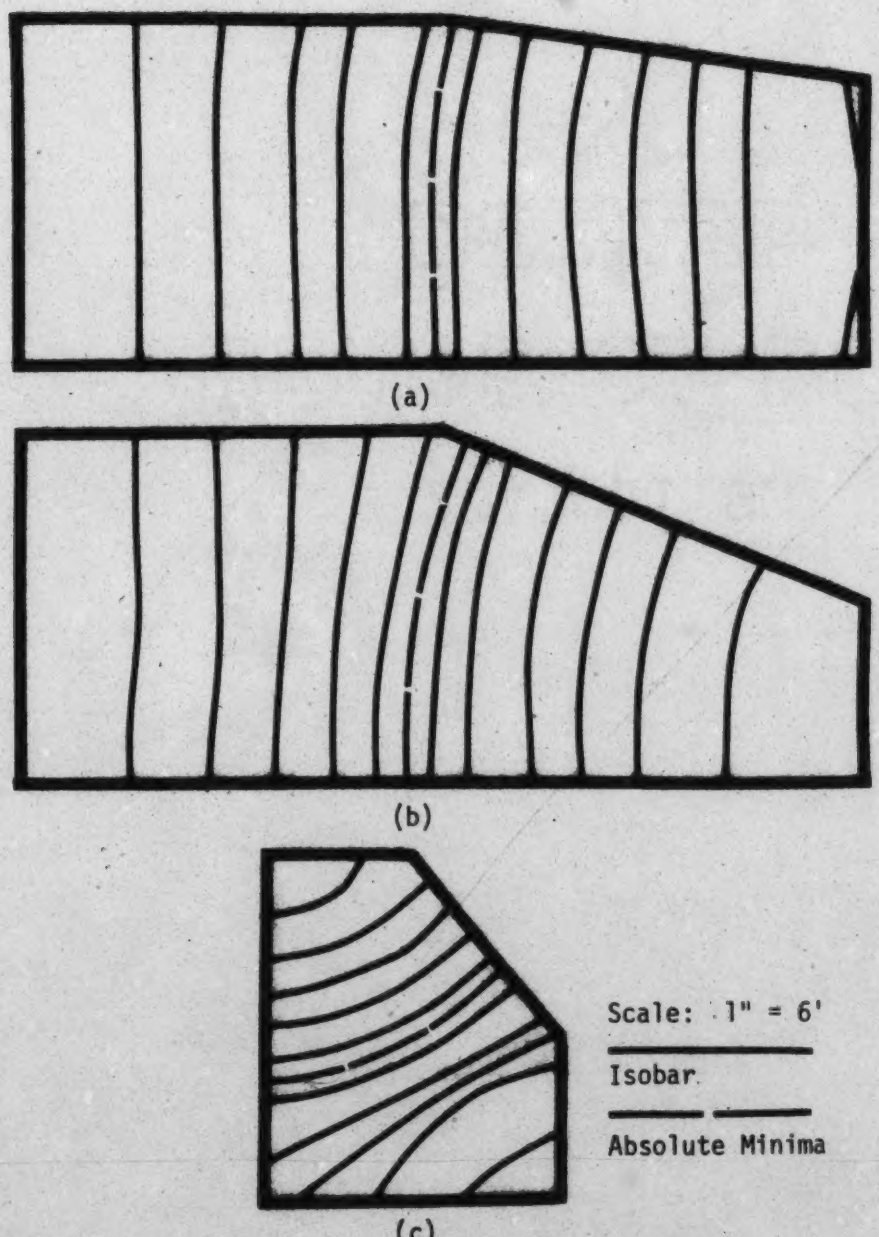

Figure 2.7 FIRST MODE - ROOMS WITH SLOPED CEILING

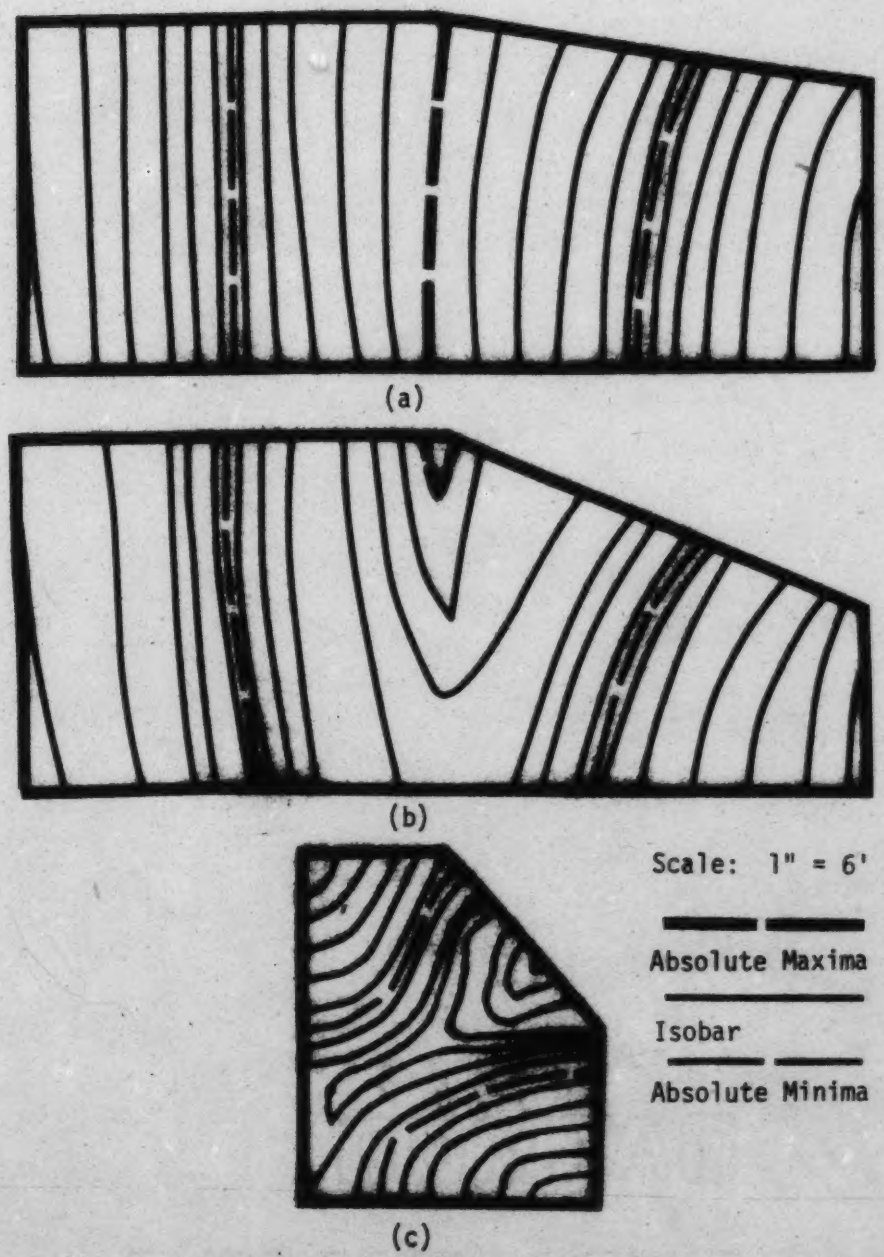

Figure 2.8 SECOND MODE - ROOMS WITH SLOPED CEILING

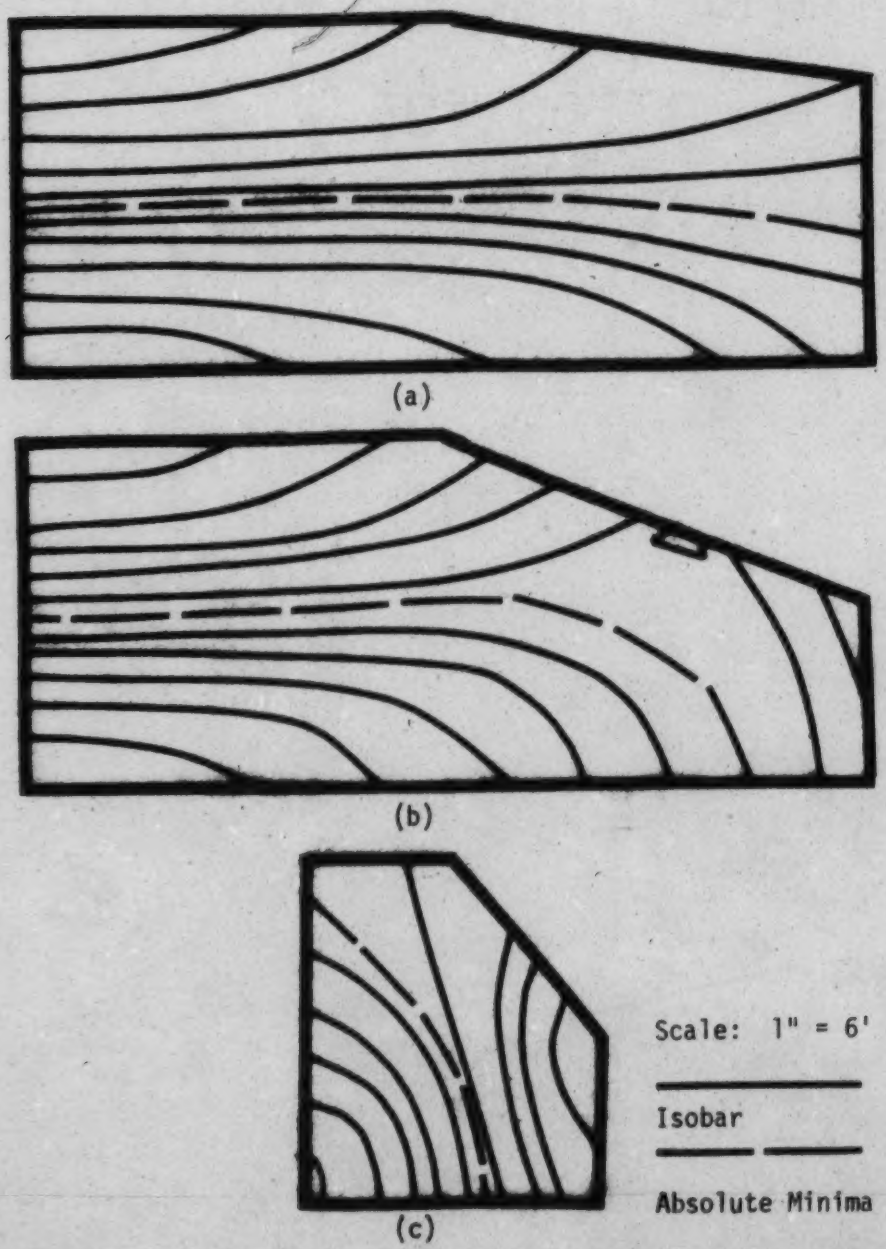

Figure 2.9 THIRD MODE - ROOMS WITH SLOPED CEILING

CHAPTER III

COUPLED ELEMENTS

The elements produced thus far have their independent applications, but have not yet been intercoupled, i.e. a displacement of the plate must cause a pressure change in the fluid and vice versa.

3.1 The Coupling Matrix

Former work by Warburton [26] and Pretlove [27] approached coupling by using the exact acoustic equation with a normal mode representation of the plate. Zimmerman and Gladwell [28] did a very complete treatment of coupled plate-acoustic systems, but encountered difficulties because they formulated the acoustic and plated elements entirely in terms of displacement or force quantities which, if nothing else, cause conceptualization problems. Using the pressure acoustic formulation and the displacement plate formulation described by Mason [29, 30] and the coupling concept advanced by Craggs [31], the ensuing formulation is easily conceptualized and relatively efficient.

To satisfy equilibrium, the forces due to the flexed panel and the pressure distribution over the surface area of the plate must be conserved. Terms whose first variation satisfies the boundary condition at the interface must be included in the respective functionals. This boundary condition is simply that the normal velocity of the fluid must be the same as the transverse velocity of the plate over the entire plate surface

$$\dot{w} = \underline{\dot{u}} \cdot \vec{n}$$

where $\underline{\dot{u}} \cdot \vec{n}$ is the normal velocity component of the fluid. By differentiating with respect to time and using equations (A8) and (A11)

$$\text{grad } p_1 \cdot \vec{n} = -\rho \ddot{w}_p = -\rho \text{ grad } \dot{\phi} \cdot \vec{n} \qquad (3.1)$$

where ρ is the acoustic density and ϕ, of course, is the velocity potential. Recalling the form of the acoustic functional, and adding to it a term whose first variation with respect to ϕ satisfies the dynamic boundary condition

$$J = \int_{t_1}^{t_2} \frac{\rho}{2} \left[\iiint_V \{\text{grad } \phi \cdot \text{grad } \phi - \frac{\dot{\phi}^2}{c^2}\} \, dV \right.$$

$$\left. - \iint_{S_c} \rho \, w_p \dot{\phi} \, dS_c \right] dt$$

where S_c is the interface surface. This last term can be physically interpreted as the pressure displacement work, B_a, at the coupling interface

$$B_a = -\iint_{S_c} \rho \, \dot{\phi} \, w_p \, dS_c = +\iint_{S_c} p_1 w_p \, dS_c \qquad (3.2)$$

It must have a stationary value and satisfy the dynamic boundary conditions. This can easily be seen by following the procedure of Appendix A3 including the extra term.

The energy added to (or extracted from) the acoustic element in the form of work, must come from (or go to) the adjacent plate element. Therefore, the work term must occur in the energy equations for the plate, but with the opposite sign. External forces, other than the acoustic pressure, can act on the plate elements but they will be excluded from this study because it is the free vibration problem which is of interest.

To form the coupling matrix proper, Θ, it is now necessary to recall the approximations for pressure and displacements used in Chapter II.

$$p_e = \{f(x^*)\ f(y^*)\}^T \{p_n\} \cos \frac{n\pi z}{d} \tag{3.3}$$

where

$$x^* = x/a$$

$$y^* = y/b$$

for the rectangular acoustic elements

$$p_e = \{g(x',y')\}^T \{p_n\} \cos \frac{n\pi z}{d} \tag{3.4}$$

where

$$x' = \frac{(\varepsilon + b)}{(a + b)}$$

$$y' = \frac{\eta}{h}$$

for the triangular acoustic element. Note the coordinate system indicated here is the localized system because this will be the system

the plate will be associated with initially.

$$w_p = \{f(\ell^*)\}^T \{w_n\} \sin \frac{k\pi z}{d}$$

where

$$\ell^* = \frac{\varepsilon}{\ell_p} \qquad 0 \le \varepsilon \le \ell_p$$

Depending on the element to be coupled to the plate element, one of the two pressure approximations will be used. The pressure formulation for the rectangular acoustic elements will be used in the following excursion because the experiments and examples to follow are based on this element.

$$B_a = \iint_{S_c} p_1 w_p \, dS_c$$

For this example, assume that the line plate element is coupled to edge 1 - 3 of Fig. 2.1 (a) where y and y* are identically zero. Also, $\ell^* = x^*$ and $\varepsilon = x$, respectively. So

$$B_a = \{p_n\}^T \left[\int_0^1 \{f(x^*)\ f(0)\} \{f(x^*)\}^T dx^* \ell_p \right.$$

$$\left. \cdot \int_0^d \cos \frac{m\pi z}{d} \sin \frac{k\pi z}{d} \, dz \right] \{w_n\}$$

where Θ_{rect} is the integral within the square brackets.

The integrals with respect to x* can be found in Appendix B2, while the integrals with respect to z are in Appendix B1.

Careful examination of Appendix B1 shows that the integrals are taken over one-half harmonic interval. This alters the orthogonality of the sine - cosine product from the standard full interval form of Fourier [32], whereas the sine - sine and the cosine - cosine product integrals are unchanged. It is obvious then when n + q is an even sum of integers, there is no coupling integral produced by this method. This would tend to indicate that in the z-direction an odd order acoustic mode would be driving an even order plate mode or vice versa. This is readily explained in such a coupling situation because for n + q = even integer, the net p - v work is zero giving an unexcitable configuration.

The integrals with respect to x* (y* = 0) were for coupling for side 1 - 3 of the rectangular element. These integrals will alter when another edge of the element is used, i.e. y* = 1, x* = 0 or x* = 1 but all can be handled by the aforementioned Appendices. The coupling formulation for a triangular acoustic element is the same; substitute (3.4) and (3.5) in equation (3.2) and multiply out the entries of matrices for a surface. Because of the random orientation in the x - y plane of any edge, it is exceedingly difficult to do the ensuing line integrals. It is initially chosen that the surface to be coupled, is co-incident with the localized x-axis, as shown in Fig. B1. The integration can then be performed with relative ease as a form of

$$(a + b) \int_0^1 x^{*m} f(x^*)\, dx \qquad m = 0, 1, 2, 3$$

$$x^* = \frac{x + a}{a + b}$$

These integrals can be done by hand (some of which are shown in the latter parts of Appendix B2). The resulting localized coupling matrix Θ'_{TRI} must be rotated by pre-multiplying by an acoustic rotational matrix $[\theta]_a$ and post-multiplying by a plate rotational matrix $[\theta]_p$ before it can be placed in the overall coupling matrix.

$$[\Theta_{TRI}] = [\theta]_a^T [\Theta'_{TRI}] [\theta]_p$$

This completes the formulation of the coupling matrix. Including the present discussion, the coupled energy functionals J_a and J_p, for the overall system can be written from equations in Appendix A4 and Chapter 2, Section 4.

$$J_a = \int_{t_1}^{t_2} \left\{ \frac{\rho_a}{2}^2 \{\phi\}^T [S] \{\phi\} + \frac{\rho_a}{2}^2 \{\dot{\phi}\}^T [P] \{\dot{\phi}\} - \rho_a \{\dot{\phi}\}^T [\Theta] \{w_p\} \right\} dt$$

$$J_p = \int_{t_1}^{t_2} \left\{ \frac{1}{2} \{\dot{w}_p\}^T [M] \{\dot{w}_p\} + \frac{1}{2} \{w_p\}^T [K] \{w_p\} \right.$$

$$\left. + \rho_a \{\dot{\phi}\}^T [\Theta] \{w_p\} \right\} dt$$

Noting that $p = \rho \dot{\phi}$

By taking the first variation of both functionals (the first with respect to ϕ and the second with respect to w_p) and equating them to zero, the coupled equations of motion can be arrived at. To give more physical significance to $\delta J_a = 0$, this functional variation should be differentiated with respect to time and the pressure formulation substituted. Then,

$$[P]\{\ddot{p}\} + [S]\{p\} - [\Theta]\{\ddot{w}_p\} = 0 \tag{3.6}$$

$$[M]\{\ddot{w}_p\} + [K]\{w_p\} + [\Theta]^T\{p\} = 0 \tag{3.7}$$

These equations of motion are for a coupled plate-acoustic system with no external force $\{\bar{F}\}$ acting on the plate elements. These external forces could be included by simply placing them in nodal form on the right hand side of (3.7). $\{p\}$ and $\{w\}$ can take any time function desired, so random vibration studies could easily be undertaken. A finite difference approach could be used for stepping through time.

Since this is a steady-state study, this discussion will not be pursued. Equations (3.6) and (3.7) can be written in a more compact matrix form

$$\left\{\begin{bmatrix} K & \Theta^T \\ 0 & S \end{bmatrix} - \omega^2 \begin{bmatrix} M & 0 \\ -\Theta & P \end{bmatrix}\right\} \begin{Bmatrix} w_p \\ p \end{Bmatrix} = 0$$

where the steady-state time function has been considered to have a frequency ω. The square brackets around the entries have been dropped for

convenience. This equation can be used in eigenvalue solutions but the matrices are unsymmetric, therefore, computation becomes tedious even by numerical methods. Irons [33] advanced an approach that makes these matrices symmetric. By partitioning the matrices and performing some basic matrix operations giving

$$\left\{\begin{bmatrix} K & 0 \\ 0 & P \end{bmatrix} - \omega^2 \begin{bmatrix} M + \theta S^{-1}\theta & -\theta^T S^{-1} P \\ -PS^{-1}\theta & PS^{-1}P \end{bmatrix}\right\} \begin{Bmatrix} w_p \\ p \end{Bmatrix} = 0$$

The result is symmetric due to the symmetry of M, K, P and S. This approach is not exactly suitable to this situation, as the M, K matrices are of the order of one-tenth the size of the S, P matrices. To do the inversion of the S matrix would therefore be exceedingly time consuming, not to mention inaccurate (because of the small values of the entries in the matrix). Instead, the M matrix was inverted and Iron's basic procedure was followed giving

$$\left\{\begin{bmatrix} KM^{-1}K & KM^{-1}\theta^T \\ \theta M^{-1}K & S + \theta M^{-1}\theta^T \end{bmatrix} - \omega^2 \begin{bmatrix} M & 0 \\ 0 & P \end{bmatrix}\right\} \begin{Bmatrix} w_p \\ p \end{Bmatrix} = 0$$

which again is symmetric and can be used for the eigenvalue problem more simply than its unsymmetric counterpart.

Initial checks were done on a simple coupled system; a cubical room with one flexible boundary (as shown in Fig. 3.1). To simplify things even further the flexible boundary was made almost rigid (i.e. plate eigenvalues are well above acoustic eigenvalues)

so as to deviate only slightly from the exact rigid room case. The computed results of the rigid boundaried room and the room with one slightly flexible boundary, are shown in Table 3.1, along with the exact results for a "rigid" room. The acoustic element is the same grid for both computed cases.

There are two noteworthy items in the results. First, when searching for an exact zero eigenvalue, the IBM eigenvalue - eigenvector routine NROOT sometimes gives a negative result. This is unrealistic for the positive definite problems for which this numerical method is designed. These negative roots must be considered as a measure of the numerical error in the calculations. Secondly, in all cases, the eigenvalues are lowered by the introduction of the slightly flexible wall. Considering only the acoustic equation of motion, this would indicate a slight increase in the potential energy (associated with [P] matrix) with no effective change in the kinetic energy.

$$\omega_a^2 = \frac{\{\psi\}^T[S]\{\psi\}}{\{\psi\}^T[P]\{\psi\}}$$

where $\{\psi\}$ is a principal mode shape.

From this point on it can be said that there are no further independent plane modes, i.e. (x, 0, 0), (0, y, 0), (0, 0, z) modes. This is indicated by the reduction of eigenvalues (square of natural frequency) for cases in which the plane wave is parallel to the flexible boundary. It can also be shown by inspection of the plate eigenvectors, which show deflected plate positions for the above mentioned case. The independent plane wave notation will still be used in

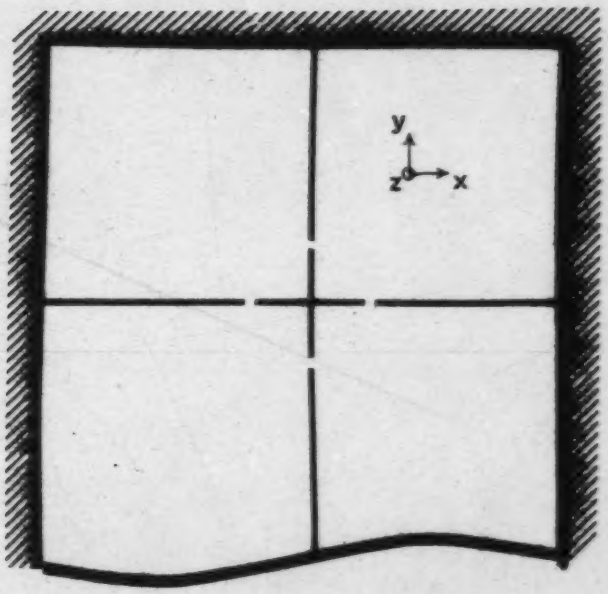

Figure 3.1 TEST ACOUSTIC MODEL

Table 3.1 RESULTS OF TEST MODEL

Equivalent Acoustic Mode (x,y,z)	Eigenvalues for a Rigid Room		Eigenvalues for Test Model
	Exact	Calculated	
(0,0,0)	0	-.000000	-.00141
(0,1,0)	9.86960	9.872300	9.70643
(1,0,0)	9.86960	9.872320	9.86831
(1,1,0)	19.73921	19.950510	19.93450
(0,2,0)	39.47842	39.529200	38.77500
(2,0,0)	39.47842	39.529300	39.52610
(1,2,0)	49.34802	49.401200	49.22090
(2,1,0)	49.34802	49.401300	49.36150
(2,2,0)	78.95684	79.058300	78.72000

following discussions, but only for descriptive purposes.

3.2 Sound Transmission Between Panel Coupled Rooms

The culmination of all foregoing work would be applicable in the study of plate-acoustic systems such as general floor areas (with a rigid floor and ceiling) enclosed by or containing flexible floor-to-ceiling panels. This is reasonably broad, and therefore the simple case of direct sound transmission between two rectangular rooms through a variable width floor-to-ceiling panel was carefully analyzed and checked. The widths of the rooms were left unchanged but the length of one room was altered. An experimental apparatus was constructed to approximate the theory. All "rigid" surfaces were made of 3/4 inch fir plywood capped on the inside surfaces with 1/8 inch masonite. A 4 inch speaker was attached to the source room, acoustically exciting the interior of the room through an orifice. Precision oscillators, frequency counters and pressure amplitude monitors were used to measure the standing wave patterns within the receiving and source rooms. The source room had fixed dimensions of 7 inches x 19 inches x 23 1/2 inches depth, while the receiving room had similar cross-sectional dimensions but of variable depth. The components of the apparatus are shown in Fig. 3.2 (a). Figure 3.2 (b) shows the "driver" for the source room as well as the basic hard wall construction of the rooms. Figure 3.3 shows the basic layout of equipment.

Detail "A" in Fig. 3.3 shows the mounting frame for the flexible plate. To approximate a zero deflection boundary condition, a length of 1/2 inch x 1/2 inch aluminum bar stock was accurately machined to

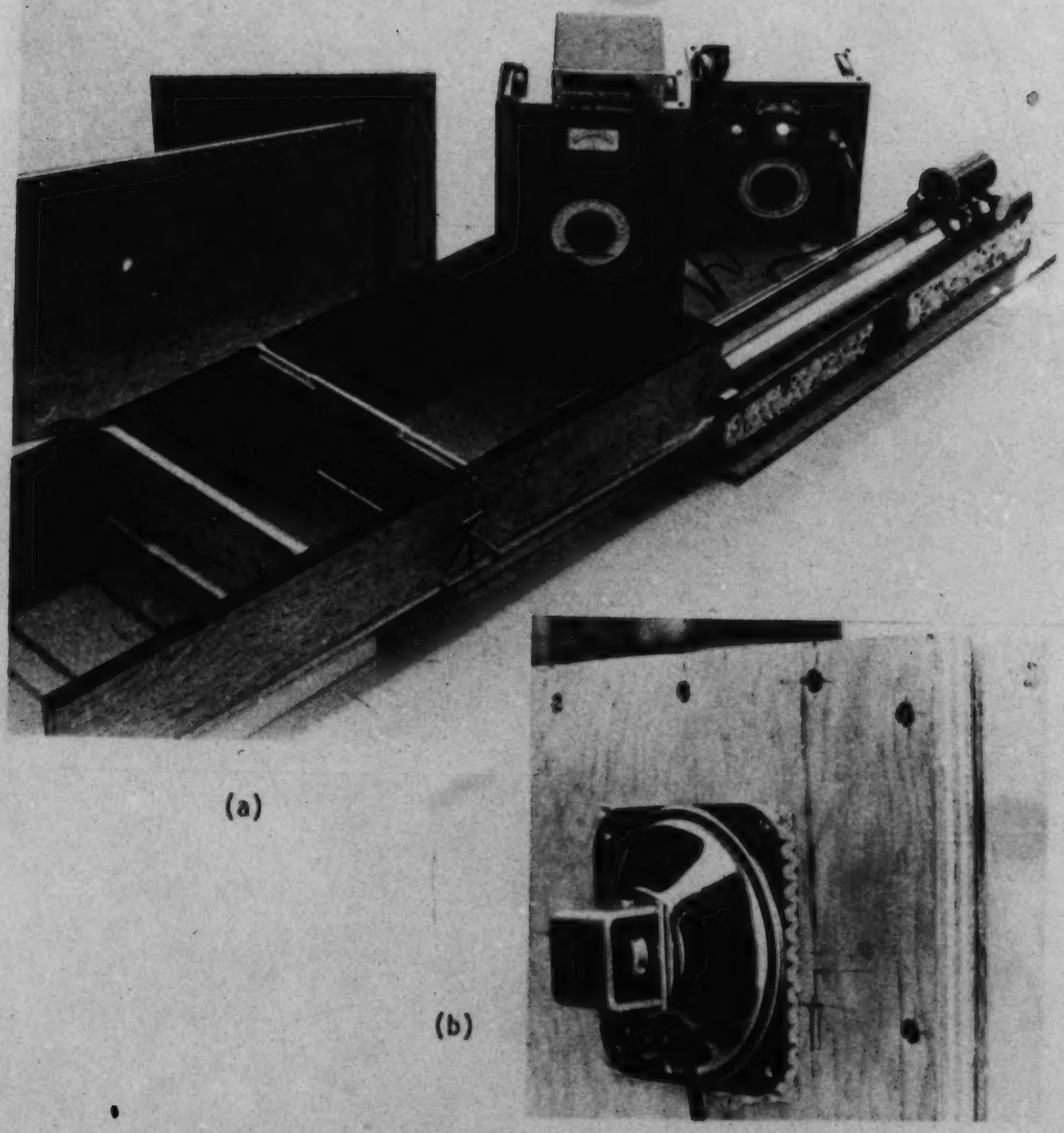

(a)

(b)

Figure 3.2 EXPERIMENTAL APPARATUS

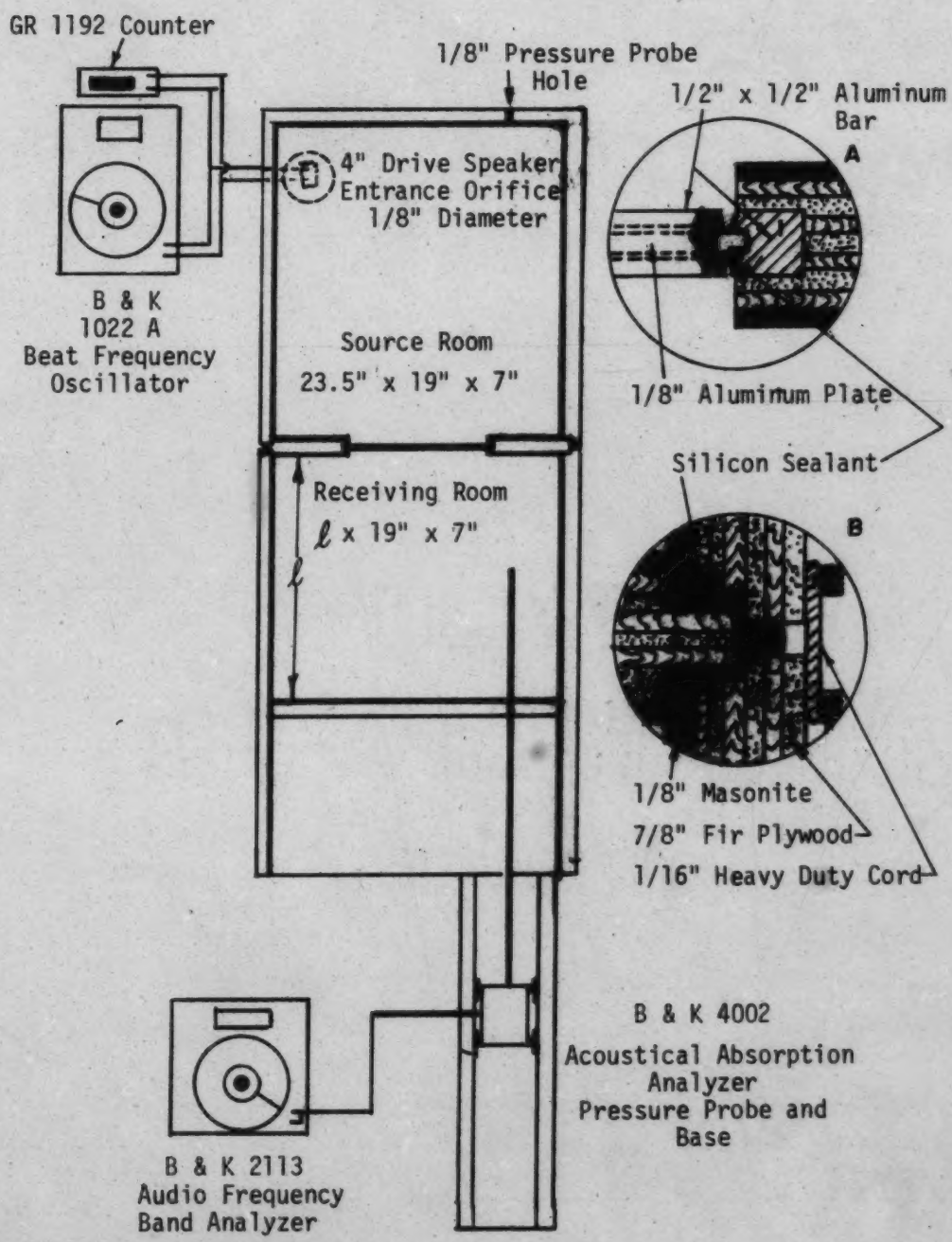
GR 1192 Counter
1/8" Pressure Probe Hole
1/2" x 1/2" Aluminum Bar
A
4" Drive Speaker Entrance Orifice 1/8" Diameter
B & K 1022 A Beat Frequency Oscillator
Source Room 23.5" x 19" x 7"
1/8" Aluminum Plate
Silicon Sealant
Receiving Room ℓ x 19" x 7"
ℓ
B
1/8" Masonite
7/8" Fir Plywood
1/16" Heavy Duty Cord
B & K 4002 Acoustical Absorption Analyzer Pressure Probe and Base
B & K 2113 Audio Frequency Band Analyzer

Figure 3.3 PICTORIAL LAYOUT OF COMPONENTS

accept all edges of a 1/8 inch aluminum plate to a depth of 1/16 inch. To assure no air leaks, the bar was carefully fitted to the rigid plywood wall and silicon sealant was used at all connections. Though not shown, the upper and lower bar stock rails were also fitted to the upper and lower panel with sealant. A well defined fixed or pinned boundary condition is not feasible by this construction. It was, therefore, necessary to give both the fixed and pinned analytical result.

Detail "B" is the edge connection between the rooms. Firstly, the rigid interior wall (or aluminum frame, depending on the flexible panel's width) was completely sealed to stop air leakage from one enclosure to another. The sealant and the saw cut isolated either room from structure-borne vibrations in the exterior walls of the other room. This eliminated a large amount of flanking transmission through the exterior boundaries which are not ideally hard. The cord binding, used to align the rooms and accurately seal the boundaries, was sufficiently limp to transmit a minimum amount of vibration. As will be seen in later results, this isolation was ineffective, in a few cases, but on the whole was very satisfactory.

On a more general scale, the entire apparatus was isolated from the laboratory tables by 3 inch foam mats. All boundaries where leaks could occur were either caulked and glued or temporarily caulked with silicon sealant. The holes for the pressure probe were sealed with brass plugs when not being used directly in tests.

It is of note that the various plates were chosen so that their fundamental modes were between 300 H_z and 500 H_z, which is well

within the range of the first few acoustic modes of either room, i.e. the plane standing wave parallel to the plate surface in the y-direction was 355 H_z.

3.2.1 Theoretical Considerations

To obtain accurate values of ρ_p (plate density) and c (velocity of sound), careful measurements were made in the test laboratory. They are, respectively

$$\rho_p = .003217 \text{ slug/in}^3 \quad \text{(for aluminum)}$$

$$c = 13{,}560 \text{ in/sec}$$

Other constants were accepted at their textbook values

$$\rho_a = 1.376 \times 10^{-6} \text{ slug/in}^3$$

$$E = 10.3 \times 10^6 \text{ lbf/in}^2 \quad \text{(for aluminum)}$$

$$\nu = 1/3 \quad \text{(for aluminum)}$$

These measurements proved to be valuable because the errors associated with published constants are of the same order as the errors due to the finite element approximation.

3.2.2 Results

The description of results is broken into two parts:

i) Effect of changing panel area and stiffness on unchanged room volumes.

ii) Effect of changing length of receiving room on unchanged source room and panel.

Figure 3.4 through Fig. 3.8 are the five lowest non-zero modes for identical source and receiving rooms. Each of the diagrams in any given figure shows a different panel stiffness and surface area. These panels represent 100 per cent, 73.7 per cent and 42.5 per cent of the coupling wall, respectively. Because the rooms are symmetric about the panel, the principal mode shapes are symmetric, therefore, only one half of the mode shape will be plotted. The positive and negative signs indicate the relative pressures and rarefactions at any given instant. This particular configuration would be equivalent to being on the lines designated as "B" on Fig. 3.13 through Fig. 3.15.

These principal mode shapes can be roughly divided into acoustically and panel dominant types. The acoustically dominant modes are characterized by mode shapes and natural frequencies fairly close to the classical acoustic cases for a hard room. Figure 3.4 is an example of this type of mode. Figure 3.6 shows a panel dominant mode shape which has a natural frequency closely related to the "in vacuo" response for the panel and a highly disturbed acoustical mode shape. For each panel dominant mode there are two acoustical dominants.

Further inspection of the mode shapes show that the nodal lines (zero pressure lines) have moved towards the flexible panel for the acoustically dominant modes and away from the panel for the panel dominant mode. This can be explained in terms of "mass" and

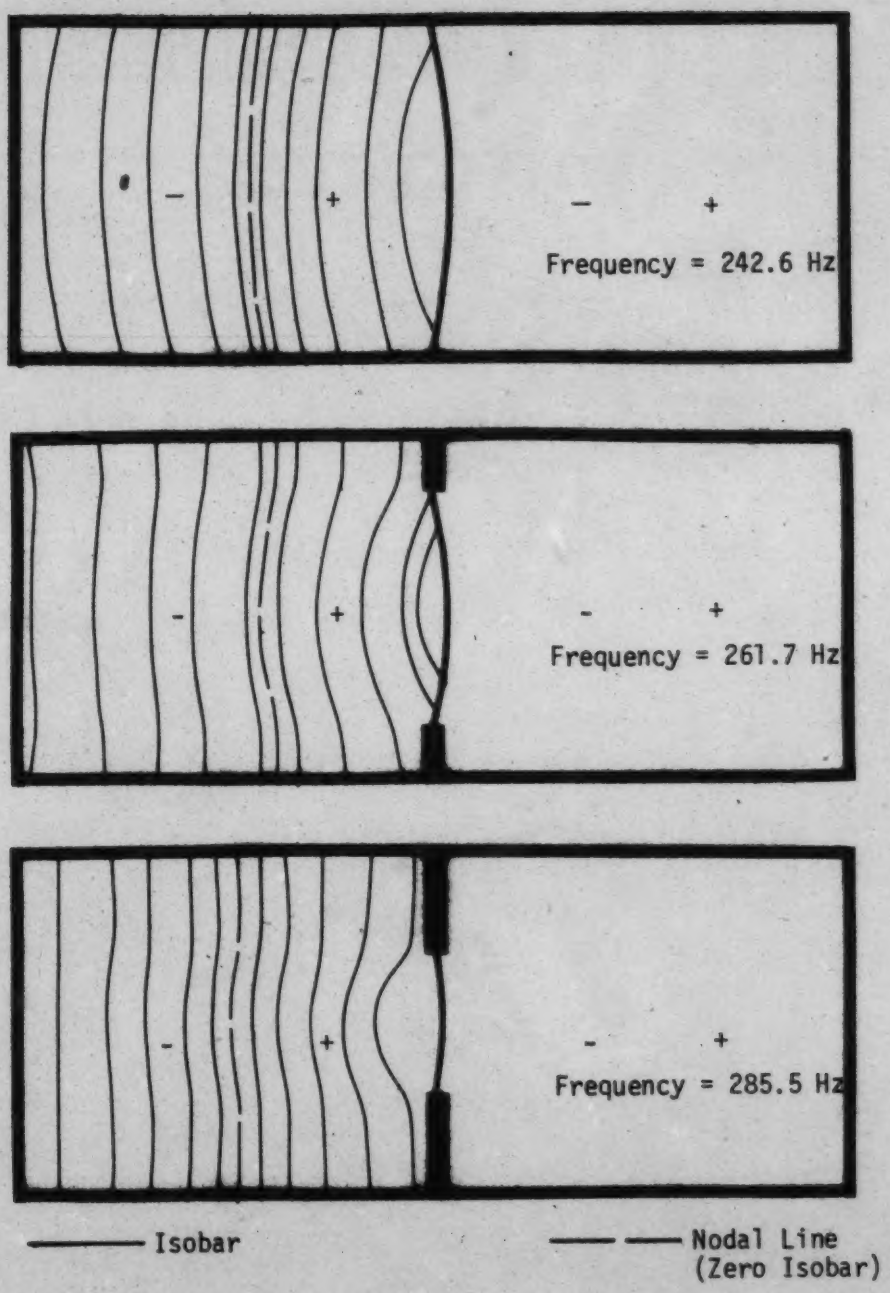

Figure 3.4 FIRST MODE - SOUND TRANSMISSION
BETWEEN SYMMETRIC ROOMS

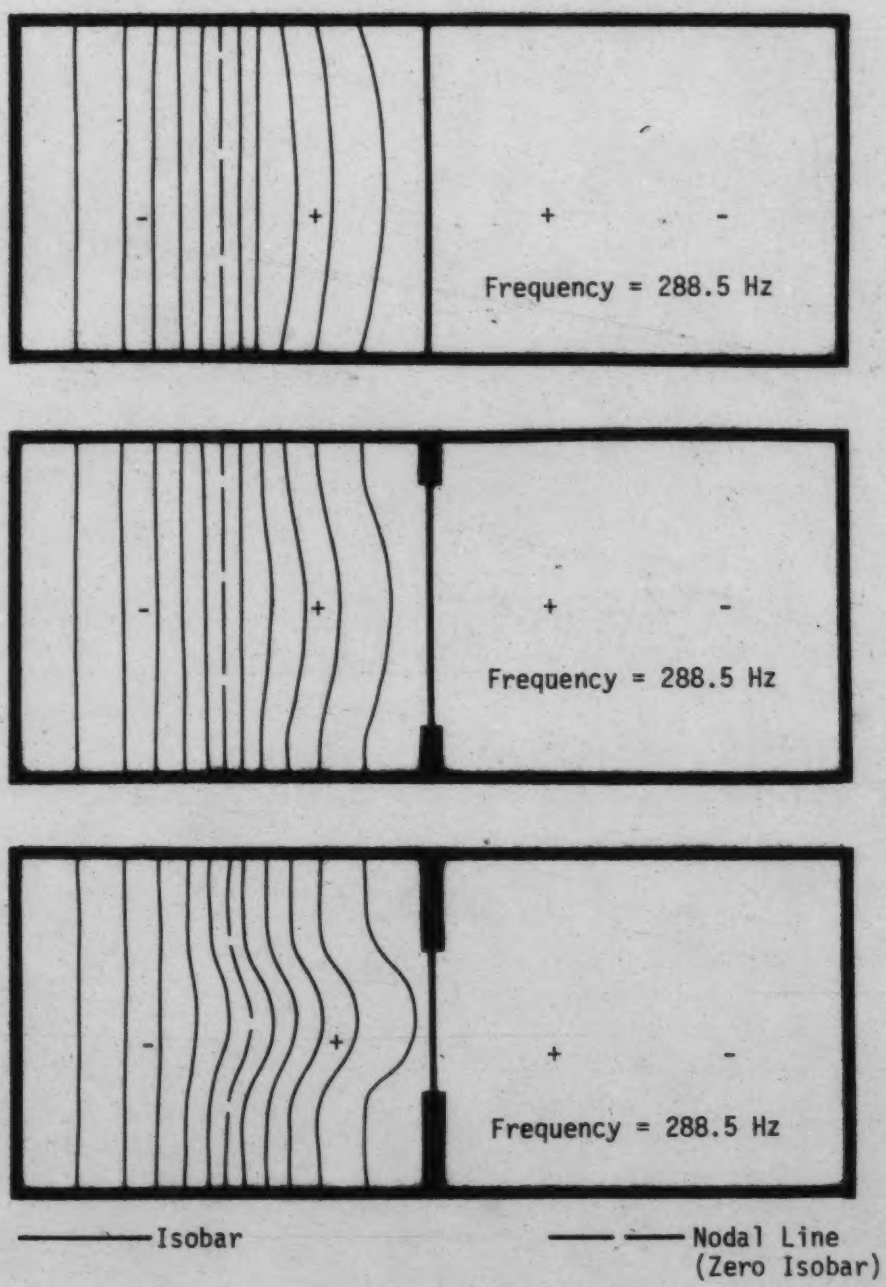

Figure 3.5 SECOND MODE - SOUND TRANSMISSION
BETWEEN SYMMETRIC ROOMS

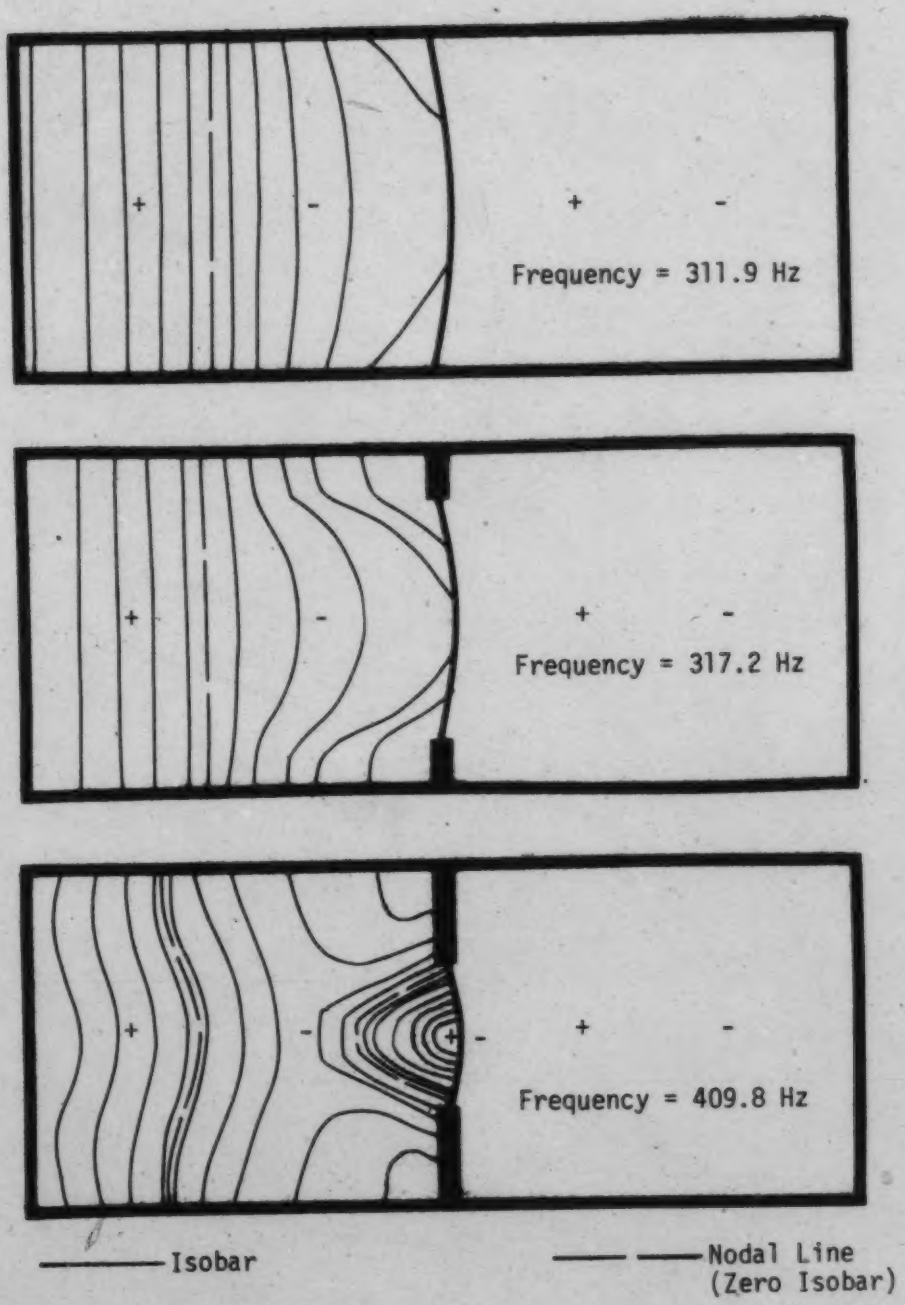

Figure 3.6 THIRD MODE - SOUND TRANSMISSION
BETWEEN SYMMETRIC ROOMS

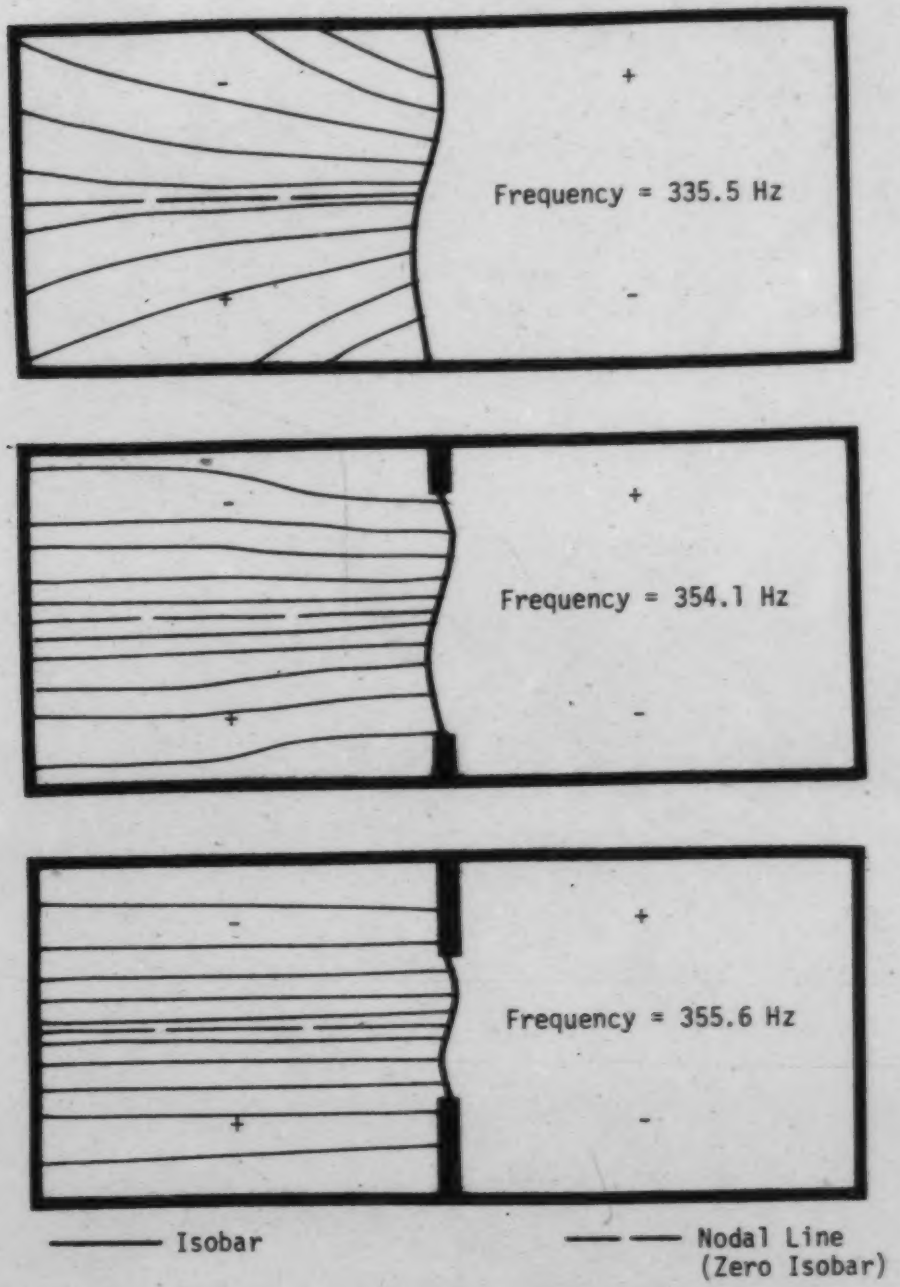

Figure 3.7 FOURTH MODE - SOUND TRANSMISSION BETWEEN SYMMETRIC ROOMS

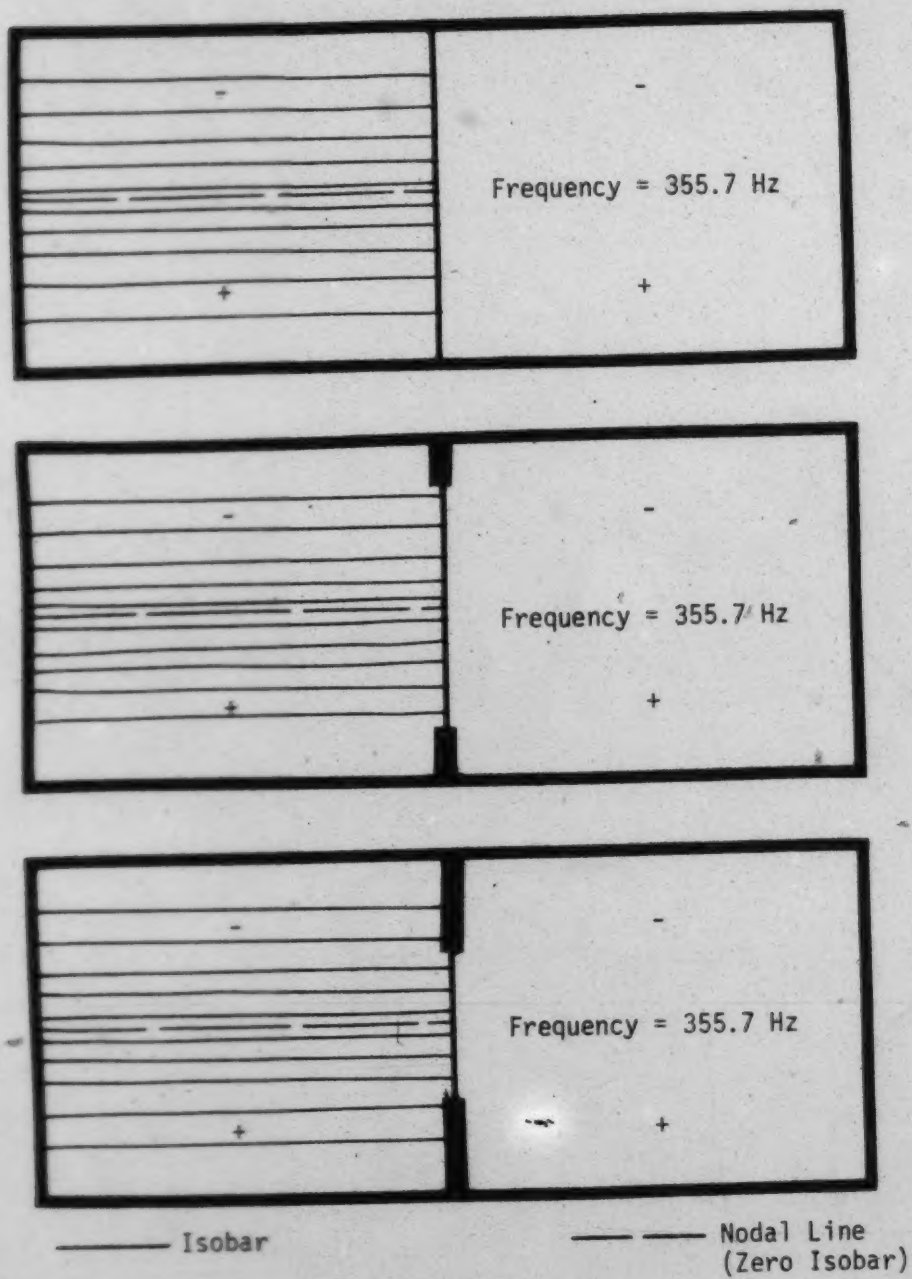

Figure 3.8 FIFTH MODE - SOUND TRANSMISSION
BETWEEN SYMMETRIC ROOMS

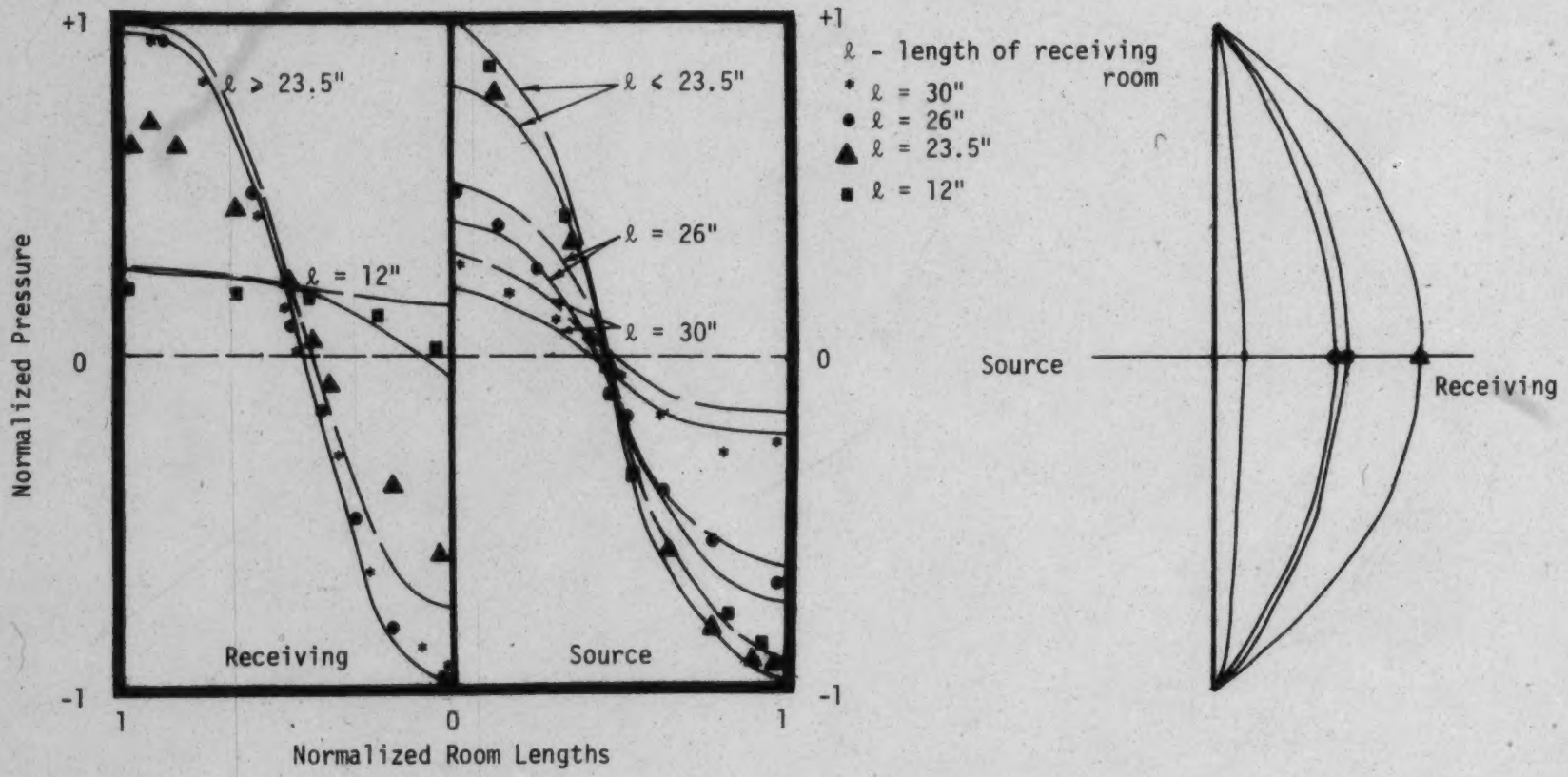

Figure 3.9 FIRST MODE - NORMALIZED LONGITUDINAL PRESSURE VARIATION AND PLATE DISPLACEMENT

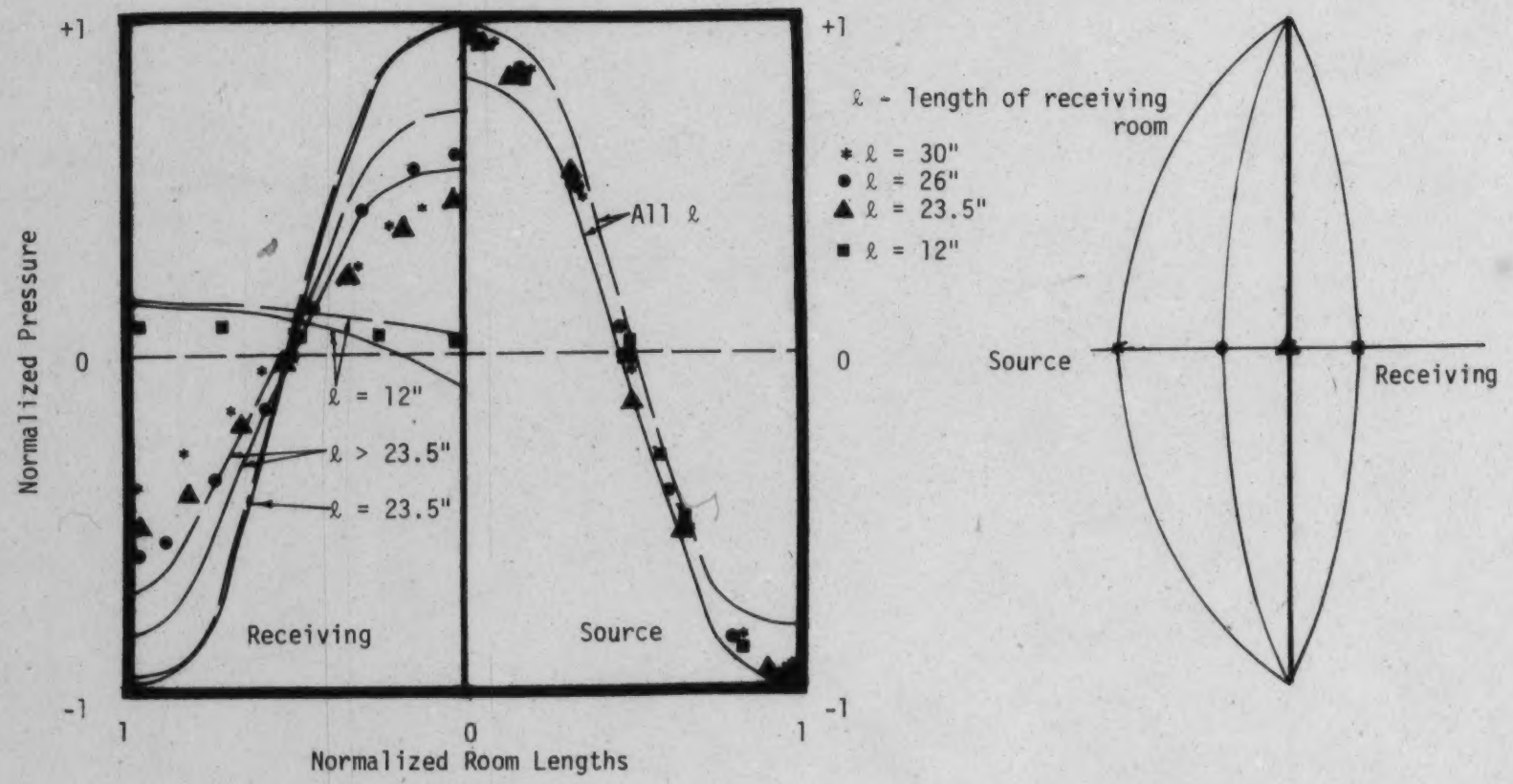

Figure 3.10 SECOND MODE - NORMALIZED LONGITUDINAL PRESSURE VARIATION AND PLATE DISPLACEMENT

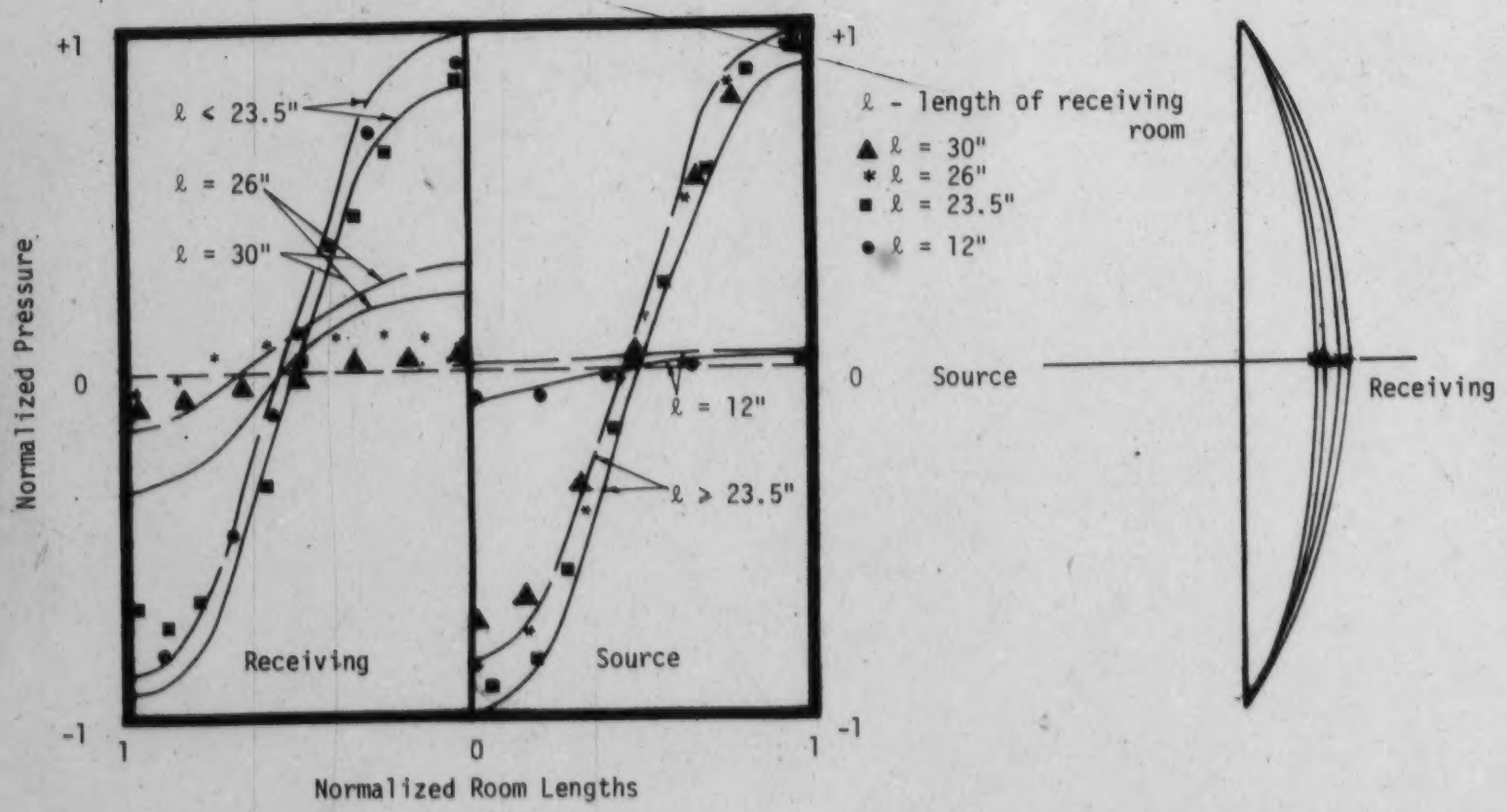

Figure 3.11 THIRD MODE - NORMALIZED LONGITUDINAL PRESSURE VARIATION AND PLATE DISPLACEMENT

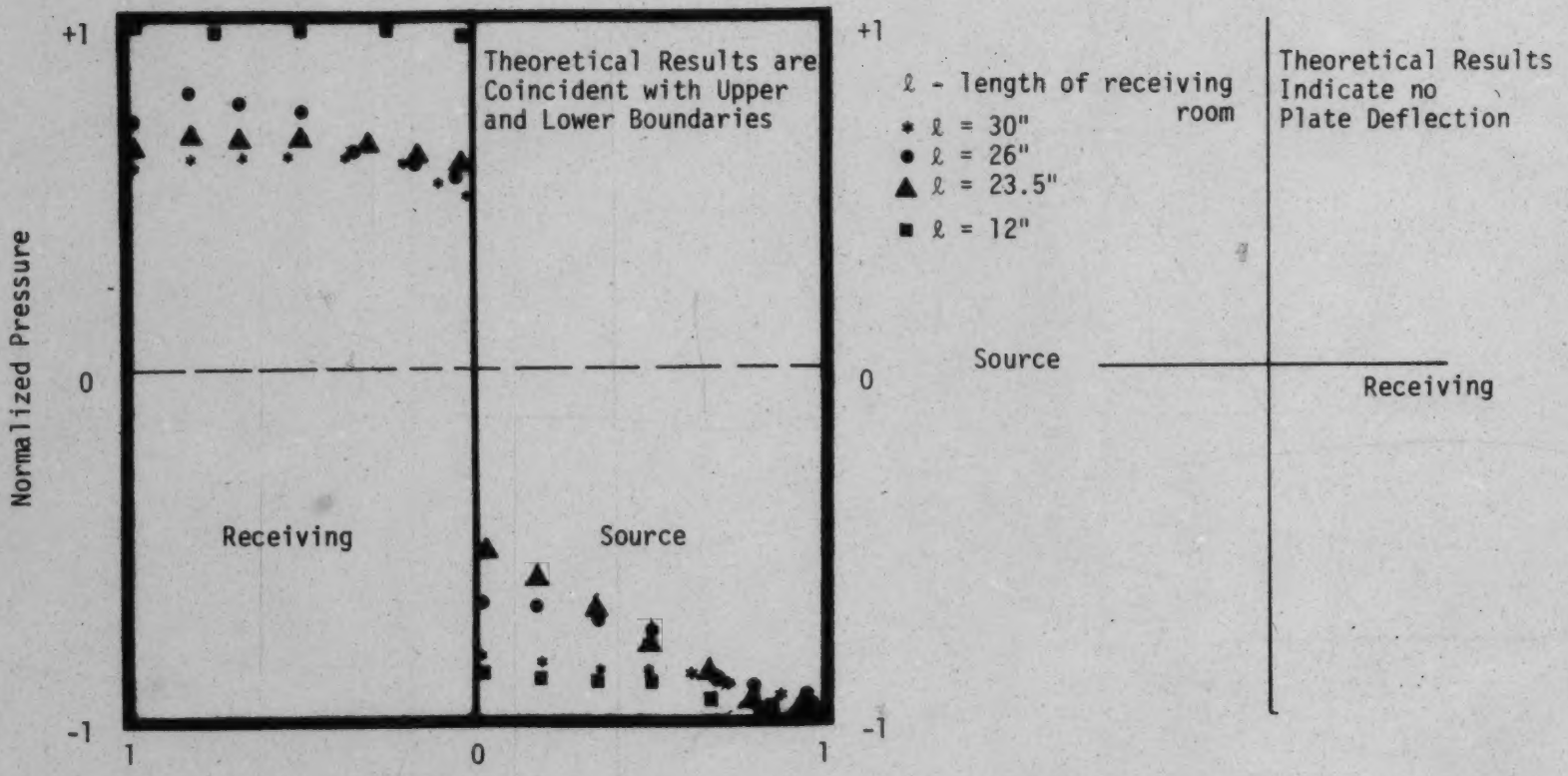

Figure 3.12 FOURTH MODE - NORMALIZED LONGITUDINAL PRESSURE VARIATION AND PLATE DISPLACEMENT

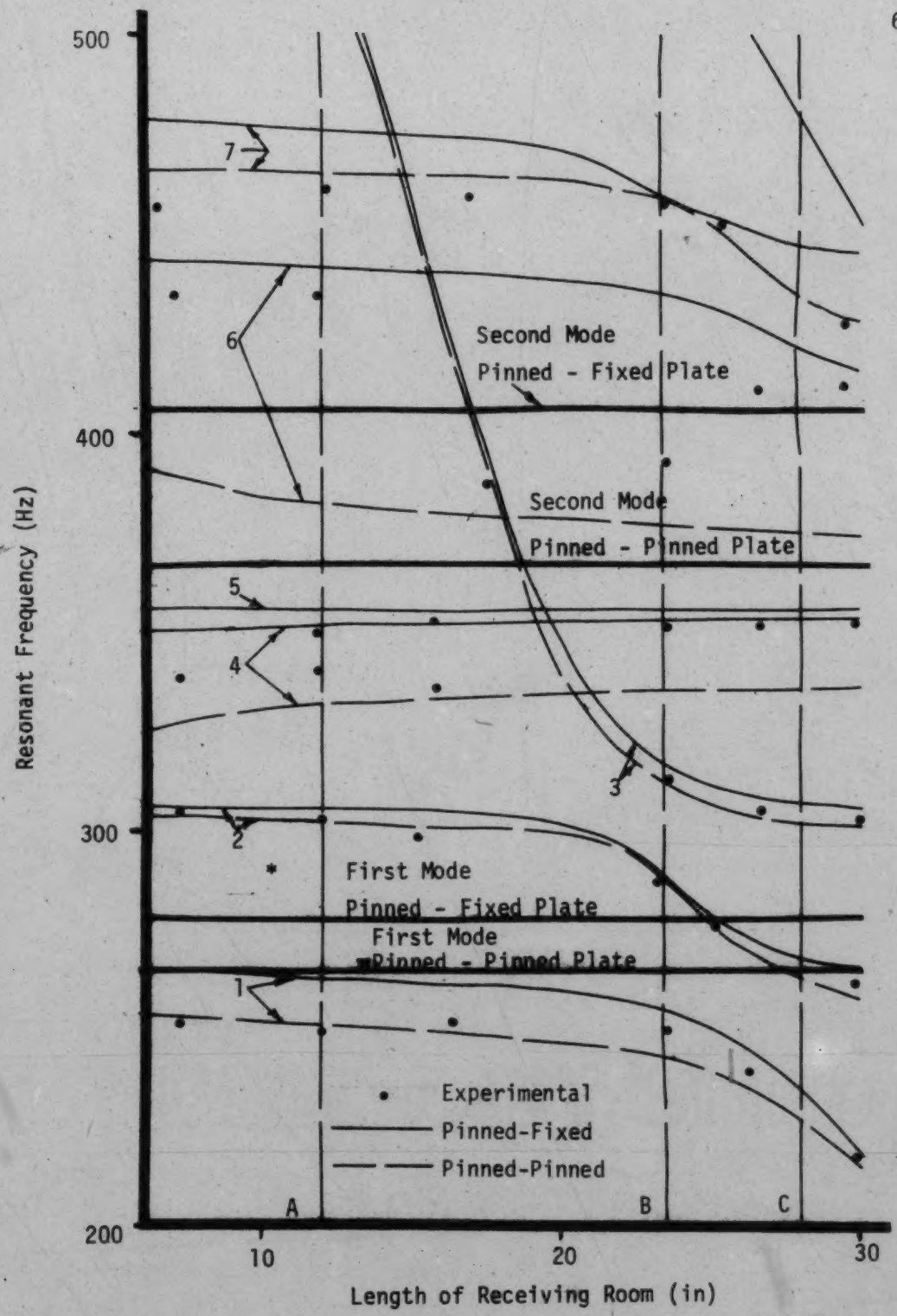

Figure 3.13 FULL COUPLING PANEL - RESONANT FREQUENCIES FOR SOUND TRANSMISSION

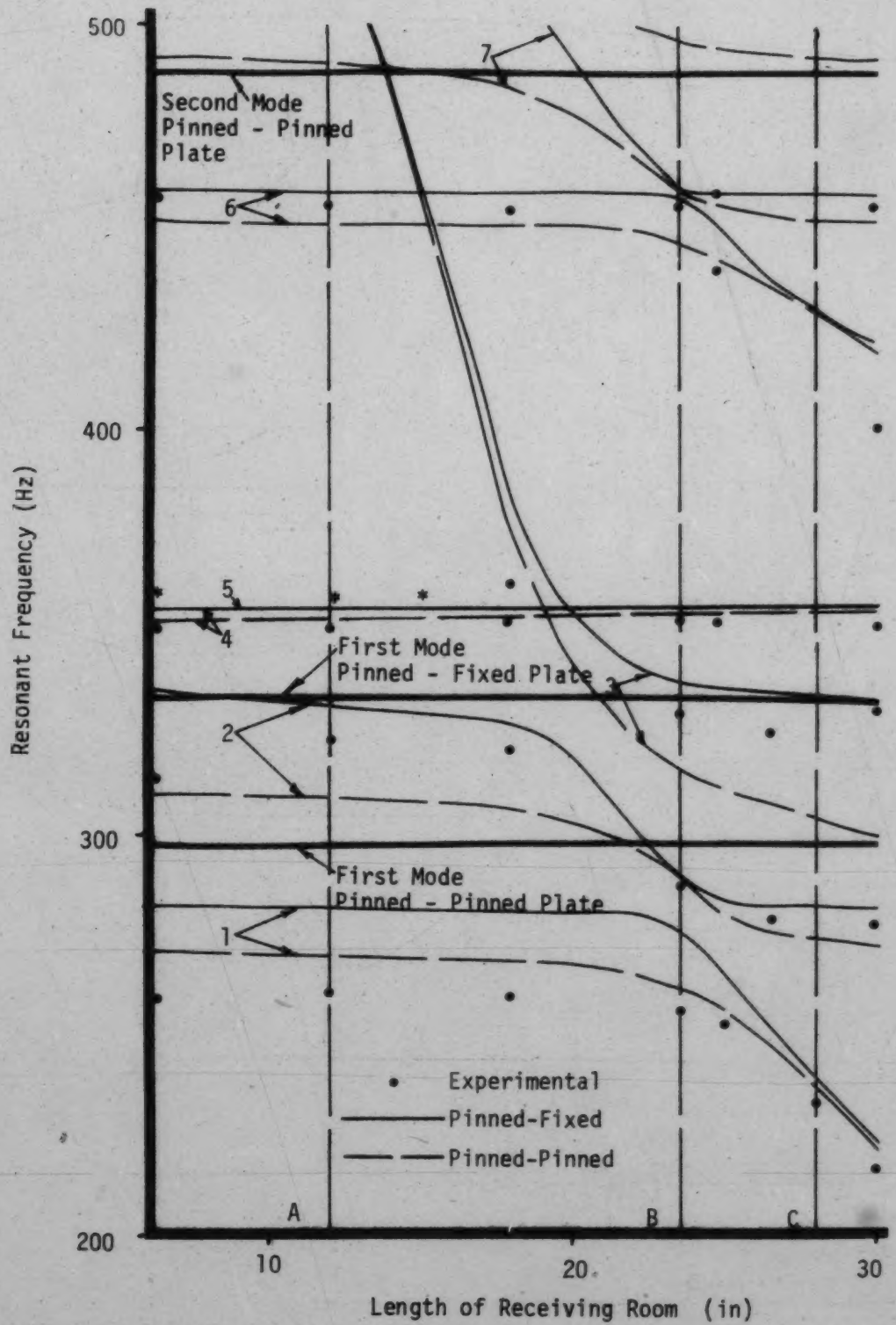

Figure 3.14 73.7 PER CENT COUPLING PANEL - RESONANT FREQUENCIES FOR SOUND TRANSMISSION

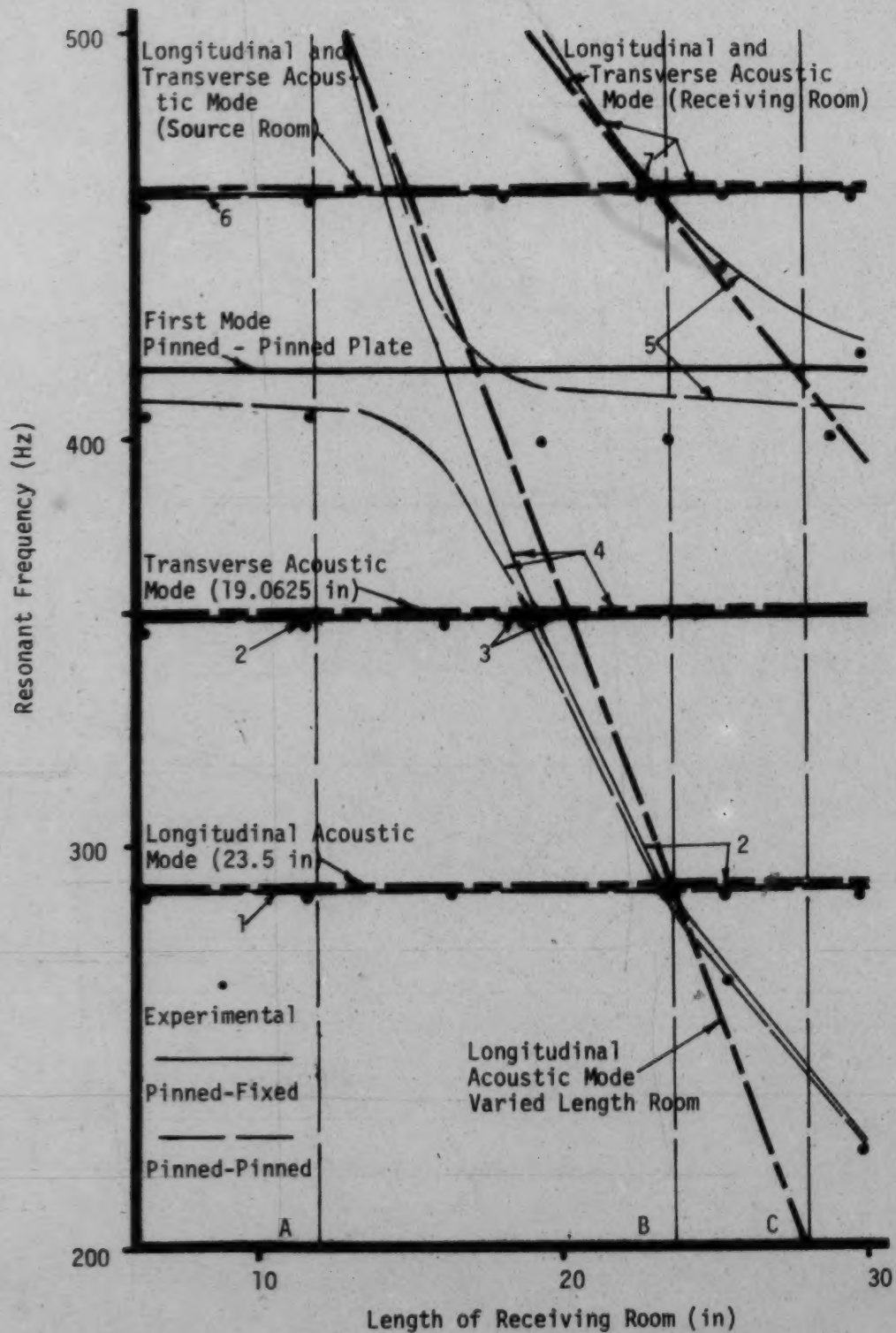

Figure 3.15 42.5 PER CENT COUPLING PANEL - RESONANT FREQUENCIES FOR SOUND TRANSMISSION

"stiffness" effects, as previously described. For any given enclosure the panel and the air in the adjacent room act as a "limp" (i.e. unstiffened) mass on the end of the enclosure to give the lower acoustically dominant mode. The second acoustically dominant mode occurs when the adjacent room reaches a frequency where it acts as a stiffener for the "limp" plate. Panel dominant modes occur at frequencies where the mass or stiffness effects of the rooms respectively decrease or increase the "in vacuo" panel frequency.

It is noteworthy that Fig. 3.5 shows the paradoxical case of sound transmission with no panel motion. Though such a case can not exist with damping present, a natural frequency closely related to the one for this configuration was measured.

Figure 3.9 through Fig. 3.15 relate the effects of changing receiving room length on the natural frequencies and principal mode shapes for any given panel. Figure 3.9 through Fig. 3.12 were scaled with respect to the maximum pressure and the individual room lengths to give a basis for comparison of theoretical and experimental results. It is to be noted that good agreement occurs for all cases except where there is little or no panel motion, i.e. transverse modes and symmetric acoustical modes. These adverse configurations are highly dependent on damping which is not considered in this thesis. To the right of the scaled pressure diagrams are scaled displacement diagrams of the plan view of the coupling panel.

The principal mode shapes within the coupled rooms can basically be described in terms of strain energy or frequency; the higher the strain energy stored, the higher the natural frequency

to maintain the energy level. Acoustically, the lowest strain energy state is the uniform pressure mode in which the room's overall pressure raises and lowers "en mass" while the second lowest is a single noded standing wave in the direction of the maximum room dimension. The panel is at its lowest potential state when unflexed, while the next higher state is a set of half-sine waves in the two planar directions, as previously described. When exciting a coupled system with any given frequency, the individual components will react more violently if the exciting frequency is near one of the components' natural frequencies. The resulting overall natural frequency will therefore be a modification of the components' natural frequencies.

The paragraphs that follow describe each of the lowest five overall natural frequencies as a function of receiving room length starting with a short receiving room. In both the acoustical and flexural sense "mass" effect lowers a component's natural frequency while "stiffness" effect increases it. Also, included is some insight as to the effect of changing the panel area and stiffness on the overall natural frequencies. The vertical lines "A", "B" and "C" in Fig. 3.13 through 3.15 will serve to locate zone points during discussion.

For the lowest overall natural frequency near point A, the receiving room has an almost zero-frequency uniform pressure which acts as a mass in tandem with the mass effect of the panel lowering the component frequency of the source enclosure. As the configuration moves towards "B" the acoustical stiffness of the receiving room drops to equal the stiffness of the source room; the wall still acts as a

limp mass, lowering the component frequency of either room. Moving towards "C" the receiving room develops a longitudinal single node standing wave, while the source room goes to a uniform pressure state. In this region the frequency is close to but above the component frequency for the receiving room. As the panel frequency increases and the panel forcing area decreases, the plate stiffness tends to raise the acoustic frequency of the system to the point where the source room appears to be acoustically hard and the frequency is that classically calculated (as in Fig. 3.15). It is to be noted that when the source room is shorter than the receiving room, the stiffness of the panel increases the frequency of the total configuration over that which would normally be calculated for the receiving room.

The second mode is extremely dependent on the frequency of the coupling plate for unsymmetric rooms (points A and C). For the first two panel widths the natural frequency is close to the frequency for an "in vacuo" panel with a slight increase due to the acoustic stiffness of both rooms. When the rooms are symmetric, sound transmission with no wall motion takes place (totally independent of the plate frequency) at the natural frequency of the hard boundaried source or receiving room. For other configurations, acoustical mass effects of either room tend to lower the frequency of the panel.

Beyond this point the overall natural frequencies and principal mode shapes become disorganized. It is best to discuss Fig. 3.13 and Fig. 3.14 and then Fig. 3.15 separately.

The third principal mode for the two larger panel configurations is governed by a single node longitudinal acoustic wave in

the receiving room in the vicinity of "A" and by the fundamental panel frequency between "B" and "C". The fourth and fifth mode shapes have transverse wave patterns in both source and receiving rooms regardless of receiving room length. In the fourth mode the wave patterns at any point near the coupling panel of one room is 180° out-of-phase with a point immediately adjacent to it in the adjacent room, causing a net force to be incident on any particular section of the panel. Since the fundamental frequency of the plate is below the overall natural frequency, the intercoupled plate-acoustic system has a natural frequency lower than that which would be calculated for similarly dimensioned "hard" rooms. The fifth mode has the adjacent wave patterns in phase so that the panel has no effect.

For the more uncoupled configuration, Fig. 3.15, the second and third modes are degenerate in the region of "A". The frequency of the coupling panel is sufficiently above the frequency of a transverse acoustic wave that the previously independent frequencies associated with the "out-of-phase" and "in-phase" acoustic mode shapes are the same. This would indicate that the rooms are effectively hard. These mode shapes are similar to the fourth and fifth mode shapes for the wider panel configurations. In the region between "A" and "B" the second mode becomes dependent on the longitudinal acoustic mode in the receiving room and from "B" to "C" on the fundamental longitudinal acoustic mode in the source room. In the region of "B" the third and fourth modes are degenerate and remain as such for further lengthening of the receiving room. The fourth acoustic mode is dependent on the "in vacuo" panel frequency near "A" but becomes

dependent on the fundamental longitudinal acoustic mode of the receiving room between "A" and "B". Beyond this, the acoustic and panel modes become coupled as the fundamental frequency of the panel is arrived at.

Cases of "weak" intercoupling produce frequency curves that are almost discontinuous at points of curvature. These lines are almost co-incident with those calculated by "hard" room and "in vacuo" panel theories. One noteworthy exception is the longitudinal standing wave in the receiving room. The panel stiffness has some effect in increasing the lower frequency results and the mass effects of the panel decreasing the higher frequencies.

In Fig. 3.13 through Fig. 3.15 the vertical distance between the pinned-pinned and pinned-fixed lines for any given mode is an indication of the mode's dependency on the panel's boundary conditions. This exemplified itself when measurements were made on the experiment apparatus. Resonances associated with narrow distances between pinned-pinned and pinned-fixed boundary conditions were pronounced over a small band width whereas resonances associated with wider distances between the boundary conditions had a much wider "skirt". An adverse effect of the different "skirt" widths was the disappearance of certain less prominant resonances. Also, a shift occurred in the peaks of two closely adjacent resonances because of the phase plane addition of the respective skirt zones. Examples of this can be seen in Fig. 3.13 and Fig. 3.14 marked with "*".

In Fig. 3.13, a '▼' denotes a resonance situation of the upper "rigid" panel of the receiving room and the coupling wall. It is given

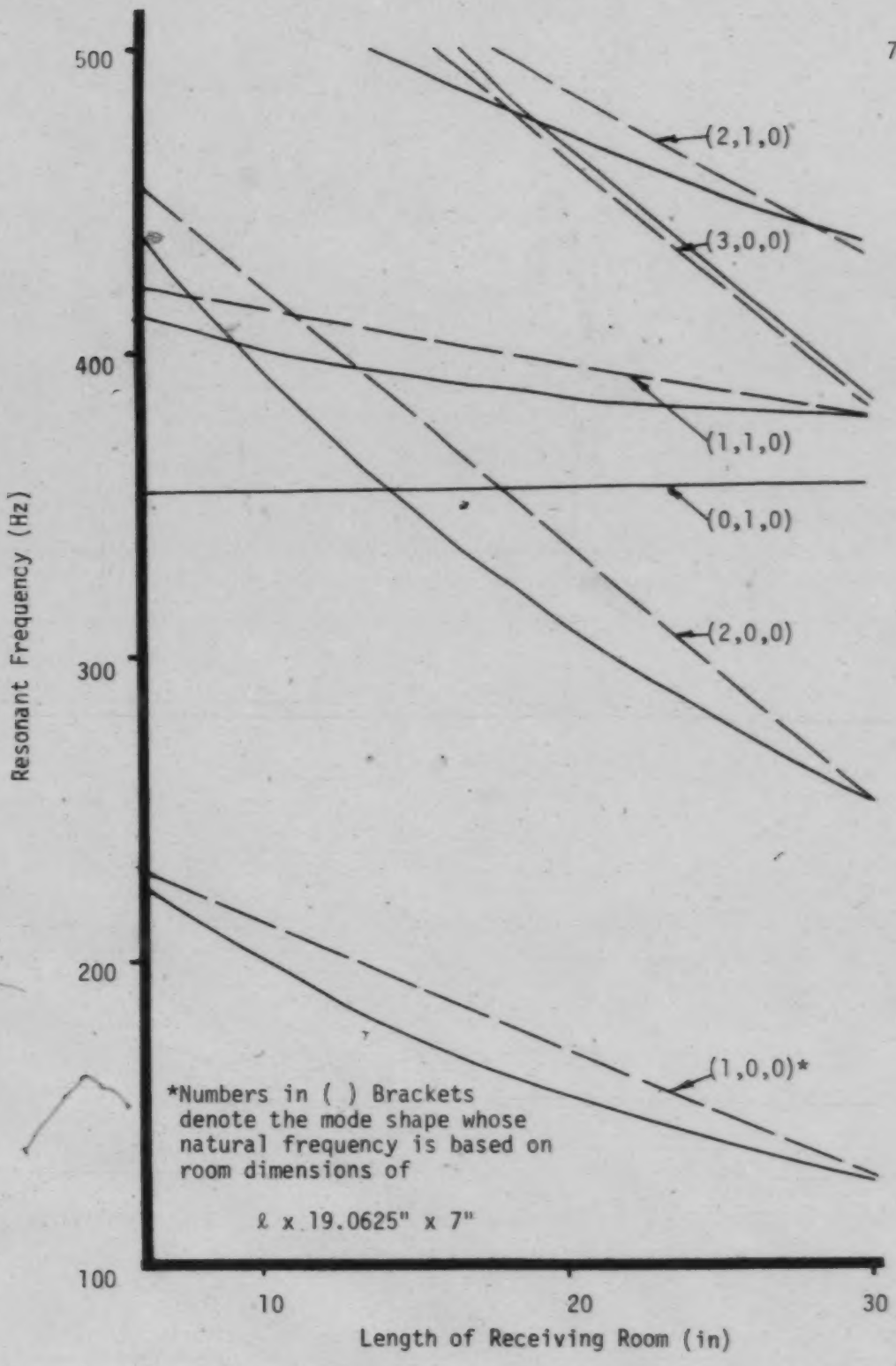

Figure 3.16 42.5 PER CENT ORIFICE COUPLING - RESONANT FREQUENCIES FOR SOUND TRANSMISSION

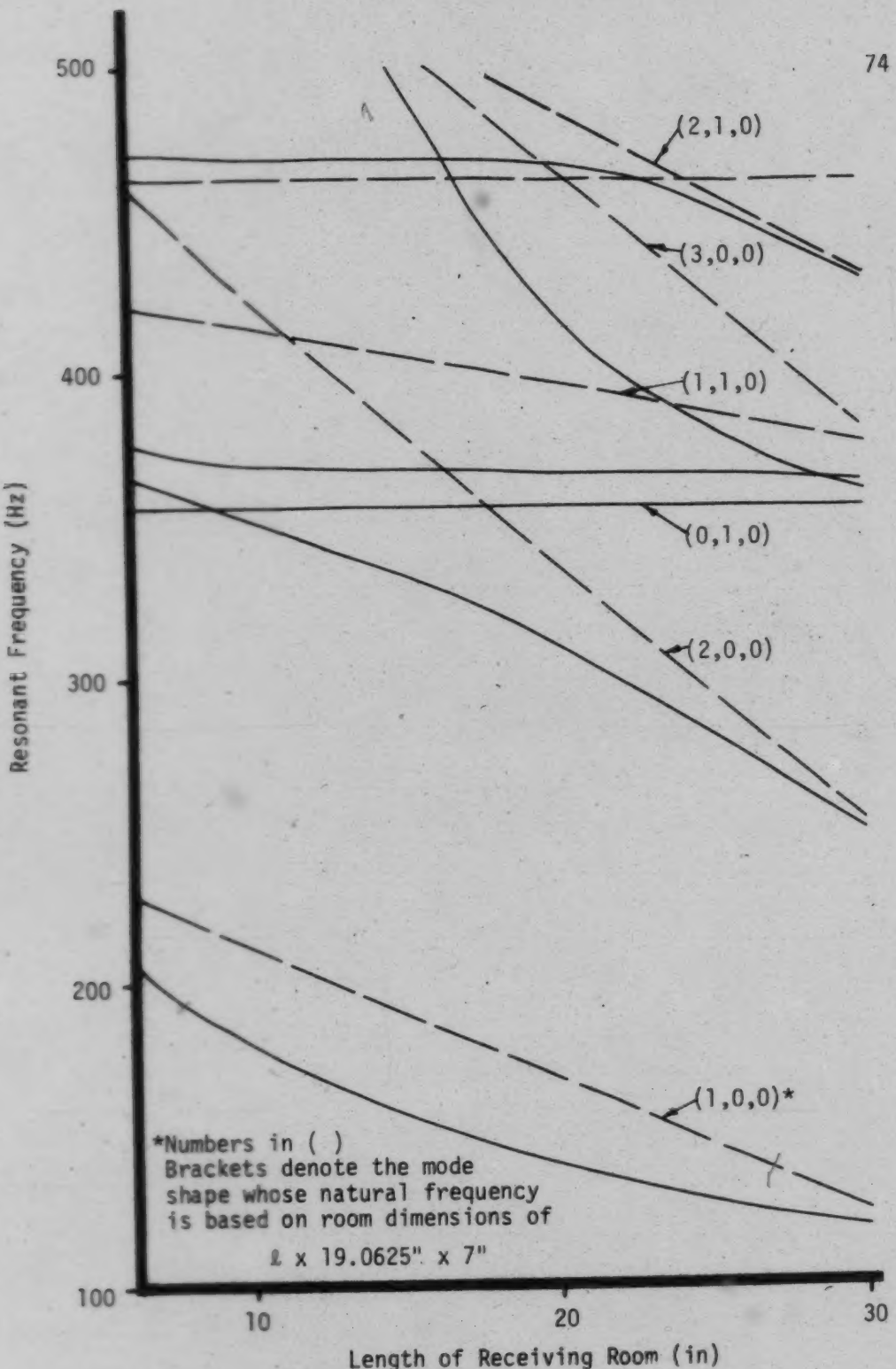

Figure 3.17 4.2 PER CENT ORIFICE COUPLING - RESONANT FREQUENCIES FOR SOUND TRANSMISSION

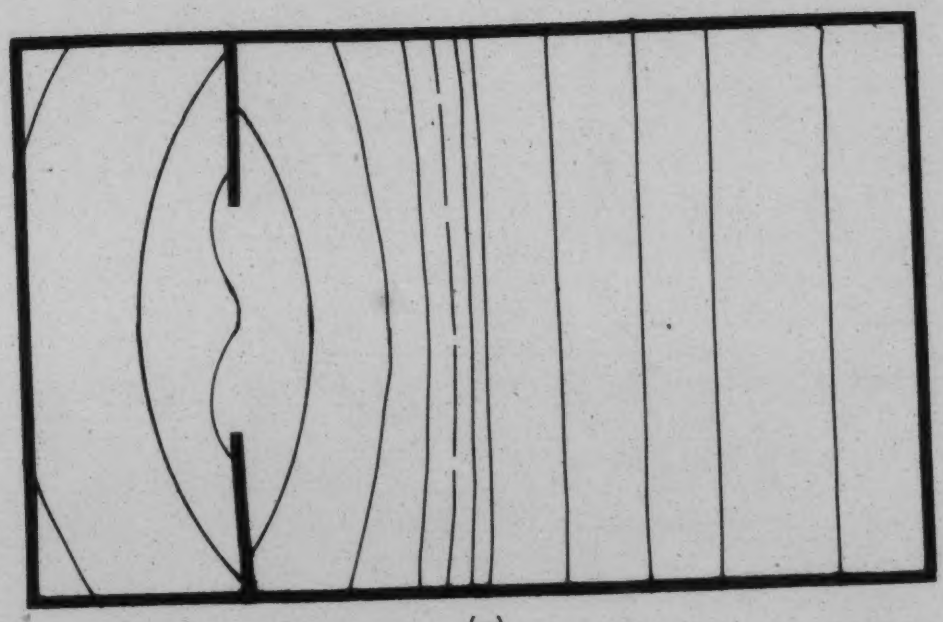

(a)

——— Isobar

— — — Nodal Line
(Zero Isobar)

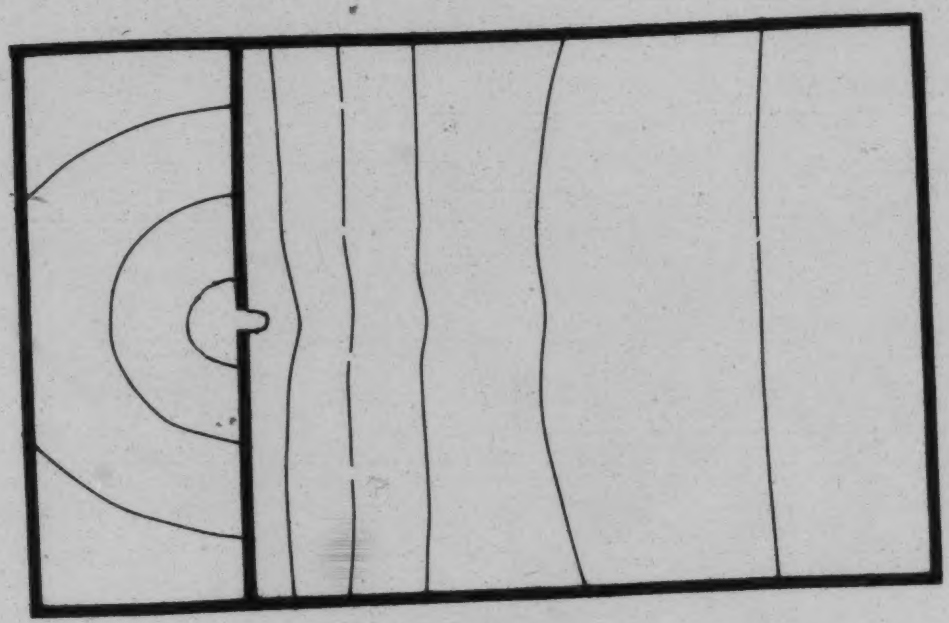

(b)

Figure 3.18 EXAMPLE OF ORIFICE COUPLING MODE SHAPES

because it appears as a resonance peak for the given configuration but is not sufficiently large in any of the other configurations.

3.3 Sound Transmission Between Orifice Coupled Rooms

Some interest was shown by Harris and Feshback [34] in the coupling of two rooms by a window. Considering the similarity in rooms studied, a slight diversion was taken to show the natural frequencies for a room with orifice coupling in a panel that represents 43.7 per cent of the coupling wall. A second set of frequencies were calculated for an orifice coupling which represented 4.25 per cent of the coupling wall. These are shown in Fig. 3.16 and Fig. 3.17, respectively.

For the large coupling window there is no extensive change of modal patterns from any given classical principal mode shape due to the excellent acoustic flow between the rooms. The constriction causes local pressure build-up in the corners adjacent to the coupling wall in longitudinal modes (shown in Fig. 3.18), which is common for both widths of constriction. The narrow window is effectively a line source of sound in the shorter room, whether it be the source or receiving room (shown in Fig. 3.18 (b)).

From Fig. 3.16 it is reasonably easy to see that the coupling window has very little effect on the principal frequency. The natural frequencies for a similar room with no window are superimposed with a dashed line and are named. The deviation is due to the slight increase in kinetic energy as the flow passes through the common boundary. It is to be noted that the computational error is small, as indicated by

the agreement of slope and only slight reversal of lines for the (3, 0, 0) mode.

For the narrow passage, the natural frequencies and mode shapes vary considerably from classical geometrically based calculations. Again, the frequencies for the lowest mode are close to those for the (1, 0, 0) mode for a similarly dimensioned room with no coupling wall. Larger deviations occur due to greater kinetic energy through the orifice (much similar to two coupled Helmholtz resonators).

For higher modes, there are indications of independence in room characteristics due to a smaller coupling surface. Modes three and four are both transverse wave patterns with the wave "in-phase" and "out-of-phase", respectively, much similar to the panel-coupled rooms. The greater frequency associated with mode four is due to a slight pressure gradient that has its peak at the orifice and declines towards the end walls.

Modes two and six also display this partially uncoupled characteristic. When the receiving room is short the receiving room has a transverse wave pattern, while the source room has a longitudinal standing wave. As the receiving room lengthens, the transverse wave in the receiving room is gradually replaced by a longitudinal wave in mode two. For mode six the transverse wave does not disperse but a longitudinal wave develops in the receiving room.

Mode five has a longitudinal wave pattern much similar to the (3, 0, 0) mode of the equivalently dimensioned uncoupled configuration. As in mode one, the frequencies are lower because of the Helmholtz resonator effect.

CHAPTER IV

DISCUSSION AND RESULTS

4.1 Discussion

There are several interesting effects which occur when the natural frequencies of the coupling plate are within the range of the natural acoustic frequencies.

1) Pressure levels in the receiving room can be higher than those in the source room.
2) Acoustically dominant modes occur at frequencies near those classically calculated with only slight deformation of the acoustic mode shapes. In this situation the exciting frequency is sufficiently removed from the natural frequencies of the panel so that the panel acts as a "passive" spring (stiffness) or "limp" mass on an acoustical system.
3) Plate dominant modes have natural frequencies that vary as much as 8 per cent from the "in vacuo" classical panel frequencies, though changes in plate mode shapes are not appreciable. The mass and stiffness effects of the adjacent acoustical systems have considerable effect on the overall frequency, but subsequently suffer considerable deformation in acoustical mode shapes.

In the orifice coupled enclosures the effect of the aperture is not significant until the opening is less than 10 per cent of the common wall area. In this range the Helmholtz resonator effect causes the natural frequency to drop considerably, while the rooms become acoustically uncoupled to some extent. As the opening becomes smaller the straight isobars of a classical hard boundaried room become distorted into curves because the orifice becomes a stronger "line" source radiating into the room that is the least acoustically exicted.

For both types of coupling, the insertion of an intermediate surface, be it a hard boundary with an air slit in it or a coupling panel, causes pressure build ups at these surfaces. This is due to the increase in potential energy and the decrease of kinetic energy because of reduced transverse velocities at a wall.

The principal mode shapes produced give an insight of the acoustic isobars and the deflected form of the panel for a given resonant condition. With the mathematical characteristics of linear combination, visualization as well as calculation of composite sound fields is readily possible.

4.2 Future Research

There are some other possible extensions of the Kantorovich approach in plate-acoustic systems. One would be to study the random dynamic response of the aforementioned rooms and structure. Another would be to change coordinate systems. By developing a cylindrical acoustic element, a circular plate element and a cylindrical shell element (with the Θ-direction being used for Fourier approximation)

and the required coupling matrices, the dynamic or resonant response of submerged closed cylindrical sections could be studied. The form of the approximating functions would be

$$r^n F(r,z) (A \cos n\theta + B \sin n\theta)$$

which would lend easily to the approximation of the Bessel Functions used in the solution of classical equations. Notably there would have to be care taken to circumvent the singularity that would occur at the origin ($r = 0$) of the element configuration.

4.3 Results

The finite elements produced give a good approximation of the principal mode shapes and natural frequencies for a coupled plate-acoustic system with two parallel surfaces and perpendicular sides. The agreement is best when the configuration is least dependent on internal hysteretic and viscous damping. Convergence of the approximate results to the exact solution is at a rate of $1/n_e^4$ or $1/n_e^5$ for all cases studied. The use of Kantorovich's approximation and Iron's symmetricization procedure produced a significant saving in computing time and storage.

Such an approach is sufficiently general to allow study of many acoustic panel configurations with little alteration to the major portions of the computing program. If the program is to be used for various problems of varying geometry, the finite element approach is much more attractive than other analytical methods (i.e. finite difference).

BIBLIOGRAPHY

1. Galilei, G., Dialogue Concerning Two New Sciences (Translated from the Italian and Latin by Henry Crew and Alfonso de Salvio), Evanston and Chicago, 1939.
2. Mersenne, M., "La Theorie et la Practique de la Musique", Harmonie Universelle, Paris, 1686.
3. Sauver, J., "Systéme General des Intervalles des Sons", Memoirs of L'Academie Royale des Science, Paris, 1701, pp. 297-299.
4. Knudsen, V. O., "Recent Developments in Architectural Acoustics", Review of Modern Physics, Vol. 6, Sec. 1, 1934.
5. Sabine, P. E., "The Beginning of Architectural Acoustics", Journal of the Acoustic Society of America, Vol. 10, Sec. 1, 1938.
6. Sabine, P. E., "Architectural Acoustics, its Past, its Present and Future", Journal of the Acoustic Society of America, Vol. 11, Sec. 21, 1939.
7. Rayleigh, J. W. S., The Theory of Sound, Vol. 1 & 2, 1896, Dover Publishers, New York.
8. Lamb, H., The Dynamic Theory of Sound, 1925, Dover Publishers, New York.
9. Morse, P. M., "Acoustics and Basic Physics", Journal of the Acoustic Society of America, Vol. 27, Sec. 2, 1955, pp. 216.
10. Morse, P. M. and Bolt, R. H., "Sound Waves in Rooms", Reviews of Modern Physics, Vol. 16, No. 2, 1944, pp. 69-150.

11. Bishop, R. E. D. and Gladwell, G. M. L., "An Investigation into the Theory of Resonance Testing", Philosophical Transactions of the Royal Society of London, Vol. 255, No. 1055, 1963, pp. 241-280.

12. Nilsson, A. C., "Reduction Index and Boundary Conditions for a Wall Between Two Rectangular Rooms", Parts 1 & 2, Acoustica, Vol. 26, 1972.

13. Lyon, R. H., Dietrich, C. W., Ungar, E. E., Pyle, R. W. and Apfel, R. E., "Low-Frequency Noise Reduction of Spacecraft Structures", NASA CR-589, 1966.

14. Pretlove, A. J. and Craggs, A., "A Simple Approach to Coupled Panel-Cavity Vibration", Journal of Sound and Vibration, Vol. 11, No. 2, 1970, pp. 207-215.

15. Craggs, A., "The Transient Response of a Coupled Plate-Acoustic System Using Plate and Acoustic Finite Elements", Journal of Sound and Vibration, Vol. 15, No. 4, pp. 509-528.

16. Craggs, A., "Computation of the Response of Coupled Plate-Acoustic Systems Using Plate Finite Elements and Acoustic Volume - Displacement Theory", Journal of Sound and Vibration, Vol. 18, No. 2, pp. 235-245.

17. Gladwell, G. M. L., "A Finite Element Method for Acoustics", presented at the 5th Congress of Acoustics 1965 (Liege).

18. Jennequin, G., "Is the Computation of Noise Level Inside a Car Feasible?", Institution of Mechanical Engineers, 1971, pp. 132-137.

19. Pin Tong, "The Finite Element Method for Fluid Flow", Recent Advances in Matrix Methods of Structural Analysis and Design, 1971, pp. 787-808, University of Alabama Press.

20. Zienkiewicz, O. C., The Finite Element Method in Engineering Science, 1971, McGraw-Hill, London.

21. Holand, I. and Bell, K., Finite Element Methods in Stress Analysis, 1970, Tapir, Norway.

22. Long, R. R., Engineering Science Mechanics, 1963, Prentice-Hall, pp. 78-88.

23. Timoshenko, S. P., Vibration Problems in Engineering, Third Edition, Van Norslrand, 1955, pp. 442.

24. Timoshenko, S. P. and Gere, J. M., Theory of Elastic Stability, Second Edition, McGraw-Hill, 1961, pp. 319-347.

25. Warburton, G. B., "The Vibration of Rectangular Plates", Proceedings of the Institute of Mechanical Engineering, Vol. 168, 1954, pp. 371-384.

26. Warburton, G. B., "Vibration of a Cylinderical Shell in an Acoustic Medium", Journal of Mechanical Engineering Science, Vol. 1, 1961.

27. Pretlove, A. J., "Free Vibration of a Rectangular Panel Backed by a Closed Rectangular Cavity", Journal of Sound and Vibration, Vol. 2, 1965.

28. Gladwell, G. M. L. and Zimmerman, "Energy Formulations of Acoustic and Structural Vibration Problems", Journal of Sound and Vibration, Vol. 3, 1966.

29. Mason, V., Ph.D. Thesis, University of Southhampton.

30. Mason, V., "Rectangular Finite Elements for Analysis of Plate Vibration", Journal of Sound and Vibration, Vol. 7, 1968, pp. 437-488.

31. Craggs, A., Ph.D. Thesis, University of Southhampton, 1969.

32. Boas, M. L., Mathematical Methods in the Physical Sciences, 1966, pp. 290-301.

33. Zienkiewicz, O. C. and Newton, R. E., "Coupled Vibration of a Structure Submerged in a Compressible Fluid", Proceedings of the Symposium on Finite Element Techniques, University of Stuttgart, Germany, 1969, pp. 371.

34. Harris, C. M. and Feshbach, H., "On the Acoustics of Coupled Rooms", Journal of the Acoustic Society of America, Vol. 22, No. 5, 1960.

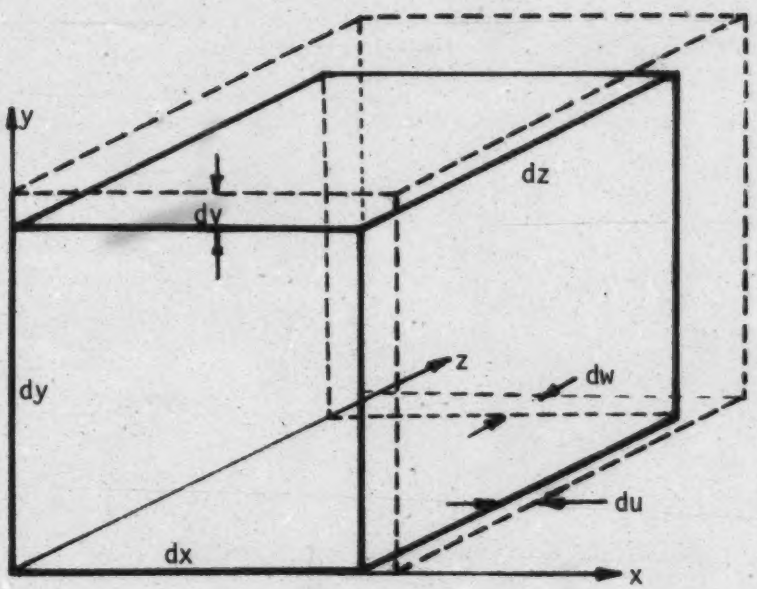

u,v,w - displacements in the x,y,z directions respectively

v_o, v - initial and final specific volumes

ρ_o, ρ - initial and final densities

dx,dy,dz - dimensions of the infinitesimal element in the x,y,z directions respectively

Figure A1 INFINITESIMAL ACOUSTIC ELEMENT

APPENDIX A

ACOUSTIC FORMULATION

A.1 Equations of Motion for Acoustics

A derivation of the equations is given by H. Lamb [8], therefore what is presented here will only represent a condensation of the above author's work.

Considering the element as shown in Fig. A1 (with the included notation) and defining the dilatation Δ as the ratio of the specific volume increment to the original specific volume, we get

$$\Delta = (v - v_0) / v_0$$

$$v = v_0 (1 + \Delta) \tag{A1}$$

Similarly, condensation s can be defined for densities

$$s = (\rho - \rho_0) / \rho_0$$

$$\rho = \rho_0 (1 + s) \tag{A2}$$

The density is the inverse of the specific volume, therefore

$$1 = (1 + s) (1 + \Delta)$$

Considering only small dilatations and condensations, it can be shown that

$$\Delta \simeq -s \tag{A3}$$

Looking more closely at the dilatation, it is defined by

$$\frac{(dx + du)\ (dy + dv)\ (dz + dw) - dxdydz}{dxdydz}$$

Neglecting second order terms, it becomes

$$\Delta = \text{div}\ \underline{u} \qquad \text{(A4)}$$

where

$$\underline{u} = (u,v,w) \quad \text{and} \quad \text{div} = \frac{\delta}{\delta x} + \frac{\delta}{\delta y} + \frac{\delta}{\delta z}$$

Poisson and Laplace consider the thermodynamics of sound to be almost adiabatic, which agreed well with experiments. Therefore, from (A2)

$$\frac{p}{p_0} = \left(\frac{\rho}{\rho_0}\right)^{\gamma} = (1 + s)^{\gamma}$$

where γ is the ratio of the specific heats. Again, assuming a small dilatation

$$p = p_0\ (1 + \gamma s) \qquad \text{(A5)}$$

By taking a force balance in each of the principal directions, we get

$$- \rho \frac{\delta^2 u}{\delta t^2} = \frac{\delta p}{\delta x}$$

$$- \rho \frac{\delta^2 v}{\delta t^2} = \frac{\delta p}{\delta y} \qquad \text{(A6)}$$

$$- \rho \frac{\delta^2 w}{\delta t^2} = \frac{\delta p}{\delta z}$$

with the minus sign indicating the direction of acceleration relative to the pressure gradient. Equation (A6) can be written in more efficient notation as

$$- \rho \frac{\delta^2 u}{\delta t^2} = \text{grad } p \qquad \text{(A7)}$$

It is worthwhile to note that the velocities in the different coordinate directions within the acoustic element can be directly related to the condensation s by

$$\frac{\delta u}{\delta t} = \frac{-p_0 \gamma}{\rho} \frac{\delta}{\delta x} \int_{-\infty}^{t_2} s \, dt$$

$$\frac{\delta v}{\delta t} = \frac{-p_0 \gamma}{\rho} \frac{\delta}{\delta y} \int_{-\infty}^{t_2} s \, dt$$

$$\frac{\delta w}{\delta t} = \frac{-p_0 \gamma}{\rho} \frac{\delta}{\delta z} \int_{-\infty}^{t_2} s \, dt$$

In acoustics the excess pressure $(p - p_0)$, is used rather than the overall pressure p. Rearranging (A5) to get the excess pressure p_1, and making substitutions from (A3) and (A4)

$$p_1 = -p_0 \gamma \text{ div } \underline{u} \qquad \text{(A8)}$$

The excess pressure can be directly substituted into (A6) and upon combination with (A7)

$$\text{div (grad } p_1) - \frac{\rho}{\gamma p_0} \frac{\delta^2 p_1}{\delta t^2} = 0$$

The divergence of the gradient of a scalar is the Laplacian operator ∇^2

$$\nabla^2 p_1 - \frac{\rho}{\gamma p_0} \frac{\delta^2 p_1}{\delta t^2} = 0$$

which is a standard form of the wave equation

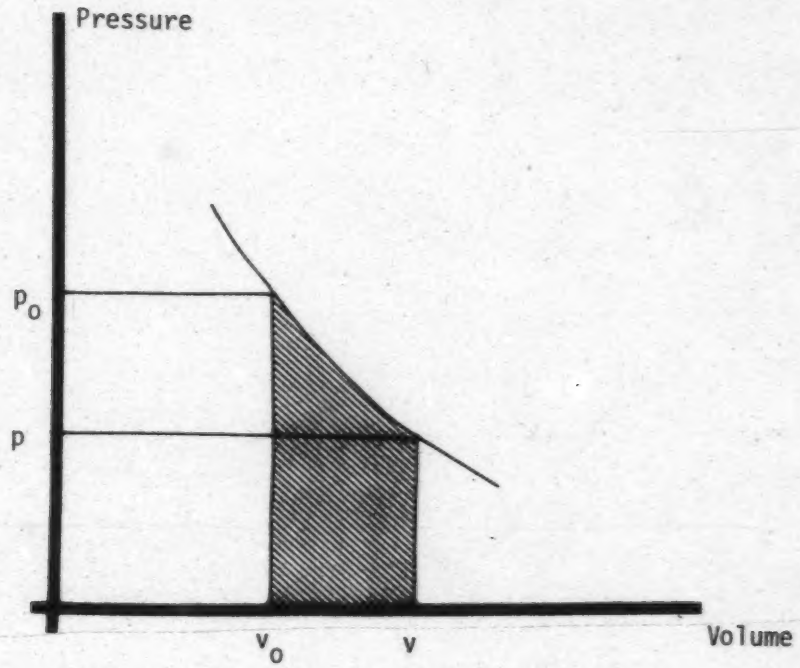

Figure A2 P-V CURVE

and $\frac{\gamma p_0}{\rho}$ is the square of the wave velocity, which from now on is c, the velocity of sound

$$c^2 = \frac{\gamma p_0}{\rho} \tag{A10}$$

A.2 Energy Equations for Acoustics

The kinetic energy T for an infinitesimal element can be written as

$$T = \frac{1}{2} \rho \iiint_V \frac{\delta \underline{u}}{\delta t} \cdot \frac{\delta \underline{u}}{\delta t} \, dV$$

The potential energy U can be found by integrating the shaded area in Fig. A2 over the whole volume V

$$U = \iiint_V \{p_0 \frac{(v-v_0)}{v_0} - \frac{1}{2} (p_0 - p) \frac{(v-v_0)}{v_0}\} \, dV$$

Since the average volume change over the whole is zero, the first term disappears and by using (A1), (A3), (A8) and (A10), it can be written that

$$U = \frac{\rho c^2}{2} \iiint_V (\text{div } \underline{u})^2 \, dV$$

To this point no assumptions have been made as to the form of wave motion. Gladwell and Zimmerman [28] assumed a periodic sound wave and continued onto the energy equations. Craggs [15] studied the tran-

sient response and, therefore, his formulation had to be more general but is, in some respects, easier to follow and will be used for the time being.

A velocity potential ϕ must be defined

$$\phi = -c^2 \int_{t_1}^{t_2} s \, dt + \Phi_0$$

where Φ_0 is the value of the integral at time, t_1.

It can be derived from the previous equations without much difficulty that

$$\frac{\delta \underline{u}}{\delta t} = \text{grad } \phi$$

$$\text{div } \underline{u} = \frac{1}{c^2} \frac{\delta \phi}{\delta t}$$

$$p_1 = -\rho \frac{\delta \phi}{\delta t} \qquad \text{(A11)}$$

Note that from here on a superscript "$\cdot$" indicates differentiation with respect to time. The value of the potential lies in its ability to define the total character of a vector quantity $\underline{u}$ by a scalar, although at a loss in physical interpretation.

A.3 Derivation of Equations of Motion from Functional Formulation

It is now worthwhile to show that the first variation of the time integral of the Lagrangian, J, actually gives the correct equation. Making substitutions from (A11) in the energy equation,

and knowing that

$$J = \int_{t_1}^{t_2} (T - V)\, dt$$

$$J = \int_{t_1}^{t_2} \{\frac{1}{2}\rho \iiint \text{grad } \phi \cdot \text{grad } \phi \, dV - \frac{1}{2}\frac{\rho}{c^2} \iiint \dot{\phi}^2 \, dV\} \, dt$$

Looking at the first variation δJ.

$$\delta J = \int_{t_1}^{t_2} \rho\{\iiint \text{grad } \phi \cdot \text{grad } \delta\phi \, dV - \frac{1}{c^2} \iiint \dot{\phi}\, \delta\dot{\phi} \, dV\} \, dt$$

Integrating the second term by parts with respect to time,

$$-\frac{\rho}{c^2} \iiint \{\dot{\phi}\, \delta\phi \Big|_{t_1}^{t_2} - \int_{t_1}^{t_2} \ddot{\phi}\, \delta\phi \, dt\} \, dV$$

Applying Greene's theorem, the first term of δJ can be written as

$$\int_{t_1}^{t_2} \rho \{-\iiint \nabla^2\phi \, \delta\phi \, dV + \iint \delta\phi \, \text{grad } \phi \cdot dS\} \, dt$$

where S is the surface of the volume of interest. But $\delta\phi$ is zero at t_1 and t_2, therefore

$$\delta J = \int_{t_1}^{t_2} \{\rho \iiint_V (\frac{1}{c^2} \ddot{\phi} - \nabla^2\phi)\, \delta\phi \, dV - \rho \iint \delta\phi \, \text{grad } \phi \cdot \delta S\} \, dt$$

Since $\delta J = 0$ and $\delta\phi$ is arbitrary between t_1 and t_2, the integrands must be zero.

$$\nabla^2\phi - \frac{1}{c^2}\ddot{\phi} = 0$$

$$\text{grad } \phi \cdot \delta S = 0 \text{ on } S \qquad \text{(A12)}$$

These equations can be derived from (A11) and represent, respectively, the wave equation and the natural boundary condition. It is only right that the "velocity potential" obey the wave equation as does the pressure p in (A9). The natural boundary condition can be translated either as the normal pressure gradient or the normal velocity being zero at a rigid boundary.

A.4 Matrix Formulation of the Functional

Let the velocity potential within an element be written

$$\Phi_e = \{F(\underline{x})\}^T \{\phi_n(t)\}_e \qquad \text{(A13)}$$

where $\{F(\underline{x})\}$ is a column vector (of some length) of functions of $\underline{x}$, the coordinates used to define the geometry, such that $\{\phi_n(t)\}_e$ (also a column vector of the same length) is the value of ϕ which varies with time at points called nodes. The right-hand side of (A13) may be differentiated and used in the desired equations containing Φ_e, but it should be realized that the equations are now approximate. Therefore,

$$\text{grad } \Phi_e = \{\text{grad } F\}^T \{\phi_n\}_e$$

and

$$\dot{\Phi}_e = \{F\}^T \{\dot{\phi}_n\}_e$$

neglecting the variables in round brackets. The energy equations for an element can now be written

$$T_e = \frac{\rho^2}{2} \{\phi_n\}_e^T \frac{1}{\rho} \iiint_V \{\text{grad } F\} \cdot \{\text{grad } F\}^T \, dV \, \{\phi_n\}_e$$

$$U_e = \frac{\rho^2}{2} \{\dot{\phi}_n\}_e^T \frac{1}{\rho c^2} \iiint_V \{F\} \{F\}^T \, dV \, \{\dot{\phi}_n\}_e \qquad \text{(A14)}$$

The products within the integral signs are now matrices, which can be integrated to give the final form of the energy equations

$$T_e = \frac{\rho^2}{2} \{\phi_n\}_e^T [S_e] \{\phi_n\}_e$$

$$U_e = \frac{\rho^2}{2} \{\dot{\phi}_n\}_e^T [P_e] \{\dot{\phi}_n\}_e \qquad \text{(A15)}$$

The square of the acoustic density ρ is kept aside for consistency of units in later work where $[S_e]$, $[P_e]$ are the elemental acoustical stiffness and pressure matrices. These matrices can easily be defined by comparison of (A14) and (A15).

Substituting these equations in the functional

$$J = \frac{\rho^2}{2} \int_{t_1}^{t_2} [\{\phi_n\}_e^T [S_e] \{\phi_n\}_e - \{\dot{\phi}_n\}_e^T [P_e] \{\dot{\phi}_n\}_e] \, dt$$

Taking the first variation of this equation and integrating the second term with respect to time gives

$$\delta J = -\{\delta\phi_n\}_e^T [P_e] \{\dot{\phi}_n\}_e \Big|_{t_1}^{t_2} + \int_{t_1}^{t_2} \{\delta\phi_n\}_e^T [[S_e] \{\phi_n\}_e + [P_e] \{\ddot{\phi}_n\}_e] \, dt = 0$$

The first term is zero because $\delta\Phi$ is zero at t_1 and t_2. This can be seen from the potential energy equation in (A14), knowing that

$$\delta\Phi = \{F(\underline{x})\}^T \{\delta\phi_n\}_e = 0 \quad \text{at } t_1 = 0 \text{ and } t_2 = 0$$

Since $\delta\Phi$ is also arbitrary between t_1 and t_2

$$[S_e] \{\phi_n\}_e + [P_e] \{\ddot{\phi}_n\}_e = 0 \tag{A16}$$

The velocity potential lacks physical significance so rather than using the nodal vector $\{\phi_n\}$, (A16) can be differentiated with respect to time and rewritten in terms of the element nodal excess pressures $\{p_n\}_e$ by using (A11)

$$[S_e] \{p_n\}_e + [P_e] \{\ddot{p}_n\}_e = 0 \tag{A17}$$

This last formula will be used in the finite element analysis of acoustic enclosures with rigid boundaries.

APPENDIX B

MATHEMATICAL TABULATIONS AND OPERATIONS

B.1 Fourier Approximation and Integrals Over One-Half Period

Let $h(z)$ be a function that satisfies the wave equation and boundary conditions that $\frac{\delta h}{\delta z} = 0$ at $z = 0$ and $z = d$. If it is piecewise continuous and finite within the interval, then

$$h(z) = \sum_{n=0}^{\infty} e_n \cos \frac{n\pi z}{d}$$

where

$$e_0 = \frac{1}{d} \int_0^d h(z)\, dz$$

$$e_n = \frac{2}{d} \int_0^d h(z) \cos \frac{n\pi z}{d} \quad \text{for } n \neq 0$$

The following integrals will be useful in future analysis

$$\int_0^d \sin \frac{q\pi z}{d} \sin \frac{n\pi z}{d}\, dz = 0 \qquad q = n \neq 0$$

$$= 0 \qquad q \neq n$$

$$= \frac{d}{2} \qquad q = n \neq 0$$

$$\int_0^d \cos \frac{q\pi z}{d} \cos \frac{n\pi z}{d}\, dz = d \qquad q = n = 0$$

$$= 0 \qquad q \neq n$$

$$= \frac{d}{2} \qquad q = n \neq 0$$

$$\int_0^d \sin \frac{q\pi z}{d} \cos \frac{n\pi z}{d}\, dz = 0 \quad \text{for all } q,n.$$

B.2 Hermitian Interpolation Polynomials

i) Polynomials: $0 \leq e \leq 1$

$$f_1(e) = 1 - 3e^2 + 2e^3$$

$$f_2(e) = e - 2e^2 + e^3$$

$$f_3(e) = 3e^2 - 2e^3$$

$$f_4(e) = e^3 - e^2$$

ii) Characteristics:

	f_1	f_2	f_3	f_4
$f(0)$	1	0	0	0
$f(1)$	0	0	1	0
$\frac{df(0)}{de}$	0	1	0	0
$\frac{df(1)}{de}$	0	0	0	1

iii) Integrals:

$$\int_0^1 f_i(e)\, f_j(e)\, de$$

	f_1	f_2	f_3	f_4
f_1	13/35	11/210	9/70	-13/420
f_2		1/105	13/420	- 1/140
f_3	Symmetric		13/35	-11/210
f_4				1/105

$$\int_0^1 f_i'(e)\, f_j'(e)\, de$$

	f_1'	f_2'	f_3'	f_4'
f_1'	1.2	0.1	-1.2	0.1
f_2'		4/30	-0.1	-1/30
f_3'	Symmetric		1.2	-0.1
f_4'				4/30

$$\int_0^1 f_i''(e)\, f_j''(e)\, de$$

	f_1''	f_2''	f_3''	f_4''
f_1''	12.	6.	-12.	6.
f_2''		4.	- 6.	2.
f_3''	Symmetric		12.	-6.
f_4''				4.

Note: f'(e) is the derivative of the function f with respect to the quantity in brackets.

$$\int_0^1 f_i(e)\, f_j''(e)\, de$$

	f_1''	f_2''	f_3''	f_4''
f_1	-1.2	-1.1	1.2	-0.1
f_2	-0.1	-4/30	0.1	1/30
f_3	1.2	0.1	-1.2	1.1
f_4	-0.1	1/30	0.1	-4/30

B.3 Triangular Integral

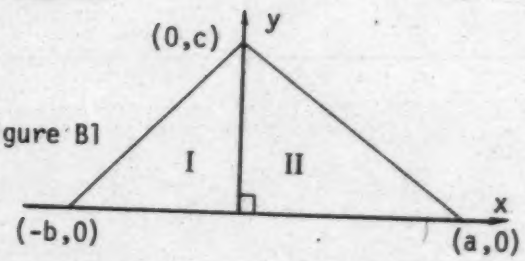

Figure B1

Section I:

$$y = \frac{c}{b}(x + b) = c\left(1 + \frac{x}{b}\right)$$

Section II:

$$y = \frac{c}{a}(a - x)$$

$$I = \int_{-b}^{0} \int_{0}^{\frac{c}{b}(x+b)} x^m y^n \, dy \, dx$$

$$= \int_{-b}^{0} \frac{x^m y^{n+1}}{(n+1)} \, dx \Big|_0^{\frac{c}{b}(x+b)}$$

$$= \left(\frac{c}{b}\right)^{n+1} \frac{n!}{(n+1)!} \int_{-b}^{0} x^m (x + b)^{n+1} \, dx$$

$$u = (x + b)^{n+1}$$

$$du = (n + 1) (x + b)^n$$

$$v = \frac{x^{m+1}}{m + 1}$$

$$dv = x^m$$

$$I = (x + b)^{n+1} \frac{x^{m+1}}{m + 1} \Big|_{-b}^{0} - \left(\frac{c}{b}\right)^{n+1} \frac{1}{(m+1)} \int_{-b}^{0} x^{m+1} (x + b)^n \, dx$$

$$= \left(\frac{c}{b}\right)^{n+1} \frac{n!(-1)^{n+1}}{(m+1+n)!} m! \int_{-b}^{0} x^{m+n+1} \, dx$$

$$= \left(\frac{c}{b}\right)^{n+1} \frac{n!m!(-1)^{n+1}}{(m+2+n)!} x^{m+n+2} \Big|_{-b}^{0}$$

$$= \frac{(-1)^{2(n+2)+m} m!}{(m+2+n)!} n! (b)^{m+n+2} \left(\frac{c}{b}\right)^{n+1}$$

$$= (-1)^m \frac{m!n!}{(m+2+n)!} b^{m+1} c^{n+1}$$

$$= - \frac{m!n!}{(m+2+n)!} (-b)^{m+1} c^{n+1}$$

$$II = \int_0^a \int_0^{\frac{c}{a}(a-x)} x^m y^n \, dy dx$$

$$= \frac{1}{n+1} \int_0^a x^m y^{n+1} \, dx \Big|_0^{\frac{c}{a}(a-x)}$$

$$= \left(\frac{c}{a}\right)^{n+1} \frac{1}{(n+1)} \int_0^a x^m (a - x)^{n+1} \, dx$$

$$u = (a - x)^{n+1}$$

$$du = - (h + 1) (a - x)^n$$

$$v = \frac{x^{m+1}}{m + 1}$$

$$dv = x^m$$

$$II = \left(\frac{c}{a}\right)^{n+1} \frac{(a-x)^{n+1}}{(n+1)} \frac{x^{m+1}}{(m+1)} \Big|_0^a + \int_0^a \left(\frac{c}{a}\right)^n \frac{x^{m+1}}{(m+1)} (a - x)^n \, dx$$

.
.

after n integrations

.
.

$$II = \left(\frac{c}{a}\right)^{n+1} \frac{m!n!}{(m+n+1)!} \int_0^a x^{m+n+1} \, dx$$

$$= \left(\frac{c}{a}\right)^{n+1} \frac{m!n!}{(m+n+2)!} a^{m+n+2}$$

$$= \frac{m!n!}{(m+n+2)!} a^{m+1} c^{n+1}$$

Total integral over area of triangle

$$\int_A x^m y^n \, dydx = \frac{m!n!}{(m+n+2)!} c^{n+1} (a^{m+1} - (-b)^{m+1})$$

B.4 Acoustic Rotational Matrix

Since the element is orientated so as to simplify the surface integral, it must be rotated to a position where the nodal characteristics are compatible with adjacent elements. The symmetry of the [P] and [S] matrices can be retained if the invariance of the energy equations are used. The rotation to a new system (x', y') from the old system (x, y) is a simple one:

p remains unchanged

$$\frac{\delta p}{\delta x'} = \frac{\delta p}{\delta x} \frac{\delta x}{\delta x'} + \frac{\delta p}{\delta y} \frac{\delta y}{\delta x'}$$

$$\frac{\delta p}{\delta y'} = \frac{\delta p}{\delta x} \frac{\delta x}{\delta y'} + \frac{\delta p}{\delta y} \frac{\delta y}{\delta y'}$$

$$\frac{\delta x}{\delta x'} = \cos \theta$$

$$\frac{\delta x}{\delta y'} = -\sin \theta$$

$$\frac{\delta y}{\delta x'} = \sin\theta$$

$$\frac{\delta y}{\delta y'} = \cos\theta$$

Thus, for any given nodal point

$$\begin{Bmatrix} p' \\ \frac{\delta p}{\delta x'} \\ \frac{\delta p}{\delta y'} \end{Bmatrix} = \begin{bmatrix} 1 & 0 & 0 \\ 0 & \cos\theta & \sin\theta \\ 0 & -\sin\theta & \cos\theta \end{bmatrix} \begin{Bmatrix} p \\ \frac{\delta p}{\delta x} \\ \frac{\delta p}{\delta y} \end{Bmatrix}$$

To rotate the total pressure vector for the triangular element, three such rotational matrices must be placed down the diagonal of a large matrix, $[\theta]$, whose remaining entries are zero

$$[p'] = [\theta]^T [p]$$

also $[p] = [\theta]^T [p']$ can be easily proven

B.5 Coordinate Relation Matrix for Triangular Acoustic Elements

$$
[A] = \begin{bmatrix}
1 & a & 0 & a^2 & 0 & 0 & 1a^3 & 0 & 0 \\
0 & 1 & 0 & 2a & 0 & 0 & 3a^2 & 0 & 0 \\
0 & 0 & 1 & 0 & a & 0 & 0 & a^2 & 0 \\
1 & b & 0 & b^2 & 0 & 0 & b^3 & 0 & 0 \\
0 & 1 & 0 & 2b & 0 & 0 & 3b^2 & 0 & 0 \\
0 & 0 & 1 & 0 & b & 0 & 0 & b^2 & 0 \\
1 & 0 & c & 0 & 0 & c^2 & 0 & 0 & c^3 \\
0 & 1 & 0 & 0 & c & 0 & 0 & c^2 & 0 \\
0 & 0 & 1 & 0 & 0 & 2c & 0 & 0 & 3c^2
\end{bmatrix}
$$

Let $u = a + b - c$

$$[A^{-1}] = \begin{bmatrix}
\frac{b^2(3a-b)}{(a-b)^3} & \frac{-b^2a}{(a-b)^2} & & \frac{a^2(a-3b)}{(a-b)^3} & \frac{-a^2b}{(a-b)^2} & & & & \\
\frac{-6ab}{(a-b)^3} & \frac{b(2a+b)}{(a-b)^2} & & \frac{6ab}{(a-b)^3} & \frac{a(a+2b)}{(a-b)^2} & & & & \\
\frac{-6a^2b^2}{c(a-b)^3u} & \frac{ab^2(2a+b)}{c(a-b)^2u} & \frac{-b(b-c)}{(a-b)u} & \frac{6a^2b^2}{c(a-b)^3u} & \frac{a^2b(a+2b)}{c(a-b)^2u} & \frac{a(a-c)}{(a-b)u} & & \frac{-ab}{cu} & \\
\frac{3(a+b)}{(a-b)^3} & \frac{-(a+2b)}{(a-b)^2} & & \frac{-3(a+b)}{(a-b)^3} & \frac{-(2a+b)}{(a-b)^2} & & & & \\
\frac{6ab(a+b)}{c(a-b)^3u} & \frac{-b(a+b)(2a+b)}{c(a-b)^2u} & \frac{-c}{(a-b)u} & \frac{-6ab(a+b)}{c(a-b)^3u} & \frac{-a(a+b)(a+2b)}{c(a-b)^2u} & \frac{c}{(a-b)u} & & \frac{a+b}{cu} & \\
\frac{-3b^2\{(3a-b)(b-c)-a(a+b)\}}{c^2(a-b)^3u} & \frac{-ab^2(a+3c-b)}{c^2(a-b)^2u} & \frac{2b(b-c)}{uc(a-b)} & \frac{-3a^2\{(a-3b)(a-c)+b(a+b)\}}{uc^2(a-b)^3} & \frac{a^2b(a-3c-b)}{c^2(a-b)^2u} & \frac{-2a(a-c)}{(a-b)uc} & \frac{3}{c^2} & \frac{2ab}{c^2u} & \frac{-1}{c} \\
\frac{-2}{(a-b)^3} & \frac{1}{(a-b)^2} & & \frac{2}{(a-b)^3} & \frac{1}{(a-b)^2} & & & & \\
\frac{-6ab}{c(a-b)^3u} & \frac{b(2a+b)}{c(a-b)^2u} & \frac{1}{(a-b)u} & \frac{6ab}{c(a-b)^3u} & \frac{a(a+2b)}{c(a-b)^2u} & \frac{-1}{(a-b)u} & & \frac{-1}{cu} & \\
\frac{2b^2\{(3a-b)(b-c)-bc\}}{uc^3(a-b)^3} & \frac{ab^2(2c-b)}{c^3(a-b)^2u} & \frac{-b(b-c)}{c^2(a-b)u} & \frac{2a^2\{(a-3b)(a-c)+ab\}}{uc^3(a-b)^3} & \frac{a^2b(2c-a)}{uc^3(a-b)^2} & \frac{a(a-c)}{uc^2(a-b)} & \frac{-2}{c^3} & \frac{-ab}{c^3u} & \frac{1}{c^2}
\end{bmatrix}$$

APPENDIX C

MATRIX FORMULATIONS

C.1 Decreasing the Order of a Matrix

The solution to the eigenvalue problem for a single triangular acoustic element gives ten eigenvectors $\{\eta\}_i$, of which $\{\eta\}_{10}$ is of the least interest for this analysis (because of its high eigenvalue). These eigenvectors are orthogonal through the $[S_e]$ or $[P_e]$ matrices of the equation

$$[[S_e] - \omega^2 [P_e]] \{p_e\} = 0$$

This would mean

$$\{\eta\}_i^T [S_e] \{\eta\}_j = \text{constant} \quad i = j$$
$$= 0 \qquad\qquad i \neq j$$

$$\{\eta\}_i^T [P_e] \{\eta\}_j = \text{constant} \quad i = j$$
$$= 0 \qquad\qquad i \neq j$$

where $i,j = 1, \cdots 10$

The orthogonality of the eigenvectors allows any pressure $\{p_e\}$ within the element to be defined by

$$\{p_e\} = \sum_{m=1}^{10} a_m \{\eta\}_m$$

By adding the constraint that the tenth eigenvector does

not contribute to the pressure distribution, a new pressure vector $\{p_e^*\}$ is arrived at such that

$$\{p_e^*\}^T [A] \{\eta\}_{10} = 0 \qquad (C1)$$

where [A] replaces the $[S_e]$ or $[P_e]$.

By partitioning the vectors and matrix as follows

$$\{p_e^*\} = \begin{bmatrix} p_1^* \\ p_2^* \\ \cdot \\ \cdot \\ \cdot \\ p_9^* \\ \hline p_{10}^* \end{bmatrix} \quad \{\eta\}_{10} = \begin{bmatrix} \eta_1 \\ \eta_2 \\ \cdot \\ \cdot \\ \cdot \\ \eta_9 \\ \hline \eta_{10} \end{bmatrix}$$

$$[A] = \left[\begin{array}{c:c} A_{11} & A_{12} \\ \hdashline A_{21} & A_{22} \end{array}\right]$$

where A_{21}, A_{12} are vectors and A_{22} is a scalar.

Let $\{p_e^*\}_c$ be a vector of the upper nine elements of $\{p_e^*\}$ and $\{\eta_c\}_{10}$ be the upper portion of $\{\eta\}_{10}$. Then (C1) can be written as

$$\{p_e^*\}_c^T [A_{11}] \{\eta_c\}_{10} + \{p_e^*\}_c^T [A_{12}] \{\eta_{10}\}$$

$$+ \{p_{10}^*\}^T [A_{21}] \{\eta_c\}_{10} + \{p_{10}^*\}^T [A_{22}] \{\eta_{10}\} = 0$$

Therefore

$$\{p_{10}^*\}^T = \{p_e\}_c^T [A_c] / B$$

where

$$A_c = [[A_{11}] \{n_c\}_{10} + [A_{12}] \{n_{10}\}]$$

$$B = - [A_{21}] \{n_c\}_{10} - [A_{22}] \{n_{10}\} \qquad (C2)$$

Again, using orthogonality

$$\{p_e^*\}^T [A^*] \{p_e^*\} = \text{constant}$$

where [A*] can also be either of the elemental matrices. The matrix can be partitioned

$$\{p_e^*\}_c^T [A_{11}^*] \{p_e^*\}_c + \{p_e^*\}_c^T [A_{12}^*] \{p_{10}^*\}$$

$$+ \{p_{10}^*\} [A_{21}^*] \{p_e\}_c + \{p_{10}^*\} [A_{22}^*] \{p_{10}^*\} = \text{constant}$$

Substituting from (C2)

$$\{p_e^*\}_c^T \left[[A_{11}^*] + [A_{12}^*] [A_c]^T / B \right.$$

$$+ [A_c] [A_{21}^*] / B$$

$$\left. + [A_c] [A_{21}^*] [A_c]^T / B^2 \right] \{p_e^*\}_c$$

It is now seen that the vector $\{p_e^*\}_c$ can be looked on as a condensed pressure vector while the result in outer square brackets is a condensed acoustic stiffness or mass matrix depending on the definition of [A*].

C.2 Applying Boundary Conditions

The overall matrices when initially assembled have no boundary conditions. The system must be "tied down" before the eigenvalue problem can be performed, because the unconstrained matrices are singular.

Several of the nodal characteristics are related to other nodal characteristics, i.e. $\frac{\delta p}{\delta x} = -\text{ctn } n \frac{\delta p}{\delta y}$, or are zero. The latter characteristics can be handled by simply removing the rows and columns which they (the zero characteristics) multiply with, because they supply nothing to the energy of the system. The zero characteristics are then deleted from the overall nodal characteristic vector $\{p_n\}$, leaving a "shrunken" energy matrix and nodal characteristic vector. The other defined nodal characteristic $\{p^*\}$ can be separated from the undefined ones $\{p_u\}$ by simply shifting rows and columns of the overall matrices so that the calculations remain the same, i.e.

$$\{p_n\}^T [B'] \{p_n\} = \begin{Bmatrix} p_u \\ p^* \end{Bmatrix}^T [B] \begin{Bmatrix} p_u \\ p^* \end{Bmatrix} = \text{constant}$$

where the left hand side is the original nodal characteristic vector and original matrix and the right hand side is the re-arranged form.

A relationship exists between $\{p^*\}$ and $\{p_u\}$

$$\{p^*\} = [R]\ \{p_u\}$$

By partitioning the matrix similarly to the way shown in Appendix C.1, a new overall energy matrix $[B^*]$ can be found in terms of the unknown nodal characters

$$[B^*] = [B_{11}] + [B_{12}]\ [R] + [R]^T\ [B_{21}]$$

$$+ [R]^T\ [B_{22}]\ [R]$$